ASSESSMENT OF VIRULENCE FACTORS OF A RESERVOIR-BORNE SARS-RELATED CORONAVIRUS BY REVERSE GENETICS

Dissertation

zur

Erlangung des Doktorgrades (Dr. rer. nat.)

der

Mathematisch-Naturwissenschaftlichen Fakultät

der

Rheinischen Friedrich-Wilhelms-Universität Bonn

vorgelegt von

Doreen Muth

aus

Rostock

Bonn, Juni 2012

Angefertigt mit Genehmigung der Mathematisch-Naturwissenschaftlichen Fakultät der
Rheinischen Friedrich-Wilhelms-Universität Bonn
am
Institut für Virologie des Universitätsklinikum Bonn
und am
Bernhard-Nocht-Institut für Tropenmedizin, Hamburg

1. Gutachter: Prof. Dr. Christian Drosten
2. Gutachter: Prof. Dr. Hans-Georg Sahl

Tag der Promotion: 05.10.2012
Erscheinungsjahr: 2013

Index

1 Introduction 1

1.1 Zoonoses and emerging infectious diseases 1

1.2 The severe acute respiratory syndrome coronavirus 2

1.2.1 SARS-CoV genome organization 4

1.2.2 SARS-CoV replication cycle 6

1.2.3 SARS-CoV accessory proteins 8

1.2.3.1 Accessory protein 6 – an IFN antagonist 8

1.2.3.2 ORF8 – subject to excessive mutations 10

1.3 Bats as the reservoir of emerging viruses 11

1.3.1 SARS-Coronavirus as a zoonotic agent 11

1.4 Reverse genetics systems for Coronaviruses 13

1.5 Aim of the thesis 15

2 Materials and Methods 16

2.1 Materials 16

2.1.1 Technical equipment 16

2.1.2 Disposables 18

2.1.3 Chemicals, buffers and solutions 20

2.1.3.1 Chemicals 20

2.1.3.2 Buffers and solutions 23

2.1.4 Cell culture media and supplements 26

2.1.5 Cell lines 27

2.1.6 Viruses 28

2.1.7 Media and antibiotics 28

2.1.8 Bacteria 29

2.1.9 Enzymes 29

2.1.9.1 Restriction endonucleases 29
2.1.9.2 Other enzymes 30
2.1.10 DNA and protein markers 30
2.1.11 Oligonucleotides 31
2.1.11.1 Cloning primers 31
2.1.11.2 Sequence PCR primers 33
2.1.11.3 Sequencing primers 34
2.1.11.4 Real-time RT-PCR primers 35
2.1.11.5 Vector primers 35
2.1.11.6 Additional primers 36
2.1.11.7 Overview of sequencing PCRs and primers 37
2.1.12 Plasmids 40
2.1.13 Kits 41
2.1.14 Antibodies 42
2.1.15 Software 43
2.2 Methods 44
2.2.1 Cell culture and virus propagation 44
2.2.1.1 General cell culture methods 44
2.2.1.2 Transfection of eukaryotic cells 44
2.2.1.3 Generation of recombinant virus 45
2.2.1.4 Production of virus stock 46
2.2.1.5 Virus infection 46
2.2.1.6 Plaque titration assay 47
2.2.1.7 Lentiviral Transduction 48
2.2.2 Molecular biological methods 50
2.2.2.1 Isolation of viral RNA 50
2.2.2.2 cDNA synthesis 50

2.2.2.3 Isolation of genomic DNA 51
2.2.2.4 Isolation of plasmid DNA 52
2.2.2.5 Purification of PCR products 53
2.2.2.6 Gel extraction of DNA fragments 53
2.2.2.7 Phenol-chloroform extraction and alcohol precipitation of nucleic acids 54
2.2.2.8 Agarose gel electrophoresis of DNA 55
2.2.2.9 Photometric determination of nucleic acid concentration 55
2.2.2.10 Sequencing of DNA 56
2.2.2.11 Generation of capped RNA transcripts 56
2.2.2.12 Generation of an RNA standard for quantification of SARS-CoV genomic RNA 58
2.2.2.13 Restriction endonuclease digestion and dephosphorylation of DNA 60
2.2.2.14 Ligation of nucleic acid fragments 61
2.2.3 Polymerase chain reaction 62
2.2.3.1 Phusion® PCR 62
2.2.3.2 Real-time RT-PCR for quantification of genomic SARS-CoV RNA 66
2.2.3.3 Site-Directed Mutagenesis 67
2.2.4 Cloning of PCR products into pEZ™ BAC vector 69
2.2.5 Production of chemically competent *E.coli* 70
2.2.6 Transformation of chemically and electrocompetent *E.coli* and preparation of glycerol stocks 70
2.2.7 Protein biochemical methods and immunodetection assays 71
2.2.7.1 Protein isolation from eukaryotic cells 71
2.2.7.2 Sodium dodecyl sulfate polyacrylamide gel electrophoresis (SDS-PAGE) 71
2.2.7.3 Western blot analysis 72
2.2.7.4 Immunofluorescence assay (IF) 73
2.2.8 RVFV-Renilla bioassay 74

3 Results 75
3.1 Technical preliminary work 75
3.1.1 Generation of recombinant SARS-CoVs 75
3.1.1.1 SARS-CoV reverse genetics system 75
3.1.1.2 Assembly of half-clone pDEF 77
3.1.1.3 Assembly of the full-length SARS-CoV clone 79
3.1.1.4 Rescue of recombinant SARS-CoVs 83
3.1.2 Generation of a SARS-CoV-susceptible bat cell line 85
3.1.3 Determination of pan-species IFN EC_{50} on primate and bat cell culture 88
3.2 Assessment of putative virulence factors of SARS-CoV and SARS-related bat-CoV. 89
3.2.1 Characterization of SARS-CoV and SARS-related bat-CoV p6 90
3.2.1.1 Cloning of SARS-CoV and SARS-related bat-CoV ORF6 into expression vector pCAGGS 91
3.2.1.2 Cellular localization of SA-p6 and BG-p6 in human and bat cells 93
3.2.1.3 Colocalization of SA-p6 and BG-p6 with human karyopherins 94
3.2.1.4 Inhibition of STAT1 nuclear translocation upon IFN stimulation by SA-p6 and BG-p6 in primate cells 96
3.2.2 Characterization of BG-p6 in the full virus context 98
3.2.2.1 Generation of an rSCV carrying the SARS-related bat CoV ORF6 98
3.2.2.2 Generation of an rSCV with a deleted ORF6 102
3.2.2.3 Rescue and quantification of ORF6 mutant rSCVs 103
3.2.2.4 Growth kinetics of ORF6 mutant viruses 104
3.2.2.5 Growth of ORF6 mutant viruses in primate and bat cells in an anti-viral state 105
3.2.3 Impact of ORF8 integrity on virus replication 109
3.2.3.1 Completion of ORF8 for the generation of O8full-rSCV 110

3.2.3.2 Deletion of ORF8 for the generation of delO8-rSCV 112
3.2.3.3 Rescue and quantification of ORF8 mutant rSCVs 115
3.2.3.4 Comparative growth kinetics of ORF8 variants 117
3.2.3.5 Replication of ORF8 mutant viruses on IFN stimulated primate and bat cell lines 118
3.2.3.6 Trans-complementation of ORF8 variants 119
4 Discussion 122
4.1 Reverse genetics 122
4.2 Transgenic bat cells 124
4.3 The potential of accessory proteins to serve as risk markers 126
4.3.1 Protein 6 126
4.3.2 Open reading frame 8 129
5 Summary 131
6 References 135
7 Abbreviations 141
Curriculum vitae 143
Publications 144

1 Introduction

1.1 Zoonoses and emerging infectious diseases

A zoonosis is defined by the World Health Organization (WHO) as "any disease or infection that is naturally transmissible from vertebrate animals to humans and vice-versa". Zoonoses are caused by bacteria (e.g. *Salmonella* – Salmonellosis, *Yersinia pestis* – Plague), parasites (e.g. *Toxoplasma gondii* – Toxoplasmosis) and viruses (e.g. Lyssaviruses – Rabies, Ebola viruses – Ebola hemorrhagic fever). An "emerging zoonosis" is described to be "newly recognized or newly evolved, or that has occurred previously but shows an increase in incidence or expansion in geographical, host or vector range".

The topic of "emerging zoonoses" came into the limelight around 1945 with increasing articles in "The Journal of Infectious Diseases" [1]. A proposed reason for this development is the increased cross-host exposure, because the separation of donor and recipient host was drastically reduced due to changes in geographical and ecological behavior [2]. Expansion of the human population results in interference with so far untouched habitats including wildlife and pathogens. Extensive global travelling enables global pathogen distribution in only a few days [2]. Agricultural expansion comes along with the exploitation of pristine habitats, bringing livestock into close contact to wildlife, which in turn increases the risk of transmission of infections to humans [3]. The disturbance of habitats by humans inevitably leads to a loss of biodiversity, which can indirectly promote the increase of emerging diseases [4]. This phenomenon has been described as the "dilution effect", postulating that a decrease in host diversity leads to an increase of prevalence of infectious diseases and vice versa [5]. Viral pathogens make up about 25% of all emerging infectious diseases (EIDs) [1].

Zoonotic viruses can be highly pathogenic for humans but in many cases the underlying factors that enable viruses to cross the species barrier are not known. It is believed that genetic relatedness of species favors cross-species transmission of pathogens [2, 6]. For successful transmission, viruses have to overcome ecological and/or molecular species barriers. Virus entry is often mediated by species-specific receptors. Even after the crossing of receptor-dependent barriers, genome replication, gene expression and morphogenesis have to adapt to new intracellular environments. Moreover, the innate immunity of the new host needs to be evaded to

establish successful replication [7, 8]. "Generalist" viruses with a broad host range, which can use different host cell mechanisms for replication, are therefore more likely to gain access to new hosts than "specialist" viruses, which infect only closely related hosts [2]. Transmission patterns play an important role in the definition of ecological species barriers. Direct zoonotic virus transmission, for instance, can occur by contaminated saliva from reservoir animals, as in the case of rabies. Viruses can also make use of "helpers", such as vectors or intermediate amplifying hosts. Arthropod-borne viruses, like Alpha-, Bunya-, or Flaviviruses, are transmitted to humans via insects or ticks, which take up the virus when feeding on infected animals. Intermediate or amplifying hosts serve as bridges between two species, possibly giving viruses a chance for stepwise adaptation and/or bringing the virus into contact with recipient hosts [2]. For example severe acute respiratory syndrome coronavirus (SARS-CoV) was not directly transmitted from bats, but underwent an adaptation in civets probably through repeated transfer of virus from civets to humans and back, resulting in the pandemic strain [9, 10]. Finally, rapid genetic evolution of zoonotic viruses is crucial for successful transmission to a new host. Here, especially RNA viruses, like SARS-CoV, with error-prone replication, insufficient or complete lack of proof-reading mechanisms and short virus generation times come into focus [11, 12].

The increasing emergence of viral zoonoses calls for research into mechanisms driving viruses from their animal hosts. New virus species are found in wild animals almost minutely these days. These viruses need to be characterized for their zoonotic potential. In addition, known zoonotic viruses have to be investigated in context of their natural reservoirs and the cellular mechanisms and *in vivo* determinants, which normally keep them confined, have to be explored. The SARS-CoV is an exceptional archetype for zoonoses research, because the virus itself has been studied intensively following the pandemic it caused and its reservoir is known.

1.2 The severe acute respiratory syndrome coronavirus

Coronavirinae are a subfamily of the *Coronaviridae* family (order *Nidovirales*). They are divided into the three genera; Alpha-, Beta- and Gammacoronaviruses. There are currently five human coronaviruses (hCoV) known, which, except for SARS-CoV, cause only mild disease of the upper respiratory tract; hCoV-229E [13] and hCoV-NL63 [14] belonging to the Alphacoronaviruses and hCoV-OC43 [15], SARS-CoV [16, 17] and hCoV-HKU1 [18] defining the Betacoronaviruses.

SARS-CoV caused the first pandemic of a transmissible disease with a previously unknown cause [19]. It started in November 2002 and was brought under control by July 2003. Until then, SARS-CoV spread to 33 countries on five continents, caused over 8000 infections and more than 700 deaths [19]. For this reason it is the most pathogenic hCoV and was subject to a huge variety of studies on coronavirus replication, interaction with the host immune response and pathogenesis, making it now the best understood coronavirus and an ideal prototype virus for studies on zoonotic disease emergence.

SARS-CoV virions are spherical enveloped particles with club-shaped spike proteins protruding from the envelope. These spikes are seen as a "crown" (lat. Corona) around the virus particles in electron microscopy, earning the virus family its name (Fig. 1.1B).

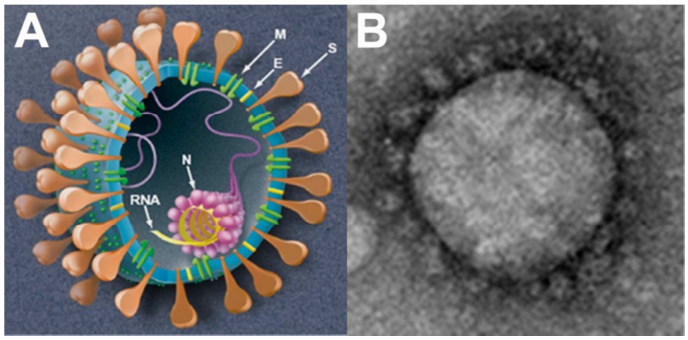

Figure 1.1: Coronavirus particle.
(A) Model of a Coronavirus particle. The virion membrane contains the spike (S), envelope (E) and matrix (M) proteins. The RNA genome is associated with nucleocapsid protein N [20]. (B) Electron microscopy showing the typical coronavirus "crown" of the S proteins (picture taken by H.R. Gelderblom, Robert Koch-Institute).

1.2.1 SARS-CoV genome organization

SARS-CoV, like all coronaviruses, contains a single stranded, 5'-capped, positive strand RNA genome [21, 22]. The first open reading frame, ORF1ab, makes up two-thirds of its 29.7 kb genome and codes for proteins contributing to virus replication. Almost all of these proteins are not packaged into virions and therefore called non-structural proteins (nsp). Most of the remaining one-third of the genome encodes 4 structural proteins. The spike (S) protein is the major surface protein (Fig. 1.1A). Neutralizing antibodies are directed against the S protein and it is responsible for virus entry and host range. The envelope protein (E) is an integral membrane protein and is involved in virus formation and budding. The matrix protein M is the most abundant structural protein in the virion whose C-terminus is located at the inside of the virus particle where it interacts with the helical nucleocapsid protein (N), which in turn is associated with the viral genome. The M protein is not transported via the Golgi apparatus to the cell membrane, but rather stays at the endoplasmatic reticulum during the whole infection cycle. There the first steps of virus assembly are initiated by interactions of the M and N protein.

Interspersed between these structural genes are eight accessory genes (Fig. 1.2A, marked in red). The encoded proteins share little amino acid identity between genera, formally termed "groups", of coronaviruses and are therefore called "group-specific". These proteins are not generally required for virus replication *in vitro* but are thought to have important roles in replication in the natural host.

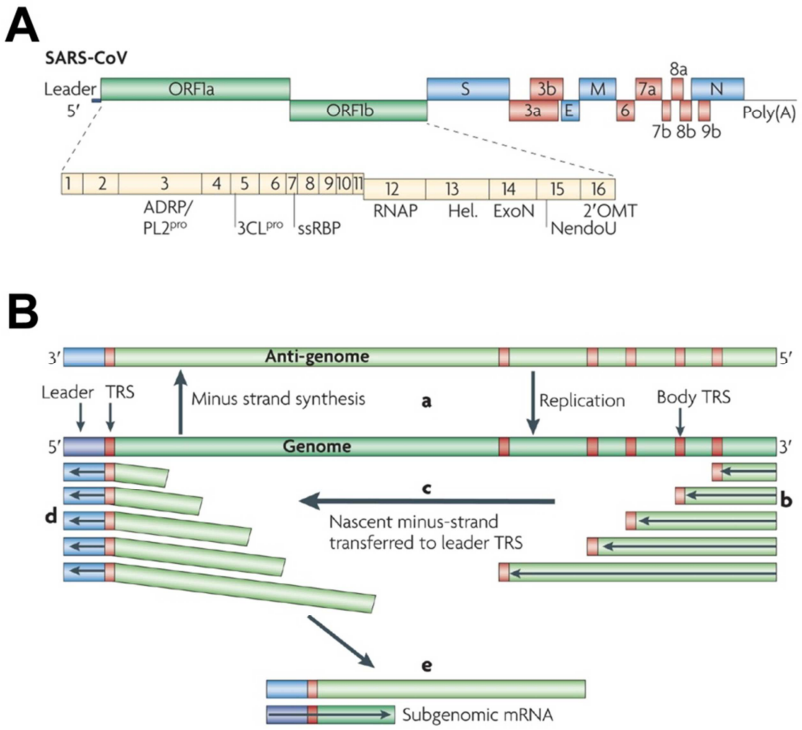

Figure 1.2: Genome organization and generation of subgenomic RNAs of SARS-CoV.
(A) Organization of the SARS-CoV genome. The replicase genes (ORF1a, ORF1b, green) make up two-third of the whole genome. Common to all coronaviruses ORFs encoding for the structural proteins are located downstream of ORF1a/b in the order S (spike), E (envelope), M (membrane) and N (nucleocapsid) protein (highlighted in blue). Interspersed between the structural genes are the genes coding for group-specific accessory proteins (red). (B) A negative-strand copy of the full-length RNA genome serves as template for genome replication (a). Subgenomic mRNAs for translation are transcribed from discontinuously transcribed negative-strand subgenomic RNAs. The viral polymerase starts transcription at the genomes 3' end (b) and stops at one of the transcription regulatory sequences (TRS) located upstream of each ORF. Then the newly synthesized strand dissociates from the template strand and fuses to the first TRS at the genomes 5' end (c). Transcription is continued through the leader sequence of the genome (d). The negative-strand subgenomic RNAs of various lengths are template for transcription of subgenomic mRNAs (e). [23]

1.2.2 SARS-CoV replication cycle

Binding of the S protein to the SARS-CoV receptor human angiotensin converting enzyme 2 (hACE2) mediates fusion of the virus envelope with the cell membrane. The infectious RNA genome is then released into the cytoplasm [21, 22]. Because the RNA genome is positive in orientation, it can serve as template for translation. ORF1ab, which codes for proteins involved in virus replication, is translated initially. The ORF1ab gene is organized in two partially overlapping ORFs (ORF1a and 1b) and translation of the full polyprotein pp1ab is achieved by a -1 ribosomal frame shift. Polyproteins pp1a and pp1ab are co- and post-translationally processed by ORF1a-encoded proteinases. These proteinases are autocatalytic and become enzymatically active before they are released from the polyprotein by cis-cleavage. All replicase proteins are found in membrane-associated "replication complexes", where viral RNA synthesis takes place. For genome replication, a full-length negative-strand genome copy is synthesized, serving as the template for synthesis of full-length positive-strand genome RNA. Negative-strand templates make up only 1-2% of total viral RNA in infected cells. All non-replicase proteins are expressed from a set of "nested" subgenomic mRNAs (Fig. 1.2B). They share common capped 5' ends ("leader sequence"), identical to the sequence of the 5' end of the genome RNA, and common poly(A) tailed 3' ends [24-26]. Usually only the ORF closest to the 5' end of subgenomic RNAs is translated. Each subgenomic mRNA is transcribed from a corresponding subgenomic negative strand RNA. These templates are generated by discontinuous transcription of the full-length positive strand RNA genome. The viral RNA polymerase starts transcription at the 3' end of the RNA genome until it reaches a transcription regulatory sequence (TRS), located directly upstream of each ORF called body TRS. There the polymerase either continues to the next body TRS or stops, dissociates from the template strand and hybridizes to the TRS directly upstream of the "leader sequence", the leader TRS. There transcription continues through the "leader sequence" and synthesis of the subgenomic negative-strand RNA is completed. This mechanism allows the virus to control the abundance of mRNAs and therefore proteins. The smaller mRNAs, coding for structural proteins needed in virus assembly, are most abundant. The assembly of virions takes place at the endoplasmatic reticulum-Golgi intermediate compartment (ERGIC) [23, 27]. M and E proteins play major roles in the formation of virus envelopes, because overexpression of both proteins is sufficient for the production of virus-like particles [28]. Interactions of M with the RNA genome containing nucleocapsid probably ensure incorporation of only full-length genomes into virions [29]. Immature virions are transported through the Golgi apparatus for

maturation. Finally, mature virions are transported in vesicles to the plasma membrane and released.

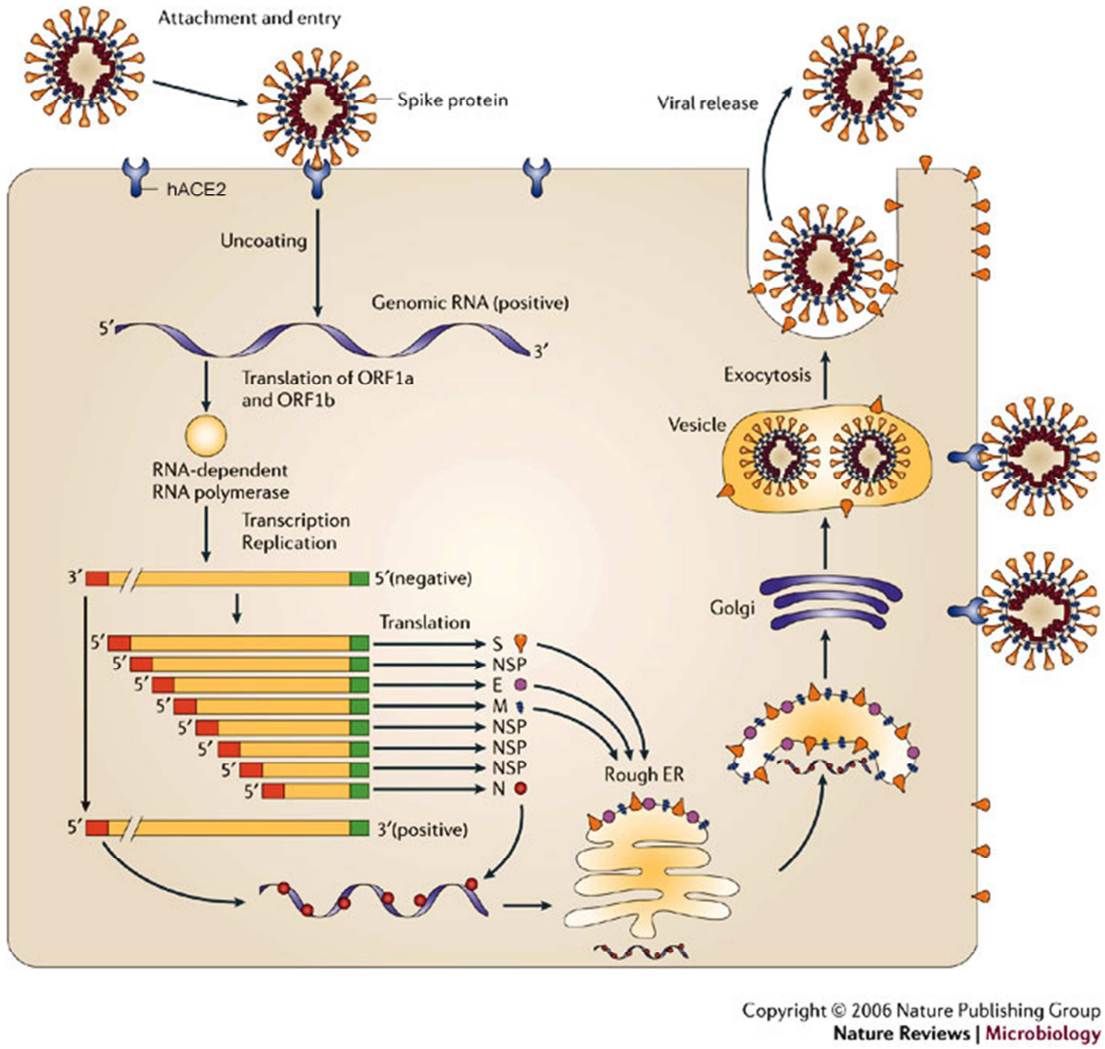

Figure 1.3: Coronavirus replication cycle.
Binding of the spike protein to the SARS-CoV specific receptor human angiotensin converting enzyme 2 (hACE2) mediates virus entry. Following uncoating of the genomic RNA, proteins necessary for virus replication are translated from open reading frame (ORF) 1a and 1ab. The remaining ORFs 2-9 are translated from a nested set of subgenomic RNAs. Virions mature while they are transported through the Golgi apparatus. Virus particles are transported in vesicles to the membrane and released by exocytosis. Replication cycle adapted from Bergmann et al. [30].

1.2.3 SARS-CoV accessory proteins

As mentioned above the group-specific ORFs of SARS-CoV are not absolutely required for *in vitro* replication but may have functions as pathogenicity factors in the natural host. Antibodies against all of these proteins have been found in patients suggesting *in vivo* expression of the accessory proteins [31-34]. Proteins 3a (p3a) and 3b (p3b) are expressed from subgenomic RNA3. P3a with its 274 amino acids is the largest group-specific protein [35] and localizes to the Golgi apparatus, the plasma membrane and to intracellular vesicles [36, 37]. Furthermore, p3a induces vesicle formation and Golgi fragmentation in full virus context [35]. The p3b, expressed from the second ORF of RNA3, localizes to mitochondria and the nucleus [38, 39] and displays IFN-antagonistic properties [40]. The proteins 7a and 7b are expressed from the bicistronic RNA7. Protein 7a induces apoptosis [41, 42] and cell cycle arrest [43]. Moreover, p7a inhibits cellular protein synthesis [44], seems to act as an RNA silencing suppressor [45] and was identified as a structural protein [46]. Protein 7b is a structural virion component [47] and localizes to the Golgi compartment during infection [48]. Furthermore, a cell culture adapted deletion in ORF7b resulted in attenuation of the corresponding virus *in vitro* and in an animal model, suggesting a function as an attenuating factor [49]. Protein 9b, expressed from the second ORF in the nucleocapsid gene, has been suggested to possess a nuclear export signal, to be predominantly localized in the cytoplasm and to induces caspase 3 mediated apoptosis [50, 51]. The proteins expressed from ORF6 and ORF8 are described in more detail below.

1.2.3.1 Accessory protein 6 – an IFN antagonist

The accessory protein 6 (p6) encoded by ORF6 is the best studied protein. P6 was found to be expressed in lung and intestine tissues of SARS patients [52] and localizes in the endoplasmatic reticulum (ER)/Golgi membrane. In a first study SARS-CoV p6 was identified as a virulence factor, whose genomic insertion turned an attenuated murine hepatitis virus (MHV) into a lethal variant. This chimeric virus caused fatal encephalitis in mice and enhanced virus growth in cell culture [53]. This enhancement is probably achieved by creating a cellular environment for optimal replication [54]. P6 colocalizes with SARS-CoV's non-structural proteins 3 and 8 [55, 56], which are found on double membrane vesicles, the sites of virus replication [23]. The N-terminus of p6 is an amphipathic helix which is able to induce membrane rearrangements to from replication complexes. Moreover, the C-terminus of p6 binds a nuclear import factor and

so antagonizes the interferon (IFN) signaling pathway by disruption of the nuclear import machinery [57, 58]. Shuttling of the IFN stimulated gene factor 3 (ISGF3) into the nucleus relies on the binding of karyopherin α1 (KPNA1) and subsequently to karyopherin β1 (KPNB1). P6 retains KPNA2 at the ER/Golgi membrane and competes with the ISGF3:KPNA1 complex for unbound KPNB1. Depletion of free KPNB1 by binding to p6:KPNA2 blocks the import of ISGF3 and inhibits the induction of transcription of IFN-stimulated genes downstream of the JAK/STAT pathway [59]. The suggested model for SARS-CoV p6 IFN antagonism is depicted in Fig. 1.4.

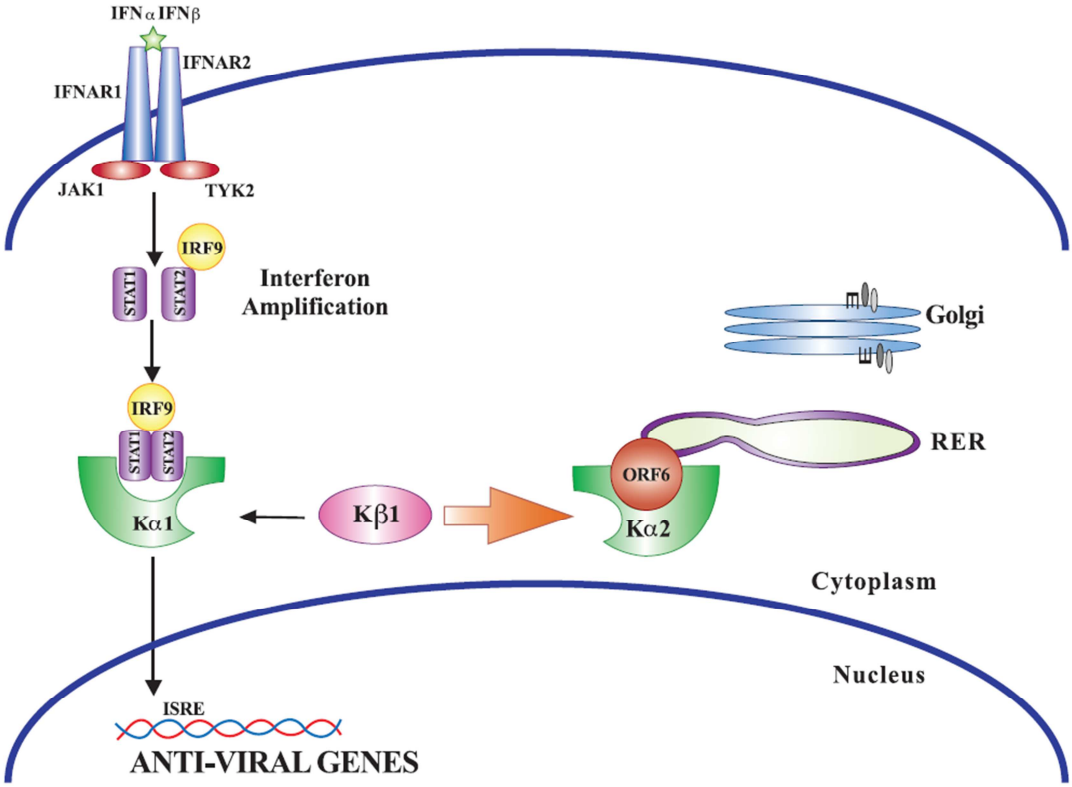

Figure 1.4: Model of SARS-CoV p6 function as an IFN antagonist.
The STAT1:STAT2:IRF9 complex (ISGF3) is formed after IFN stimulation and recognized by KPNA1 (Kα1) for nuclear import. Protein 6 (here ORF6) retains KPNA2 (Kα2) at the ER and competes with KPNA1 for unbound KPNB1 (Kβ1), which is necessary for nuclear translocation of ISGF3 [59].

The deletion of ORF6 in recombinant SARS-CoVs did not reduce virus growth in cell culture after infection at a high MOI [60]. However, infections at a low MOI revealed disadvantages in replication at early time points post infection. Furthermore, although a mechanism for IFN antagonism of p6 has been described, deletion of ORF6 did not result in an increased IFN sensitivity of the virus [54, 59].

Despite the rather modest influence of p6 on virus growth in cell culture, its expression in context of MHV greatly enhanced mortality in mice and implies an important role in virus infection in the natural host [53].

1.2.3.2 ORF8 – subject to excessive mutations

Genetic analysis of SARS-CoV strains from different phases of the epidemic revealed that the ORF8 region underwent unusually excessive changes within a short time [61]. Strains isolated from humans in the early phase of the pandemic and those isolated from palm civets (*Paguma larvata*) carried either a single full-length ORF8 or showed an 82 nucleotide (nt) deletion [26, 61]. SARS-CoV strains isolated in the intermediate phase of the pandemic displayed a 29nt-deletion within ORF8 resulting in two ORFs, ORF8a and ORF8b [61]. This genotype was dominant during the rest of the epidemic. In a very late cluster of SARS cases a genotype with a 415nt deletion resulting in the loss of ORF8 was isolated from two patients [61]. The deletion mutations within ORF8 might either mean that ORF8 is non-coding or codes for a non-functional protein. Many studies have been conducted comparing the proteins of the full-length ORF8 and the pandemic variants ORF8a and 8b to elucidate their roles in human to animal transmission or viral pathogenesis and persistence [62-68]. Recombinant viruses carrying either the full-length ORF8 or ORF8 with the 29nt-deletion showed no differences in virus replication in cell culture [60]. Both viruses grew to same titers in mice and showed no differences in replication efficiency, pathology, or duration of virus persistence [60]. Experimentally infected palm civets were equally susceptible to both viruses, however civets infected with SARS-CoV carrying the full-length ORF8 had higher body temperatures and slightly stronger antibody responses [69]. The ORF8a protein was found to enhance viral replication and induce apoptosis when overexpressed and anti-ORF8a-antibodies were found in patients [62]. Expression of ORF8b was questioned because of its unusual location within ORF8a and its poor context for translation initiation [26]. In addition, overexpressed protein 8b degrades *in vitro* within a few hours [67]. Nevertheless, protein 8b was found to be expressed late in viral infection and to reduce virus replication by down-regulating the expression of the envelope protein [63, 64, 66]. Whether changes within the ORF8 region are a result of viral adaptation or genomic instability remains unclear. The 29nt-deletion appeared to be unnecessary for human-to-animal transmission, because isolates from a second zoonotic transmission after the declared end of the SARS epidemic carried the full-length ORF8 [64].

1.3 Bats as the reservoir of emerging viruses

Bats represent an outstanding reservoir for viral zoonoses because of their high species diversity, broad geographic distribution, ability for long-distance migration and roosting behavior in large groups. Bats make up 20% of the about 4600 species currently classified as mammals [70]. They are distributed around the world except for northern and southern polar areas. With their unique ability among mammals to fly, bats even cross continents [70]. This ability allows exchange of novel viruses between different bat species and other vertebrates. Bats live in great population densities with up to several million individuals [70]. This roosting behavior creates optimal conditions for intra- and inter-species transmission of viruses [70].

Only little is known about the bat immune system and how it supports persistence of a variety of viruses. Because bats share a relatively old common ancestor with other mammals, their immune response might have important qualitative and quantitative differences as compared to rodents and primates. Similar to other mammals, bats apparently develop a virus-specific adaptive T- and B-cell response despite persistent virus infection [70-73].

In the past years, bats have been demonstrated to be natural reservoirs for an increasing number of emerging zoonotic viruses, e.g. rabies virus [74], filoviruses [73, 75], henipaviruses [71, 76], as well as SARS-CoV [10, 72].

1.3.1 SARS-Coronavirus as a zoonotic agent

The animal origin of the SARS pandemic was based, amongst others, on the findings that SARS-CoV was a new virus without genetic relatedness to known hCoVs. Early case patients lived near animal markets or were food traders with animal contact. SARS-CoVs isolated from humans were almost identical to isolates from market animals [77]. An initial study found viruses closely related to SARS-CoV in palm civets (*Paguma larvata*), one raccoon dog (*Nyctereutes procyonoides*) and ferret badgers (*Melogale moschata*) [78]. The question arose, if other species are also susceptible to SARS-CoV, but no systematic studies were conducted. However, a total of 13 mammalian species proved to be susceptible in experimental infections [77]. The close genetic relation between human and civet SARS-CoV isolates strongly suggested a transmission from civets, but interestingly neutralizing antibodies against SARS-CoV were exclusively found in civets from

animal markets, not farmed civets [79-81]. So, apparently civets are not generally infected with SARS-CoV. Furthermore, it is widely accepted that a reservoir host shows no clinical signs of an infection [82], but experimentally infected palm civets did [69]. Therefore, palm civets definitely played an important role in transmission, but were unlikely to be the natural reservoir of SARS-CoV. In 2005 bats from the genus *Rhinolophus* were identified as the most likely reservoir of SARS-CoV [10, 72]. The high seroprevalence and wide distribution of seropositive *Rhinolophus* bats are typical for natural hosts [82]. This finding led to intensive studies on bats and coronaviruses around the world. Indeed a huge variety of alpha- and betacoronaviruses were found in many different bat species, suggesting that bats are not only the natural reservoir of SARS-CoV but of most CoVs [83-87]. Furthermore, these studies revealed that bat CoVs seem to be specifically associated with their hosts. Different bat species from same locations harbored different CoVs, while similar CoVs were found in the same bat species of geographically distant regions [85, 88].

This wide distribution of CoVs in bats, the fact that SARS-CoV entered the human population at least two times independently [89] and hints that there is an ongoing evolution of CoVs in bats [85] open the possibility of future transmissions of CoVs to the human population and emphasize the need to understand reservoir distribution and transmission to prevent future outbreaks.

1.4 Reverse genetics systems for Coronaviruses

Reverse genetics provides a valuable tool to study viral protein functions in whole virus context. Studies in overexpression systems, looking at only one protein in particular, are rather unreliable and leave out virus-host and intra-viral protein interactions.

First viral reverse genetics systems have already been established in the early 1980s for DNA-viruses [90-92] and positive-strand RNA-viruses with small genomes [93-95]. All systems for positive-strand RNA-viruses are plasmid-based. The cDNA copy of the whole RNA genome is inserted into a vector and maintained in bacteria.

Coronaviruses possess the largest genomes of all known RNA-viruses with about 27-32 kb in length. The genetic instability of such large inserts in conventional vectors and the suspected toxicity to *Escherichia coli* (*E.coli*) of certain genome regions of coronaviruses, e.g. replicase genes, represent major obstacles in creating a cDNA clone. Different approaches were successfully used to overcome these obstacles. Baric and colleagues established a system of step-wise *in vitro* ligation of cloned subgenomic cDNAs, completely avoiding the generation of a full-length genome plasmid [96-98]. Here, the coronavirus genome is segmented into 6 fragments, which are cloned into conventional vectors. All fragments are cloned using the restriction endonuclease BglI, which cuts the sequence GCCNNNN↓NGGC. The unspecified nucleotides represented by N leave a statistical variation of 64 different asymmetrical ends, allowing a unidirectional assembly of the fragments. Genomic mutations can be easily inserted into corresponding fragments due to their small sizes. Thiel et al. overcame the problems of cloning of the large cDNA genome by using a poxvirus vector [99]. These vectors are especially suitable for cloning of large fragments, because inserts are kept stable in a non-bacterial host system. Nevertheless, subgenomic fragments have to be cloned into plasmids or be prepared as PCR products for subsequent insertion into the poxvirus genome. In the end, the cDNA genome of the coronavirus has to be cut out from purified poxvirus DNA. Both mentioned systems use a T7 promoter, cloned in front of the coronavirus genome, for *in vitro* transcription of infectious genomic RNA. The RNA is either electroporated or chemically transfected into eukaryotic cells for virus replication. The group of Enjuanes established the first plasmid-based cloning system for the whole coronaviral cDNA genome [100, 101]. Here the cDNA genome is cloned step-wise into a bacterial artificial chromosome (BAC) vector. BAC vectors are only present in one or two copies per bacterium and inserts are therefore kept stable. The viral genome is under control of the cytomegalovirus immediate-early promoter and therefore transcribed in the nucleus of

chemically transfected eukaryotic cells. This system avoids potentially error-prone *in vitro* RNA transcription, but exposes the viral genome to RNA modifications and processing, e.g. by splicing, within the nucleus. Potential splicing sites can be predicted and deleted by inserting silent mutations into the genome. But changing the genome in any way to study modified viral proteins might lead to the introduction of other splicing sites, hence making more modifications of the viral genome necessary. The reverse genetics system established by our group combines BAC vector-based cloning of the coronaviral full-length cDNA genome with *in vitro* RNA transcription of the genome using the T7 polymerase [49]. The genome is divided into six fragments, which are first cloned into high copy vectors. During the step-wise assembly of the full-length genome, the vector backbone is switched to pBeloBAC11, stabilizing the growing inserts. Because cDNA inserts are subject to modifications by the bacteria they are maintained in, like deletions or nucleotide exchanges, careful handling of the plasmids and sequencing of each assembly step is necessary. Nevertheless, mutations can be easily introduced on subclone level and assembly is straightforward. In contrast to the other systems, recombinant virus does not have to be passaged and plaque purified. Four times passaging and three times plaque titration is done by other groups leading to increased virus titers [100]. However, this might already be due to genome mutations in the course of cell culture adaptation.

1.5 Aim of the thesis

SARS-CoV encodes for an exceptionally high number of accessory proteins whose features are not yet fully characterized. These proteins are dispensable for virus replication in cell culture models but are believed to serve important functions in the natural reservoir.

By sequencing the full-length genome of a Bulgarian SARS-related bat-CoV new sequence information on a reservoir-borne CoV became available.

The aim of the present study was to compare accessory proteins from the newly discovered SARS-related bat-CoV with their corresponding proteins of the human pathogenic SARS-CoV. The purpose of this comparison was the evaluation of the bat-CoV derived proteins to function in primate cell culture models, thus assessing their zoonotic potential.

Protein 6, encoded by ORF6, was chosen because it is a well characterized IFN antagonist. In addition, ORF8 was chosen because, intriguingly, it is absent in the Bulgarian SARS-related bat-CoV, while it is present in Asian SARS-related bat-CoVs and the human pandemic strain.

Viral proteins derived from a bat-CoV were to be compared to proteins from a human pathogenic CoV. In addition to studies on primate cell cultures a cell culture model of the bat reservoir was to be established. Therefore, a *Rhinolophus* lung cell line was produced and made susceptible to SARS-CoV infection.

.

2 Materials and Methods

2.1 Materials

2.1.1 Technical equipment

Equipment	Type	Source
Autoclave	V120	Systec GmbH, Wettenberg
Balance	SPO 61	Scaltec Instruments GmbH, Göttingen
Blotting system	Fastblot B44	Biometra GmbH, Göttingen
Blue-light transilluminator	Flu-O-Blu	Biozym Scientific GmbH , Hessisch Oldendorf
Centrifuges	Centrifuge 5424	Eppendorf, Hamburg
	Centrifuge 5810R	Eppendorf, Hamburg
	Sorvall Evolution RC	Thermo Fisher Scientific, Schwerte
Chemiluminescence detection system	FusionFx7	PeqLab/Vilbert Lourmat, Erlangen
Chemiluminescence reader	Synergy™ 2	BioTek, Bad Friedrichshall
Electrophoresis system	Mini-PROTEAN® Tetra Cell	Bio-Rad Laboratories, Munich
Electroporation system	Gene Pulser Xcell	Bio-Rad Laboratories, Munich
Freezer	-20°C Liebherr premium	Liebherr, Biberbach a. d. Riß
	-80°C/Typ499	Kaltis Europe GmbH, Niederweningen, Switzerland

	Liquid Nitrogen LS 750	Taylor Wharton Germany GmbH, Husum
Gel electrophoresis	PerfectBlue Gelsystem Mini	PEQLAB Biotechnologie GmbH, Erlangen
Gel electrophoresis documentation	E-Box 3028, WL/26M	Vilbert Lourmat, Marne-la-Vallee, France
Heating block	Thermomixer comfort	Eppendorf, Hamburg
Hood (Bioflow)	Gelaire BSB-4A	ICN Biochemicals, Eschwege
Incubators	HERAcell® 240	Thermo Fisher Scientific, St. Leon-Roth
	Heraeus® B6126	Thermo Fisher Scientific, St. Leon-Roth
Magnetic plate	Agencourt SPRIPlate Supermagnet Plate	Beckman Coulter GmbH, Krefeld
Magnetic stirrer	REO basic IKAMAG	IKA®-Werke GmbH & CO. KG, Staufen
Microscopes	TELAVAL31	Carl Zeiss Jena GmbH, Jena
	IMAGER.M1	Carl Zeiss Jena GmbH, Jena
PCR cycler	Mastercycler epgradient S	Eppendorf, Hamburg
pH meter	766 Calimatic	Knick Elektronische Meßgeräte GmbH & Co. KG, Berlin
Photometer	NanoDrop 2000c	PEQLAB Biotechnologie GmbH, Erlangen
Pipette assistance	Accu-jet® pro	Brand, Wertheim

Pipettes	Research, PhysioCare (100-1000 µL, 20-200 µL, 2-20 µL, 0.5-10 µL)	Eppendorf, Hamburg
Power supply	Standard Power Pack P25	Biometra GmbH, Göttingen
Real-time PCR cycler	LightCycler® 1.5	Roche Diagnostics Deutschland GmbH, Mannheim
	LightCycler® 480	Roche Diagnostics Deutschland GmbH, Mannheim
Rotating incubator	GFL-3033	GFL, Burgwedel
Thermocycler	Mastercycler ep	Eppendorf, Hamburg
Vertical shaker	Mini Rocker MR.1	PEQLAB Biotechnologie GmbH, Erlangen
Vortexer	Vortex VF2	IKA®-Werke GmbH & CO. KG, Staufen
Water purification system	Milli-Q® Biocel	Millipore GmbH, Schwalbach

2.1.2 Disposables

Article	**Source**
Blotting paper	Whatman GmbH, Dassel
C-Chip, Disposable Neubauer improved counting chamber	Biochrom AG, Berlin
Cell culture flask with filter cap (25, 75, 175 cm^2)	SARSTEDT AG & Co., Nümbrecht
Cell culture plates (6well, 24well)	SARSTEDT AG & Co., Nümbrecht

Cell scraper	TPP Techno Plastic Products AG, Trasadingen, Switzerland
Centrifuge tubes (15, 50 mL)	SARSTEDT AG & Co., Nümbrecht
Cover glass slips (13 mm round)	Thermo Fisher Scientific, St. Leon-Roth
Cryotubes	SARSTEDT AG & Co., Nümbrecht
Electroporation cuvettes (1 mm, 2 mm gaps)	Biozym Scientific GmbH , Hessisch Oldendorf
Immobilion-P^{SQ} PVDF membrane, 0.2 µm	Millipore GmbH, Schwalbach
LightCycler® Capillaries (20 µL)	Roche Diagnostics Deutschland GmbH, Mannheim
Microplates 96-well LUMITRAC, white	VWR, Darmstadt
LightCycler®480 Multiwell Plate 96, white	Roche Diagnostics Deutschland GmbH, Mannheim
PCR reaction tubes (0.2 µL)	SARSTEDT AG & Co., Nümbrecht
Petri dishes	SARSTEDT AG & Co., Nümbrecht
Pipette Tips (10, 20, 200, 1000 µL)	SARSTEDT AG & Co., Nümbrecht
Reaction tubes (1.5, 2 mL)	SARSTEDT AG & Co., Nümbrecht
Scalpel	Aesculap AG, Tuttlingen
Serological pipettes (1, 2, 5, 10, 25 mL)	SARSTEDT AG & Co., Nümbrecht
Stericup and Steritop Vacuum Filter Cups (500 mL)	Millipore GmbH, Schwalbach
Westran® Clear Signal PVDF membrane, 0.45 µm	Whatman GmbH, Dassel

2.1.3 Chemicals, buffers and solutions

2.1.3.1 Chemicals

Chemical	Source
2-Mercaptoethanol (β-Mercaptoethanol)	Carl Roth GmbH + Co. KG, Karlsruhe
2-Propanol ≥99.5%	Carl Roth GmbH + Co. KG, Karlsruhe
30% Acrylamid (Rotiphorese® Gel 30)	Carl Roth GmbH + Co. KG, Karlsruhe
4x NuPAGE® LDS Sample Buffer	Life Technologies, Darmstadt
Acetic acid, 100%, Ph.Eur., reinst	Carl Roth GmbH + Co. KG, Karlsruhe
Agarose Broad Range	Carl Roth GmbH + Co. KG, Karlsruhe
Agarose GTQ	Carl Roth GmbH + Co. KG, Karlsruhe
Ammonium persulfate (APS)	Carl Roth GmbH + Co. KG, Karlsruhe
Ampuwa® (sterile, pyrogen-free water)	Fresenius Kabi, Bad Homburg
Bovine Serum Albumin (special quality for molecular biology)	Roche Diagnostics, Mannheim
Bovine Serum Albumin (BSA)	New England Biolabs GmbH, Frankfurt am Main
Bromphenol blue	Sigma-Aldrich Chemie GmbH, Munich
Calcium Chloride ($CaCl_2$)	Carl Roth GmbH + Co. KG, Karlsruhe
Carrier RNA (Poly A RNA solution, 10 mg/mL)	QIAGEN, Hilden
Chloric acid (HCl)	Carl Roth GmbH + Co. KG, Karlsruhe
Chloroform	Carl Roth GmbH + Co. KG, Karlsruhe

Crystal Violet	Carl Roth GmbH + Co. KG, Karlsruhe
Dako Fluorescent Mounting Medium	Dako North America Inc., Carpineteria, USA
Diethylpyrocarbonate (DEPC)	Carl Roth GmbH + Co. KG, Karlsruhe
Dithiothreitol (DTT), 0.1 M	Life Technologies, Darmstadt
Disodium hydrogen phosphate - dihydrate (Na_2HPO_4-$7H_2O$)	Merck KGaA, Darmstadt
dNTP set (dATP, dTTP, dGTP, dCTP)	QIAGEN, Hilden
Ethanol ≥99.9%, Ph.Eur., reinst	Carl Roth GmbH + Co. KG, Karlsruhe
Ethidium Bromide (10 mg/mL)	Carl Roth GmbH + Co. KG, Karlsruhe
Ethylenediaminetetraacetic acid (EDTA)	SERVA Electrophoresis GmbH, Heidelberg
EUROIMMUN sample buffer	EUROIMMUN AG, Lübeck
Formaldehyde 37%	Carl Roth GmbH + Co. KG, Karlsruhe
FuGENE® HD Tranfection Reagent	Roche Diagnostics, Mannheim
GelStar® Nucleic Acid Gel Stain	Lonza, Rockland, USA
Glycerol	Carl Roth GmbH + Co. KG, Karlsruhe
Glycin	Carl Roth GmbH + Co. KG, Karlsruhe
IGEPAL® CA-630	Sigma-Aldrich Chemie GmbH, Munich
Magnesium chloride ($MgCl_2$)	Sigma-Aldrich Chemie GmbH, Munich
Methanol (99%)	Carl Roth GmbH + Co. KG, Karlsruhe
Milk powder	Carl Roth GmbH + Co. KG, Karlsruhe
Phenol (Rotiphenol®)	Carl Roth GmbH + Co. KG, Karlsruhe

Potassium chloride (KCl)	Carl Roth GmbH + Co. KG, Karlsruhe
Potassium dihydrogen phosphate (KH_2PO_4)	Merck KGaA, Darmstadt
Protease Inhibitor Cocktail III, EDTA-free	Merck KGaA, Darmstadt
Re-Blot Plus-Strong, 10x	Millipore GmbH, Schwalbach
RNA*later*® RNA Stabilization Reagent	QIAGEN, Hilden
Roti®-Histofix 4% (pH7)	Carl Roth GmbH + Co. KG, Karlsruhe
Sodium chloride (NaCl)	Carl Roth GmbH + Co. KG, Karlsruhe
Sodium deoxycholate	Carl Roth GmbH + Co. KG, Karlsruhe
Sodium dodecyl sulfate (SDS), ultra pure	Carl Roth GmbH + Co. KG, Karlsruhe
Sodium hydroxide (NaOH)	Carl Roth GmbH + Co. KG, Karlsruhe
Sucrose	Sigma-Aldrich Chemie GmbH, Munich
SuperSignal® West Chemiluminescent Substrate (Pico, Femto)	Thermo Fisher Scientific p/a Perbio Science Deutschland, Bonn
Tetramethylethylenediamine (TEMED), 99%	Carl Roth GmbH + Co. KG, Karlsruhe
Tris hydroxymethyl aminomethane (Tris)	Carl Roth GmbH + Co. KG, Karlsruhe
Triton X-100	Sigma-Aldrich Chemie GmbH, Munich
Tween® 20	Sigma-Aldrich Chemie GmbH, Munich
X-tremeGENE DNA Transfection Reagent	Roche Diagnostics, Mannheim
Xylene cyanol FF	Sigma-Aldrich Chemie GmbH, Munich

2.1.3.2 Buffers and solutions

Name	Ingredients
6x Loading Dye	40% Sucrose
	0.15% Bromphenol blue
	0.15% Xylene cyanol FF
	in deionized water
APS working solution	10% APS
	in deionizede water
	store at -20°C
Crystal violet stock solution	10 g Crystal violet
	50 mL Formaldehyde (37%)
	100 mL Ethanol (99.9%)
	350 mL deionized water
Crystal violet working solution	100 mL Crystal violet stock solution
	100 mL Formaldehyde (37%)
	800 mL deionized water
DEPC water	1 mL DEPC
	in 1 L deionized water
	stir over night, autoclave

PBS-Tween	0.1% Tween® 20
	10% 10x PBS
	in deionized water
Phosphate buffered saline (PBS), 10x, pH7.0	80 g NaCl
	2 g KCl
	26.8 g Na_2HPO_4-$7H_2O$
	2.4 g KH_2PO_4
	adjust pH with 37% HCl
	add 1 L deionized water
	autoclave
RIPA lysis buffer	150 mM NaCl
	1% IGEPAL® CA-630
	0.5% Sodium deoxycholate
	0.1% SDS
	50 mM Tris (pH8.0)
	in deionized water
	steril filtrate, store at 4°C
add freshly before use:	10 µL Proteinase Inhibitor Cocktail
	1 µL Benzonase
	50 µL 0.1 mM DTT
	to 939 µL RIPA lysis buffer

SDS working solution, 10%	100 g SDS
	in 900 mL deionized water
	heating to 68°C to dissolve SDS
	adjust pH to 7.2 with HCl
Transfer buffer, 10x	250 mM Tris-acetate
	1.5 M Glycin
	in deionized water
Transfer buffer working solution	10% Methanol
	10% Transfer buffer 10x
	in deionized water
Tris-acetate-EDTA (TAE) buffer, 50x, pH7.8	2 M Tris-acetate
	0.05 M EDTA
	1 M Acetic acid (100%)
	in deionized water
Tris-HCl buffer, 1.875 M, pH8.8	227.14 g Tris-acetate
	adjust pH with 37% HCl
	Add 1 L deionized water
Tris-HCl buffer, 0.6 M, pH6.8	72.68 g Tris-acetate
	adjust pH with 37% HCl
	add 1 L deionized water

Western blot antibody buffer	1% dry milk in PBS-Tween
Western blot blocking solution	5% dry milk in PBS-Tween

2.1.4 Cell culture media and supplements

Name	Source
Accutase™ (50 mL)	PAA Laboratories GmbH, Cölbe
Amino Acids Non Essential (100x, 50 mL)	PAA Laboratories GmbH, Cölbe
Avicel® RC581	FCM BioPolymer, Brussels, Belgium
CryoMaxx S (50 mL)	PAA Laboratories GmbH, Cölbe
Dulbecco's MEM (DMEM)	Biochrom AG, Berlin
Dulbecco's Modified Eagles Medium (high glucose, 4.5 g/L, 500 mL)	PAA Laboratories GmbH, Cölbe
Dulbecco's PBS (1x, 500 mL)	PAA Laboratories GmbH, Cölbe
Fetal Bovine Serum (FBS) "Gold" (500 mL)	PAA Laboratories GmbH, Cölbe
L-glutamine (100x, 50 mL)	PAA Laboratories GmbH, Cölbe
Opti-MEM® I Reduced-Serum Medium (1x, 50 mL)	Life Technologies, Darmstadt
OptiPRO ™ serum-free medium (1 L)	Life Technologies, Darmstadt
Penicillin/Streptomycin (100x, 50 mL)	PAA Laboratories GmbH, Cölbe
Polybrene	Sigma-Aldrich Chemie GmbH, Munich

Poly-L-Lysine (50 mL)	Sigma-Aldrich Chemie GmbH, Munich
Puromycin Dihydrochloride Ready Made Solution (10 mg/mL, 10 mL)	Sigma-Aldrich Chemie GmbH, Munich
Sodium pyruvate (100x, 50 mL)	PAA Laboratories GmbH, Cölbe
Trypsin-EDTA (1x, 50 mL)	PAA Laboratories GmbH, Cölbe

2.1.5 Cell lines

Name	Source
293T	Human fetal liver cell line (cell culture collection BNI[a])
BHK-J	Baby hamster kidney cell line (cell culture collection BNI[a])
Huh7	Human liver cell line (ATCC CCL-185)
MA104	Monkey kidney cell line (cell culture collection BNI[a])
RhiLu-hACE2	Transgenic embryonic Rhinolophus landeri lung cell line expressing human ACE2 (made in house)
VeroE6	Monkey kidney cell line (ATCC CRL-1586)
VeroFM	Monkey kidney cell line (kind gift of Jindrich Cinatl, Universtiy of Frankfurt)

Legend: [a]BNI (Bernhard Nocht-Institute for Tropical Medicine, Hamburg)

2.1.6 Viruses

Name	Description/Source
BGO6-rSCV	Recombinant SARS Coronavirus strain Frankfurt (NC_004718) with ORF 6 from BtCoV/BM48-31/BGR/2008 (NC_014470), Doreen Muth
O8full-rSCV	Recombinant SARS Coronavirus strain Frankfurt (NC_004718) with 29 nucleotide insertion in ORF 8 between position 27882 and 27883, Doreen Muth
delO6-rSCV	Recombinant SARS Coronavirus strain Frankfurt (NC_004718) with 2 stop codons instead of amino acid 4 and 5 in ORF 6, Doreen Muth
delO8-rSCV	Recombinant SARS Coronavirus strain Frankfurt (NC_004718) without ORFs 8a and 8b, Doreen Muth
rSCV	Recombinant SARS Coronavirus strain Frankfurt (NC_004718), Susanne Pfefferle
RVFV-Luc	*Renilla* Luciferase expressing recombinant Rift Valley fever virus, Prof. Dr. Friedemann Weber, University of Marburg
SARS-CoV FRA1	SARS Coronavirus strain Frankfurt (NC_004718), Institute of Virology, Bonn

2.1.7 Media and antibiotics

Name	Source
Ampicillin	Sigma-Aldrich Chemie GmbH, Munich
Chloramphenicol	Sigma-Aldrich Chemie GmbH, Munich
Lysogeny Broth (LB) Broth (Lennox)	Carl Roth GmbH + Co. KG, Karlsruhe
Lysogeny Broth (LB) Agar (Lennox)	Carl Roth GmbH + Co. KG, Karlsruhe

S.O.C. Medium	Life Technologies, Darmstadt
Recovery Medium	Lucigen Corporation, Middleton, USA

2.1.8 Bacteria

Name	Source
BAC-Optimized Replicator v2.0 elctrocompetent cells	Lucigen Corporation, Middleton, USA
E. cloni 10G (supreme, elite) electrocompetent cells	Lucigen Corporation, Middleton, USA
One Shot® Stbl3™ chemically competent cells	Life Technologies, Darmstadt/made in-house
One Shot® TOP10 chemically competent cells	Life Technologies, Darmstadt/made in-house

2.1.9 Enzymes

2.1.9.1 Restriction endonucleases

Name	Source
BamHI FastDigest®	FERMENTAS GmbH, St. Leon-Roth
EcoRI FastDigest®	FERMENTAS GmbH, St. Leon-Roth
MluI	New England Biolabs GmbH, Frankfurt am Main
NcoI	New England Biolabs GmbH, Frankfurt am Main
NotI FastDigest®	FERMENTAS GmbH, St. Leon-Roth
PspOMI	New England Biolabs GmbH, Frankfurt am Main

2.1.9.2 Other enzymes

Name	Source
Antarctic Phosphatase	New England Biolabs GmbH, Frankfurt am Main
Benzonase® Nuclease HC, purity >99%	Merck KGaA, Darmstadt
Phusion® High-Fidelity DNA Polymerase	Thermo Fisher Scientific (Finnzymes), St. Leon-Roth
RNaseOUT™ Recombinant Ribonuclease Inhibitor	Life Technologies, Darmstadt
RNase H	Life Technologies, Darmstadt
SuperScript™ III Reverse Transcriptase	Life Technologies, Darmstadt
T4 DNA Ligase (5 u/µL)	Roche Diagnostics, Mannheim

2.1.10 DNA and protein markers

Name	Source
GeneRuler™ 1 kb DNA Ladder	FERMENTAS GmbH, St. Leon-Roth
GeneRuler™ 1 kb Plus DNA Ladder	FERMENTAS GmbH, St. Leon-Roth
GeneRuler™ 100 bp Plus DNA Ladder	FERMENTAS GmbH, St. Leon-Roth
Supercoiled DNA Ladder	New England Biolabs GmbH, Frankfurt am Main
Supercoiled DNA Marker Set	EPICENTRE, Madison, USA
PageRuler™ Prestained Protein Ladder	FERMENTAS GmbH, St. Leon-Roth

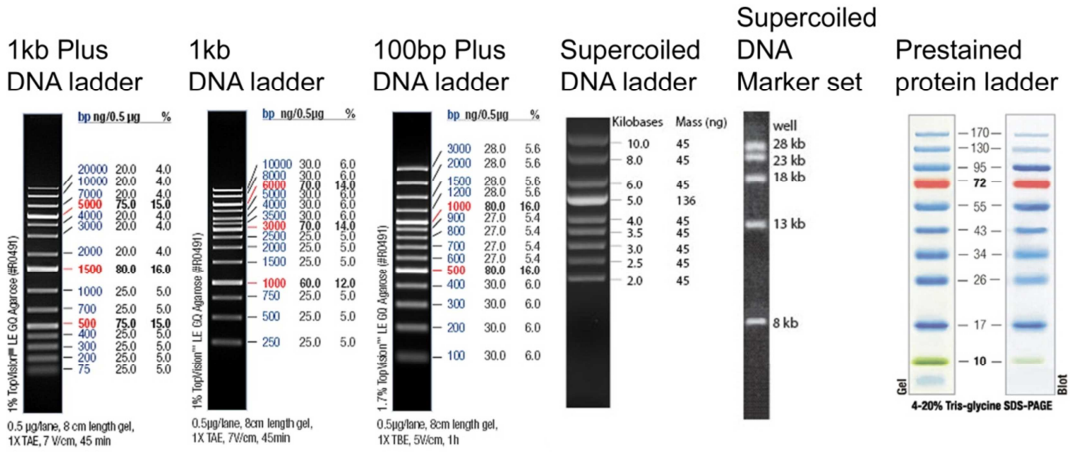

Figure 2.1: DNA and protein markers

2.1.11 Oligonucleotides

2.1.11.1 Cloning primers

BGO6 cloning primers

BG-ORF6-for	ATGTTTAGTCTAGTTGCTTTCCA
BG-ORF6-rev	TTAAGGATGATCAATTTCCATAGG
F 25778 F	GAAGGTGACGGCATTTCAAC
F 29260 R	TTTGTATGCGTCAATGTGCTTG
H-BG-ORF6-rev	TGGAAAGCAACTAGACTAAACATCTGTTGTCACTTACTGTACTAG
H-BG-ORF6-for	CCTATGGAAATTGATCATCCTTAAAACGAACATGAAAATTATTCTCTTC
RT-BG-ORF6	GTTCTGCTGATGCTATACTTAC

Underlined: BG-CoV sequence

delO6 cloning primers

delORF6-for	GACAACAGATGTTTCATTAATGAGACTTCCAGGTTACAATAGC
delORF6-rev	ACTTACTGTACTAGCAAAGCAATATTGTCGTTGCTACCG

Underlined: double stop codon

O8full cloning primers

29nt-for	CTGGTTACCAACCTGAATGGAATATAAGGTACAACACTAGGGGTAATACT
29nt-rev	TCCATTCAGGTTGGTAACCAGTAGGACAAGGATCTTCAAGCACATGA
F 26020 F-P	CGGCTCTTCAGGAGTTGCTA

Underlined: additional 29nts

delO8 cloning primers

delORF8-1-for	AATGTCTGATAATGGACCCCAATCAAACCAACGTAGTGC
delORF8-1-rev	GTTCGTTTAGACTTTGGTACAAGGTTCTTCTAGATCC
delORF8-2-for	TAAAATGTCTGATAATGGACCCCAATCAAACCAACG
delORF8-2-rev	TTGTTCGTTTAGACTTTGGTACAAGGTTCTTCTAGATCC

Underlined: sequence replacement for ORF8

SARS-CoV ORF6 with C-terminal HA-tag

Eco-Koz-SAO6-F	ccgccG**gaattc***GCCACC***atg**TTTCATCTTGTTGACTTCCAGG
SAO6-HA-Not-R	atagtttaGCGGCCGC**tta***agcgtaatctggaacatcgtatgggt a*TGCAGCTGCTGGATAATCTAACTCCATAGGTTCTTC

SARS-related bat-CoV ORF6 with C-terminal HA-tag

Eco-Koz-BGO6-F	ccgccg**gaattc***GCCACC***atg**TTTAGTCTAGTTGCTTTCCAAGT TAC
BGO6-HA-Not-R	atagtttaGCGGCCGC**tta***agcgtaatctggaacatcgtatggg ta*TGCAGCTGCAGGATGATCAATTTCCATAGGTTCTTC

Legend:	**gaattc**	EcoRI site
	GCGGCCGC	NotI site
	***GCCACC*atg**	Kozak sequence
	tacccatacgatgttccagattacgct	HA-tag
	GCAGCTGCA	3x alanine spacer

2.1.11.2 Sequence PCR primers

A 2335	F	AGGCACTCGAAATGTGCATTG
B 5663	F	TACAGCAAGGTACATTCTTATG
C 9013	F	TTGTTATGACACTAATTTGCTAG
D 12200	F	CAAGTTGGAAAAGATGGCAGATC
D 15010	F	ACTCAAATGAATCTTAAGTATGC
D 18969	F	AATCCAAAGGCTATCAAGTGTG
E 21249	F	CAAGCCGAAGGAACAAATTGATG
E 22748	F	TGCCAGATGATTTCATGGGTTG
F 24444	F	AGCCTTCAAACCTATGTAACAC
F 27420	F	GGCAATTCACCATTTCACCCTCTTG
A 2860	R	CGGATTCAACAGTGTAGACAGAGCA
B 6490	R	CAGCCATAAGATCCTCATGA
C 9740	R	GCAGCCTCCTCGAAGGTACT
D 13779	R	CCTCATCAAAATGACGTAGAGCATAGAC
D 16166	R	CTGCAAGACTGTATGTGGTGTGTACAT
E 19430	R	GCATCGTGTAATACACGTAGCAGA
E 22427	R	ATCTCCTGAGGGAACAACCC
F 24481	R	GCCCTGATTAGTTGTTGTGTTA
F 25594	R	ATAGAGGTACAAAAATTGCGCC
F 29260	R	TTTGTATGCGTCAATGTGCTTG

2.1.11.3 Sequencing primers

A	324	F	GTCCAACTCAGTTTGCCTGTC
A	1067	F	GGGAATGCCCAAAGTTTGTG
A	1849	F	ACATTGGACAACAGAGATCAG
A	2587	F	AATGGAGCTATCGTTGGCAC
A	3366	F	CTCTGTCTACACTGTTGAATC
A	3970	F	AATGGTAAGCTTTACCATGATTC
B	4622	F	CTTAAAGCTCCTGCCGTAGTG
B	5304	F	TGCTGGTGATGCTGCTAAC
B	6022	F	CAAATGACAGGCTTCACAAAG
B	6782	F	GAATTAGAGCTTCACTACCTAC
B	7468	F	ACTATTGTTAATGGCATGAAGAG
B	8185	F	GAAGTGACAGGTGACAGTTG
C	8884	F	TACACACCTTCCAAACTCATTG
C	9578	F	CATTCTTGGCTCACCTTCAATG
C	10297	F	CGTATCCAACCTGGTCAAAC
C	11063	F	GGTATTATGGCAATTGCTGC
C	11570	F	TAGGCTATTGTTGCTGCTG
D	12200	F	CAAGTTGGAAAAGATGGCAGATC
D	12924	F	CTAAATAGAGGTATGGTGCTG
D	13700	F	AAGATTGTCCAGCGGTTGCTGTC
D	14510	F	GTATGCTGCTGATCCAGCTATG
D	15264	F	ATAATGGCCTCTCTTGTTCTTG
D	16059	F	AAGTTACATGATGAGCTTACTG
D	16779	F	TATGGTGATGCTGTTGTGTAC
D	17532	F	TGACACTGTGAGTGCTTTAG
D	18034	F	CATTACTGGTCTTCATCCTACAC
D	18656	F	TTCTGTGGGTTTTGACTATGTC
E	19250	F	GTGAATAAGCATGCATTCCAC
E	19984	F	AAGGTTCAGTCAAAGGTCTAAC
E	20738	F	ATGTCGCAAAGTATACTCAACTG
E	21452	F	TGTGGTTTCAAGTGATATTCTTG
E	22225	F	TTCACCTGCTCAAGACATTTG
E	22900	F	CTGCTCTTAATTGTTATTGGCC

E 23658 F	AAACCTCCGTAGATTGTAATATG

F 24252 F	ACAACAACATCAACTGCATTGG
F 24905 F	CAAAGAAGAGCTGGACAAGTACTTC
F 25462 F	GAGCGCTACCAAAATAATTGCGCTC
F 26176 F	TCTTGCTTTCGTGGTATTCTTG
F 26918 F	GATCACTGTGGCTACATCACGAAC
F 27659 F	GACTTCTATTTGTGCTTTTTAGC
F 28462 F	GATGGTACTTCTATTACCTAG
F 29149 F	GATCCACAATTCAAAGACAACG

2.1.11.4 Real-time RT-PCR primers

SARS-CoV RNA

SARS-F	CCCGCGAAGAAGCTATTCG
SARS-P	Fam-ACGTTCGTGCGTGGATTGGCTTTG-BHQ
SARS-R	AGTTGCATGACAGCCCTCTACA

2.1.11.5 Vector primers

pBeloBAC

pBELOscfwd	GCCCTTAAACGCCTGGTTGCTAC
pBELOscrev	CGACAGGTGCTGAAAGCGAGC
Seq9	CCCGTATTCAGTGTCGCTG

pCAGGS vector

pCAGGS-F_mod	GCCTTCTTCTTTTTCCTACAGC
pCAGGS-R_mod	CTTTATTAGCCAGAAGTCAGATGC

pEZ™ BAC vector

BEZ-F1	CACTTTATGCTTCCGGCTCGTATG
BEZ-R1	GGGATGTGCTGCAAGGCGATTAAG

2.1.11.6 Additional primers

SARS-CoV N PCR

Ngenefwd	GGCCATTTAGGTGACACTATAGATGTCTGATAATGGACCCCAATC
	underlined = SP6 promoter
Frev	TTTTTTTTTTTTTTTTTTTTGTCATTCTCCTAAGAAGC

SARS CoV real-time RT-PCR standard

T7-SAR S1	TAATACGACTCACTATATTATCACCCGCGAAGAAGCT
	underlined = T7 promoter sequence
E 19031 R	CTGAGCATCGTAGAACTTCC

Forward primers

F 27626 F	GAGAAAGACAGAATGAATGAGC

Reverse primers

F 27900 R	CCCTAGTGTTGTACCTTACAAG
F 27990 R	ACCATAGTGTGCCATCTATGA
F 28182 R	GGGTCCACCAAATGTAATGCGG

hACE2-puromycin resistance gene

hACE2 1737F	GAATGTAAGGCCACTGCTCAACTA
pQC.Puro R	TCAGGCACCGGGCTTGC

2.1.11.7 Overview of sequencing PCRs and primers

Table 2.1: Sequencing PCRs and primers for subclone pEF

PCR/Amplicon No.	**Forward primer**	**Reverse Primer**	**Fragment length**
1	Seq9	F 26100 R	5,292 bp
2	F 25462 F	pBELOscfwd	4,423 bp
Annealing temperature: 60°C, extension time: 80 sec			
Seq. primer PCR No. 1		**Seq. primer PCR No. 2**	
pBELOscrev		F 25462 F	
E 21452 F		F 26176 F	
E 22225 F		F 26918 F	
E 22900 F		F 27659 F	
E 23658 F		F 28462 F	
F 24252 F		F 29149 F	
F 24905 F			

Table 2.2: Sequencing PCRs and primers for subclone pDEF

PCR/Amplicon No.	**Forward primer**	**Reverse Primer**	**Fragment length**
1	Seq9	D 16166 R	3,369 bp
2	D 16059 F	E 19430 R	3,363 bp
3	D 18969 F	E 22427 R	3,459 bp
4	E 21249 F	F 24481 R	3,255 bp
5	E 22748 F	F 25594 R	2,869 bp
6	F 24444 F	F 29260 R	4,762 bp
7	F 27420 F	pBELOscfwd	2,130 bp
Annealing temperature: 57°C, extension time: 72 sec			
Seq. primer PCR No. 1	**Seq. primer PCR No. 2**	**Seq. primer PCR No. 3**	**Seq. primer PCR No. 4**
pBELOscrev	D 16059 F	D 19250 F	E 22225 F
D 13700 F	D 16779 F	D 19984 F	E 22900 F
D 14510 F	D 17532 F	D 20738 F	E 23658 F
D 15264 F	D 18034 F	E 21452 F	
	D 18656 F		
Seq. primer PCR No. 5	**Seq. primer PCR No. 6**	**Seq. primer PCR No. 7**	
F 24252 F	F 25462 F	F 28462 F	
F 24905 F	F 26176 F	F 29149 F	
	F 26918 F		
	F 27659 F		

Table 2.3: Sequencing PCRs and primers for the SARS-CoV full-length clone

PCR/Amplicon No.	**Forward primer**	**Reverse Primer**	**Fragment length**
1	Seq9	A 2860 R	3,370 bp
2	A 2335 F	B 6490 R	4,182 bp
3	B 5663 F	C 9740 R	4,090 bp
4	C 9013 F	D 13779 R	4,789 bp
5	D 12200 F	D 16166 R	3,975 bp
6	D 15010 F	E 19430 R	4,413 bp
7	D 18969 F	E 22427 R	3,459 bp
8	E 21249 F	F 24481 R	3,255 bp
9	E 22748 F	F 25594 R	2,869 bp
10	F 24444 F	F 29260 R	4,762 bp
11	F 27420 F	pBELOscfwd	2,465 bp
Annealing temperature: 56°C, extension time: 72 sec			
Seq. primer PCR No. 1	**Seq. primer PCR No. 2**	**Seq. primer PCR No. 3**	**Seq. primer PCR No. 4**
pBELOscrev	A 2587 F	B 6022 F	C 9578 F
A 324 F	A 3366 F	B 6782 F	C 10297 F
A 1067 F	A 3970 F	B 7468 F	C 11063 F
A 1849 F	A 4622 F	B 8185 F	C 11570 F
	B 5304 F	C 8884 F	D 12200 F
Seq. primer PCR No. 5	**Seq. primer PCR No. 6**	**Seq. primer PCR No. 7**	**Seq. primer PCR No. 8**
D 12924 F	D 16059 F	D 19250 F	E 22225 F
D 13700 F	D 16779 F	D 19984 F	E 22900 F
D 14510 F	D 17532 F	D 20738 F	
D 15264 F	D 18034 F	E 21452 F	
	D 18656 F		
Seq. primer PCR No. 9	**Seq. primer PCR No. 10**	**Seq. primer PCR No. 11**	
E 23658 F	F 24905 F	F 27659 F	
F 24252 F	F 25462 F	F 28462 F	
	F 26176 F	F 29149 F	
	F 26918 F		

2.1.12 Plasmids

Name	Source
pCAGGS-MCS	Prof. Dr. Stephan Becker, University of Marburg
pEZ BAC	Lucigen Corporation, Middleton, USA
pBeloBAC11	New England Biolabs GmbH, Frankfurt am Main

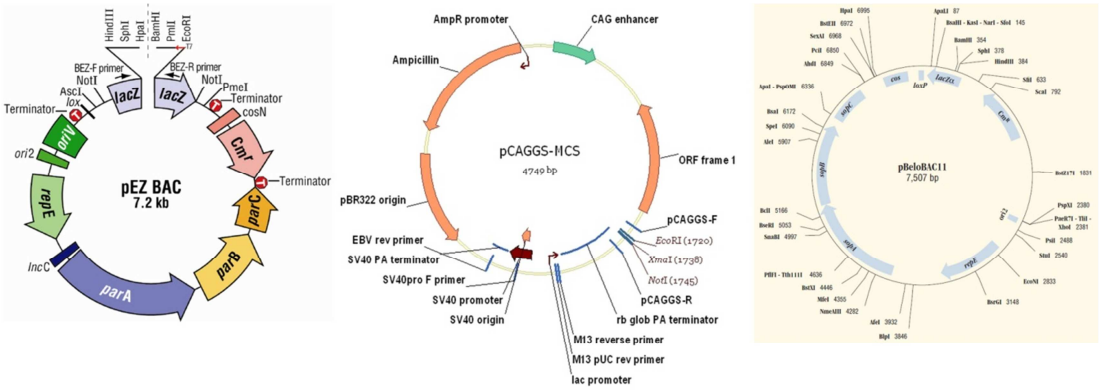

Figure 2.2: Vector maps.
PEZ BAC was used for blunt end cloning of PCR products. PBeloBAC11 was used for cloning of the SARS-CoV cDNA clone. PCAGGS-MCS was used for eukaryotic gene expression.

2.1.13 Kits

Name	Source
Agencourt® AMPure®	Beckman Coulter GmbH, Krefeld
GeneJET™ Plasmid Miniprep Kit	FERMENTAS GmbH, St. Leon-Roth
mMESSAGE mMACHINE® Kit	Ambion/Applied Biosystems, Darmstadt
MEGAscript® Kit	Ambion/Applied Biosystems, Darmstadt
NucleoBond® Xtra Midi	Macherey-Nagel, Düren
Phusion™ Site-Directed Mutagenesis Kit	Thermo Fisher Scientific (Finnzymes), St. Leon-Roth
QIAamp DNA Blood Mini Kit	QIAGEN, Hilden
QIAamp® Viral RNA Mini Kit	QIAGEN, Hilden
QIAEXX II® Gel Extraction Kit	QIAGEN, Hilden
Renilla Luciferase Assay System	Promega, Mannheim
RNeasy® Mini Kit	QIAGEN, Hilden
SuperScript™ III One-Step RT-PCR System with Platinum® *Taq* DNA Polymerase	Life Technologies, Darmstadt

2.1.14 Antibodies

Primary antibodies

Name	Target (antigen)	Species	Dilution (Application)	Source
β-actin	β-actin	mouse	1:2000 (WB)	Sigma-Aldrich, Munich
anti-FLAG	FLAG-tag epitope	mouse/ rabbit	1:5000 (WB), 1:100 (IF)	Sigma-Aldrich, Munich
anti-Golgi 58K	Golgi protein 58K/ cytoplasmic part	mouse	1:100 (IF)	Sigma-Aldrich, Munich
anti-HA	HA-tag epitope	mouse/ rabbit	1:5000 (WB), 1:100 (IF)	Sigma-Aldrich, Munich
Delseith serum	SARS-CoV	human	1:100 (IF)	BNI

Legend: Western blot (WB), Immunofluorescence assay (IF), Bernhard Nocht-Institute (BNI)

Secondary antibodies

Name	Label	Species	Dilution (Application)	Source
anti-human	Cy2	goat	1:200 (IF)	Dianova, Hamburg
anti-mouse	Cy3	goat	1:200 (IF)	Dianova, Hamburg
anti-mouse	HRP	goat	1:20,000 (WB)	Dianova, Hamburg
anti-rabbit	Cy2	goat	1:200 (IF)	Dianova, Hamburg
anti-rabbit	HRP	goat	1:20,000 (WB)	Millipore GmbH, Schwalbach

Legend: Immunofluorescence assay (IF), horseradish peroxidas (HRP), Western blot (WB)

2.1.15 Software

Name
AxioVision Rel. 4.8
BioEdit Sequence Alignment Editor version 7.0.9.0
DNASTAR Lasergene 7 (EditSeq, SeqMan)
SigmaPlot 11.0
Vector NTI 10.3.0

2.2 Methods

2.2.1 Cell culture and virus propagation

2.2.1.1 General cell culture methods

All cells were maintained in DMEM with high glucose (4.5 g/L) supplemented with 5% Penicillin/Streptomycin, 5% non-essential amino acids, 5% sodium pyruvate, 5% L-glutamine and 10% FBS in an incubator with a 5% CO_2 environment at 37°C. Passaging was done dependent on cell growth. Confluent cells were washed once with PBS and treated with Trypsin (or Accutase™ in case of RhiLu-hACE2 cells) at 37°C until detachment was completed. Cells were then suspended in supplemented DMEM and seeded in a new cell culture flask at a dilution according to their growth between 1:3 and 1:10. Cell culture flasks were filled with supplemented DMEM according to their sizes (T25 = 6 mL, T75 = 12 mL, T175 = 25 mL)

For cryopreservation cells were detached as described above and counted. Cell amount was adjusted to 5x 10^6 cells/cryo tube, the cell suspension was centrifuged at 300x g for 3 min. The cleared supernatant was discarded, the cell pellet was resuspended in 1 mL CryoMaxx/cryo tube and cells were aliquoted. In order to freeze cells controlled at 1°C/min cryo tubes were placed in an insulated box filled with isopropanol and placed in a -70°C freezer. After 16 h cells were transferred to liquid nitrogen.

2.2.1.2 Transfection of eukaryotic cells

Eukaryotic cells were transfected using Roches FuGENE® HD or X-tremeGENE Transfection Reagent for analysis of protein expression in Western blot analysis or Immunofluorescence assays.

Cells were seeded according to their size and speed of growth between 1x 10^5 and 3x 10^5 cells/mL, seeding 500 µL/24well or 2 mL/6well. Confluency between 70-80% is desired for optimal transfection efficiency with FuGENE® HD or X-tremeGENE. After cultivation over night in an incubator, medium was exchanged by fresh supplemented DMEM, 400 µL/24well or 1.5 mL/6well and the transfection complex was set up. The amount of plasmid DNA and the ratio of transfection reagent to DNA used varied in accordance to the cell lines transfection efficiency and downstream application. The transfection complex was prepared according to manufacturer's instructions. Briefly, plasmid DNA was diluted in OptiPRO™ serum-free medium

in a 1.5 mL reaction tube, 100 µL/24well or 500 µL/6well. FuGENE® HD was pipetted into the diluted plasmid DNA without getting in contact with the plastic wall of the reaction tube. The transfection complex was then vortexed, briefly centrifuged and incubated at room temperature for 15 min. Thereafter, the transfection complex was pipetted drop-wise into the fresh supplemented DMEM. Cells were further incubated for 24h and subsequently used for Western blot analysis or Immunofluorescence assay.

2.2.1.3 Generation of recombinant virus

The generation of recombinant SARS-CoV and all cell culture works with them were carried out under biosafety level 4 conditions.

For generation of recombinant viruses 7-methyl guanosine capped, poly-A-tailed *in vitro* transcribed SARS-CoV genomic full-length RNA was used (2.2.2.11). In order to improve translation efficiency of viral proteins [96] capped nucleocapsid transcript was co-electroporated.

BHK-J and Vero FM cells were grown to confluency and detached as described above. Resuspended cells were counted in a Neubauer improved counting chamber. 4x 10^6 BHK-J cells were needed for one electroporation reaction. The amount of cells was adjusted according to the number of electroporations, cells were centrifuged at 300x g for 3 min at 4°C and washed twice in 20 mL ice cold PBS. Cells were then resuspended in 1 mL OptiMEM™ and centrifuged again as described above. OptiMEM™ was discarded qualitatively and the BHK-J cells were resuspended in 100 µL OptiMEM per electroporation reaction. Cells were kept on ice until further use.

2 mm electroporation cuvettes and 1.5 mL reaction tubes were placed on ice for cooling. RNA *in vitro* transcripts were thawed on ice. Per electroporation reaction 10 µg of SARS-CoV genomic full-length RNA and 2 µg of nucleocapsid transcript were pipetted into one pre-cooled 1.5 mL reaction tube. 100 µL cell suspension was mixed with the *in vitro* transcripts by carefully pipetting up and down twice, and then the RNA-cell-suspension was transferred to a pre-cooled electroporation cuvette and placed on ice until electroporation. The cuvette containing the RNA-cell-suspension was placed in the shock pod of the Gene Pulser Xcell™ and one pulse was applied (pre-set protocol for BHK-J cells; 25 msec, 140 V, exponential decay). The cells were left at room temperature for 10 min. Thereafter, the cells were resuspended in 12 mL supplemented DMEM, seeded in a T75 cell culture flask and transferred to the incubator.

5-6x 10^6 VeroFM cells were seeded in a T175 cell culture flask in 20 mL supplemented DMEM and cultured overnight in an incubator for virus recovery.

After 24h electroporated BHK-J cells were scraped off and cells and recombinant virus containing cell culture supernatant were decanted into a 50 mL centrifuge tube and spun at 300x g for 3 min. 2.5 mL of the cleared supernatant was transferred to the T175 cell culture flask containing VeroFM cells, the remaining supernatant and cells were stored at -70°C if retry was necessary. The infected cell culture flask was transferred to an incubator for virus growth for 3-4 days. At day 0, 2, 3 and if necessary 4, 140 µL supernatant were sampled for isolation of viral RNA (2.2.2.1) to monitor virus replication in real-time RT-PCR (2.2.3.3). When virus growth could be confirmed the virus containing supernatant was decanted into a 50 mL centrifuge tube, cleared from cell debris at 300x g for 3 min and aliquoted á 500 µL in cryo tubes. Recombinant virus was stored at -70°C. Plaque assays were done for determining the amount of infectious particles in plaque forming units per mL (2.2.1.6).

When virus growth was not sufficient after 3 days, the cell culture was incubated for another day before harvesting the supernatant.

2.2.1.4 Production of virus stock

5-6x 10^5 VeroFM cells were seeded in a T175 cell culture flask in 25 mL supplemented DMEM and cultivated overnight in an incubator. Cells were infected at a multiplicity of infection (MOI) of 0.0001 (50-60 PFU per flask) for 1 h at 37°C in a total volume of 10 mL. Thereafter, the cell culture flask was filled up with 10 mL fresh supplemented DMEM and the infected cell culture was further incubated for 3 days. 140 µL cell culture supernatant were sampled at day 0 and 3 for isolation of viral RNA (2.2.2.1) and verification of virus growth in real-time RT-PCR (2.2.3.3). 3 days after infection the virus containing supernatant was harvested and centrifuged at 300x g for 3 min. The cleared supernatant was aliquoted á 500 µL in cryo tubes, virus stocks were stored at -70°C. After confirmation of virus growth in real-time RT-PCR the amount of infectious particles was determined by plaque titration (2.2.1.6).

2.2.1.5 Virus infection

For virus infection studies cells were detached and counted in a Neubauer improved counting chamber as described above. The cell concentration was adjusted to 4x 10^5 cells/mL. Cells were

seeded in 24- or 6-well plates á 500 µL or 2 mL, respectively and cultivated overnight in an incubator.

Virus stocks were diluted in OptiPRO™ according to the desired MOI prior to infection (e.g. 800 PFU/mL for an MOI of 0.001).

Cell culture supernatant was removed from the cells and 250 µL or 1 mL virus master mix were pipetted to one 24-well or 6-well, respectively. After 1 h virus adsorption in an incubator the virus master mix was removed, cells were washed once with PBS and wells were refilled with supplemented DMEM (250 µL/24-well, 2 mL/6-well). Cell culture plates were placed back in an incubator for cultivation.

2.2.1.6 Plaque titration assay

The amount of infectious particles in plaque forming units per mL (PFU/mL) was determined with the help of a plaque titration assay. This method is based on the assumption that one virus particle upon infection of a single cell only spreads horizontally to neighboring cells when overlayed with high viscous medium. So one infectious particle creates a hole in a confluent cell monolayer (plaque) and the amount of PFU in a given volume can be calculated. In case of SARS-CoV the optimal high viscous overlay proved to be a 1:2 dilution of 2.4% Avicel in 2xDMEM.

500 µL VeroE6 cells were seeded per 24-well at a concentration of 3x 10^5 cells/mL 16-24h prior to titration.

The virus containing samples were serially diluted 1:10 (60 µL sample in 540 µL supplemented DMEM). Each dilution step was titrated in duplicates. After removal of the cell culture supernatant from the VeroE6 plates, 200 µL of diluted sample were pipetted into one 24-well, the plate was placed back into an incubator for 1 h for virus adsorption. Next, the diluted virus samples were removed and the cells overlayed with 500 µL Avicel-2xDMEM per 24-well. After 3 days of incubation the overlay was removed and cells were fixated for at least 20 min in 6% Formaldehyde. Cells were washed once with 1x PBS and stained with 500 µL crystal violet working solution for 15 min. Following removal of crystal violet the stained cell layer was washed with water and left for drying until analysis. All dilutions with distinct plaques were counted and PFU/mL calculated according to the following equation:

$$Titer[PFU/mL] = \frac{(\Sigma\ plaques\ x\ lowest\ countable\ dilution)}{(\Sigma\ applied\ volume)}$$

2.2.1.7 Lentiviral Transduction

Lentiviral transduction is a highly efficient method for the transfer of genes into a broad variety of cell lines [102]. The major characteristic of lentiviruses is their ability to integrate their genetic information into the genome of an infected cell. This way, foreign genes can be permanently transferred into host cells.

The method of lentiviral transduction utilizes the ability of Vesicular stomatitis virus glycoprotein (VSV-G) pseudotyped lentiviruses to infect most mammalian cell cultures and to integrate a transgene (here *hACE2* or viral genes and a puromycin selection marker) into the genome of the infected cell [100]. The G protein thereby mediates receptor-independent virus entry. For safety reasons the structural proteins of the lentiviruses are provided in trans to produce single-cycle infectious particles. Therefore a packaging cell line is transfected with three different plasmids encoding proteins for assembly of the lentiviruses, which are subsequently released into the cell culture supernatant. The packaging plasmid encodes the lentiviral polymerase and the group-specific antigens but lacks the envelope protein. This is substituted by VSV-G located on a second plasmid. The third plasmid carries the gene of interest. Upon cellular entry of the lentiviral vector the viral RNA genome is reverse transcribed and the produced cDNA is integrated into the cell genome. Integration occurs randomly and can lead to the disruption of cellular genes.

All used lentiviruses were kindly provided by Alexander Pfeifer (Institute of Pharmacology and Toxicology, University of Bonn).

Generation of a bat cell line stably expressing human ACE2

In order to establish reservoir-related cell culture models for SARS-CoV infection studies, a new bat cell line from the reservoir host had to be generated. All *Rhinolophus* bats are environmentally protected. Since our working group had an exemption license for bat catching in Ghana, the endemic species *Rhinolophus landeri* was caught.

The generation of a SARS-CoV susceptible bat cell line stably expressing human ACE2 was done in the course of the bachelor thesis of Hanna Roth [103]. Briefly, immortalized RhiLu cells were seeded at a concentration of 2x 10^5 cells/mL in a 6-well and cultivated overnight. Cells were then infected with lentiviruses carrying the sequence information of hACE2 at an MOI of 0.0005 (determination of the biological titer is described in the reference). Infection was done in 800 µL supplemented DMEM containing 12 mg/mL polybrene, for better attachment of viruses to the cellular membrane. 24h p.i. 1.2 mL fresh supplemented DMEM was added to the 6-well and cells were further incubated. 48h p.i. virus containing medium was removed, cells were washed twice with PBS and 2 mL selection medium (supplemented DMEM containing 4 µg/mL puromycin) were added to the well. The use of selection medium leads to the die off of cells which did not successfully integrate hACE2 and the attached puromycin resistance gene into their genome. The selection medium was changed every 3 days while the puromycin concentration was gradually increased to 6 µg/mL in order to increase the selection pressure. 10 days p.i. cells were detached with Accutase™, seeded in a fresh 6-well and further incubated in selection medium. When the cells reached confluency, they were expanded into a T25 culture flask. The so generated mixed culture of RhiLu cells stably expressing hACE2 was propagated by using selection medium containing only 4 µg/mL puromycin only after every second passage.

Transduction of primate and bat cells for transient expression of a transgene

Lentiviral transduction can also be used for the temporary expression of a foreign gene for example in the context of a tans-complementation experiment. Here cells are not selected for successful genome integration. Therefore, within the produced cell culture not all cells express the transduced gene. This method is generally used for short termed experiments, since expression levels of the transduced gene gradually ceases. In this work lentiviral transduction was used for the transient expression of the proteins encoded by SARS-CoVs ORF8.

VeroFM and MA104 cells were seeded at a concentration of 1x 10^5 /mL, RhiLu-hACE2 cells at a concentration of 3x 10^5 /mL in 24-well plates and cultivated overnight. Cells were infected with a physiological titer of 50 ng reverse-transcriptase activity per 24-well in supplemented DMEM and cultivated for 48h, when protein expression generally reaches its maximum.

2.2.2 Molecular biological methods

2.2.2.1 Isolation of viral RNA

Viral RNA from cell culture supernatant was extracted with QIAGENs QIAamp® Viral RNA kit according to manufacturer's instructions. Briefly, 70 µL or 140 µL virus containing cell culture supernatant were added to 560 µL AVL containing carrier RNA, puls-vortexed and incubated for 10 min at room temperature. Samples were stored at -20°C or immediately processed. 560 µL ethanol were added to the samples and puls-vortexed again for 15 sec. Samples were then applied to a QIAamp Mini column and RNA bound to the columns membrane by brief centrifugation. Bound RNA was washed with Buffer AW1 and AW2. To eliminate all residual buffer, the column was spun at full speed for 3 min. RNA was eluted in 60 µL AVE pre-heated to 80°C. The eluate was stored at -20°C.

2.2.2.2 cDNA synthesis

Transcription of RNA into cDNA was done with Invitrogens SuperScript™ III Reverse Transcriptase according to manufacturer's instructions, generally using specific reverse primers. Master mix I and II were prepared according to the following reaction set up:

Master mix I for cDNA synthesis

dNTPs (10 mM each)	0.5 µL
Reverse primer (10 µM)	0.5 µL
RNase-free water	2.0 µL
BSA (Roche, 1 mg/mL)	0.5 µL
Template RNA	2.5 µL
Total	**6.0 µL**

Master mix II for cDNA synthesis

5x First-Strand Buffer	2.0 µL
DTT (0.1 M)	0.5 µL
SuperScript™ III Reverse Transcriptase	1.0 µL
RNaseOUT™	0.5 µL
Total	**4.0 µL**

Reverse Transcription was done according to the following temperature profile:

Temperature profile for cDNA synthesis

Denaturation	65°C	5 min	Master mix I
Primer annealing	4°C	1 min	
cDNA synthesis	55°C	60 min	After 1 min add master mix II
Inactivation	70°C	5 min	
Storage	4°C	∞	Add 0.5 µL RNaseH
Elimination of template RNA	37°C	15 min	
Storage	4°C	∞	

CDNAs were stored at -20°C until used in downstream applications.

2.2.2.3 Isolation of genomic DNA

Cellular genomic DNA was extracted using QIAGENs QIAamp® DNA Blood Mini Kit according to manufacturer's instructions. Briefly, cells were washed once with PBS and detached using trypsin or Accutase™. Detached cells were resuspended in PBS and pelleted for 3 min at 1000x g. Supernatant was removed and cells resuspended again in 200 µL PBS. 20 µL protease and 200 µL Buffer AL were added. The sample was incubated at 56°C for 10 min for cell lysis and protein degradation. 200 µL ethanol were added to the sample and the mixture was applied to a QIAamp Mini spin column. DNA was bound to the membrane by centrifugation at 6000x g

for 1 min. Bound DNA was washed with Buffer AW1 and AW2, the membrane was dried by centrifugation at 16,100x g for 3 min. DNA was eluted in 100 µL Buffer AE pre-heated to 80°C. Extracted DNA was stored at -20°C.

2.2.2.4 Isolation of plasmid DNA

Plasmid DNA was isolated in small scale with Fermentas' GeneJET™ Plasmid Miniprep Kit or in medium scale with MACHEREY-NAGELs NucleoBond® Xtra Midi kit according to the manufacturer's instructions.

For small scale plasmid preparations overnight cultures of a quarter petri dish plate of bacteria carrying low copy plasmids or ⅛ of a petri dish plate of bacteria carrying high copy plasmids were used. The culture was scraped and resuspended by vigorous vortexing in 250 µL Resuspension Solution. 250 µL of Lysis Solution were added for cell lysis. After addition of 350 µL Neutralization Solution cell debris were pelleted at 11,000x g for 5 min and the supernatant was transferred to a GeneJET™ spin column by decanting. Plasmid DNA was bound to the filter membrane by centrifugation. The column washed twice with 500 µL Wash Solution. In order to eliminate residual buffer the column was spun dry at full speed for 2 min. Plasmid DNA was eluted in 50 µL Elution Buffer. For elution of low copy plasmids the membrane was incubated twice with 25 µL 37°C pre-warmed Elution Buffer. Plasmid DNA containing eluate was stored at -20°C. Integrity of the plasmids was verified by agarose gel electrophoresis (2.2.2.8) of 20 µL low copy plasmid or 5 µL high copy plasmid.

For medium scale plasmid preparations 5-10 petri dishes of an overnight culture were used. The bacteria were scraped off and resuspended in 8-16 mL Buffer RES by vortexing in a 50 mL centrifuge tube. The bacteria were lysed with 8-16 mL Buffer LYS for 5 min at room temperature. Meanwhile, the NucleoBond® Xtra column and column filter were equilibrated with Buffer EQU. 8-16 mL Buffer NEU were added to the lysed bacteria and the bacteria suspension was applied to the NucleoBond® Xtra column filter. Following loading of the whole bacteria suspension the column filter was washed with Buffer EQU and afterwards discarded. Next, the column was washed with Buffer WASH. After washing the plasmid DNA was eluted from the column with 5 mL Buffer ELU and precipitated out of the eluate by addition of 3.5 mL 100% isopropanol and centrifugation at 15,000x g and 4°C for 30min. The plasmid DNA pellet was

washed once with 70% ethanol, centrifuged again at 15,000x g and room temperature for 5 min and air dried. The pellet was resuspended in an appropriate amount of Ampuwa® (100-200 µL). Plasmid DNA was stored at -20°C.

2.2.2.5 Purification of PCR products

PCR products were routinely purified with Beckman Coulters Agencourt® AMPure® XP in order to remove excess primers, dNTPs, salts and enzymes.

The procedure was done according to the manufacturer's instructions. Briefly, Agencourt® AMPure® XP was resuspended by vortexing and 1.8x the volume of the PCR reaction was mixed with the PCR product by pipetting. The mixed sample was incubated at room temperature for 10 min, then the sample containing PCR tube was placed on an Agencourt SPRIPlate 96 Super Magnet Plate for 10 min. The magnetic beads carrying the bound PCR products separate from the solution. The cleared solution was discarded and the beads washed twice with 70% ethanol. All residual ethanol was removed and the beads were left at room temperature for complete drying. The dried magnetic beads were resuspended in an appropriate volume of Ampuwa® and PCR products were eluted by repeated pipetting.. Magnetic beads were either left in the suspension and the purified PCR product was stored at 4°C or the PCR tube was placed on the magnetic plate to separate beads from PCR products, cleared PCR product was transferred to a fresh tube and stored at 4°C for short term or at -20°C for long term.

2.2.2.6 Gel extraction of DNA fragments

In order to eliminate undesired DNA fragments after digestion of plasmid DNA or unspecific PCR products, restriction or PCR reactions were separated on an Roti®garose Broad Range gel, DNA fragments or PCR products of interest were cut out of the gel with a scalpel and purified using QIAGENs QIAEX II® Gel Extraction Kit according to manufacturer's instructions.

Briefly, excised gel slices were put in a 1.5 mL reaction tube and weighed. Depending on the size of the fragments 3 volumes of Buffer QX1 or 3 volumes of Buffer QX1 and 2 volumes of Ampuwa® for fragments of 100 bp – 4 kb or > 4 kb respectively were added to the tube (100 mg gel = 100 µL). QIAEX II® silica particles were resuspended by vortexing for 30 sec and 15 µL were added to the gel containing buffer. Agarose was solubilized and DNA bound to QIAEX II® silica particles by incubation for 10 min at 50°C on a thermo shaker rotating at 1400 rpm.

Thereafter, samples were centrifuged and the supernatant was removed carefully. The pellet was washed once with Buffer QX1 and twice with Buffer PE. Resuspension of the pellets was done by inverting and flicking the tube in order to minimize shear forces on large DNA fragments. After washing, the pellet was air-dried until it became white. DNA fragments were eluted in 20 µL Ampuwa® by incubation for 5 min at room temperature, 5 min at 50°C, or 10 min at 50°C according to fragment sizes of ≤ 4 kb, 4 – 10 kb, or ≥ 10 kb, respectively. After incubation the samples were centrifuged and the supernatant was transferred to a clean 1.5 mL reaction tube. DNA fragments were ideally used immediately for downstream applications or stored at -20°C.

2.2.2.7 Phenol-chloroform extraction and alcohol precipitation of nucleic acids

Since *in vitro* transcriptions require very clean templates for optimal yields, linearized SARS-CoV full-length plasmids were purified by phenol-chloroform extraction. *In vitro* transcribed RNAs used in cell culture for electroporation were also phenol-chloroform extracted for optimal purity.
Briefly, 1 volume of phenol-chloroform was added to one reaction, mixed by inversion and phases were separated by centrifugation for 5 min at 4°C and 11,000x g. The upper nucleic acid containing aqueous phase was transferred to a clean 1.5 mL reaction tube and 1 volume of chloroform was added. Phase separation was done by centrifugation for 5 min at 4°C and 11,000x g. The upper nucleic acid containing phase was again transferred into a fresh 1.5 mL reaction tube and the nucleic acids were precipitated by ethanol precipitation.

Alcohol precipitation is a standard method for eliminating proteins, salts and small nucleotides such as enzymes, buffers, or primers from nucleic acids in restriction or PCR reactions and can be done with ethanol or isopropanol.
Ethanol precipitation was done by adding 0.1 volume of 3 M sodium acetate (pH 6.6) and 2.5 volumes of 99.9% ethanol to the reaction and centrifugation at 4°C and 11,000x g for 30 min. The pellet was washed once or twice with 70% ethanol, centrifuged at room temperature and 11,000x g for 5 min, air dried and resuspended in an appropriate volume of Ampuwa®.
Isopropanol precipitation was done by adding 0.7 volume of 99.9% isopropanol to the reaction and centrifugation at 4°C and 11,000x g for 30 min. The pellet was washed once or twice with 70% ethanol, centrifuged at room temperature and 11,000x g for 5 min, air dried and resuspended in an appropriate volume of Ampuwa®.

When precipitating RNAs all steps were carried out at 4°C, DEPC treated water was used for diluting ethanol and pellets were resuspended in RNase-free water.

2.2.2.8 Agarose gel electrophoresis of DNA

Electrophoretic analysis of DNAs on agarose gels was done to verify successful restriction or PCR amplification and to separate DNA fragments within a reaction for subsequent extraction. The percentage of agarose in the gel varied between 0.8 and 2% for very large and very small DNA fragments, respectively. Roti®garose GTQ was used for standard gel electrophoresis, Roti®garose Broad Range for preparative gels. In addition, 50x TAE was sterile filtrated for preparative gels.

The appropriate amount of agarose was weighed and dissolved in 1x TAE buffer by heating in a microwave oven. After complete dissolving the agarose was cooled down without letting it solidify again and 1.5 µL of 1% ethidium bromide were added per 50 mL agarose. The agarose was poured under a fume hood into the gel tray and left for solidification.

An appropriate amount of DNA (200-300 ng plasmid DNA, 5 µL PCR product) was mixed with 6x loading dye and applied to one lane. 500 ng per lane of a suitable DNA marker were used to determine the size of DNA fragments.

Separation of DNA fragments was done applying 80-120 V, depending on the size of the electrophoresis chamber.

Preparative gels were not stained with ethidium bromide but incubated after electrophoresis with Lonzas GelStar® Nucleic Acid Gel Stain (diluted 1:1000 in 1x TAE).

2.2.2.9 Photometric determination of nucleic acid concentration

Nucleic acid concentrations were determined using PeqLabs NanoDrop 2000c. The instrument was blanked with the liquid the nucleic acid was dissolved in, usually Ampuwa® or AVE. Then 1 µL of nucleic acid sample was applied and measured 3 times. The mean value was calculated and accepted as the concentration.

2.2.2.10 Sequencing of DNA

Agencourt® AMPure® XP purified PCR products (2.2.2.5) or plasmid minipreparations (2.2.2.4) were sent to SeqLab Sequence Laboratories Göttingen for sequencing.

Sequence reaction set up

Sequencing primer (10 mM)	1.0 µL
DNA	400 ng
Ampuwa®	add to 7.0 µL

Sequence data was viewed with BioEdit 7.0.9.0 and sequence alignments were generated with DNASTER Lasergene 7.

2.2.2.11 Generation of capped RNA transcripts

In vitro transcription of capped full-length SARS-CoV genomic RNAs was done with Ambions mMESSAGE mMACHINE® Kit according to manufacturer's instructions with minor changes for the transcription of long templates.

In front of the SARS-CoV genome the minimum T7 promoter sequence needed for transcription was added. A NotI restriction site, directly following the poly-A-tail, was used for linearization of the plasmid containing the full-length SARS-CoV genome.

6 µg of full-length SARS-CoV plasmid were linearized with 5 µL Fermentas FastDigest® NotI for at least 30 min in a total volume of 200 µL (2.2.2.13). Completeness of linearization was checked by agarose gel electrophoresis (2.2.2.8). Linearized plasmid was purified by phenol-chloroform extraction (2.2.2.7). The plasmid was resuspended in 20 µL RNase-free water; the plasmid concentration was determined (2.2.2.9) and adjusted to 1 µg/5 µL. The *in vitro* transcription reaction was pipetted on ice according to the following set up:

Reaction set up for in vitro transcription of SARS-CoV genomic RNA

2x NTP/CAP	15 µL
10x Reaction Buffer	3 µL
GTP	4 µL
Enzyme Mix	3 µL
Linearized plasmid (1 µg)	5 µL
Total	**30 µL**

The reaction was placed in a thermo mixer and incubated at 37°C for 3 h. After 3 h 1 µL of TURBO DNase was added to the reaction and residual DNA template was degraded at 37°C for 15 min. Thereafter, 15 µL Ammonium Acetate Stop Solution and 105 µL nuclease-free water were added to the reaction and the *in vitro* transcript was phenol-chloroform extracted (2.2.2.7). Isopropanol precipitation was started only after incubation of RNA with isopropanol at -20°C overnight. The RNA pellet was resuspended in 20 µL nuclease-free water, concentration was determined and adjusted to 5 µg/µL. *In vitro* transcripts were stored at -70°C.

For generation of capped nucleocapsid RNA the template for *in vitro* transcription was generated by PCR using the primer Ngenefwd, which contains the minimum SP6 promoter sequence and Frev with Phusion™ polymerase (2.2.3.1). The PCR product was purified with Agencourt® AMPure® XP (2.2.2.5) and adjusted to a concentration of 1 µg/7 µL.

The *in vitro* transcription reaction was pipetted on ice according to the following set up:

Reaction set up for in vitro transcription of capped nucleocapsid RNA

2x NTP/CAP	15 µL
10x Reaction Buffer	3 µL
GTP	2 µL
Enzyme Mix	3 µL
PCR product (1 µg)	7 µL
Total	**30 µL**

The reaction was placed in a thermo mixer and incubated at 37°C for 2 h.
Degradation of DNA template and purification of RNA by phenol-chloroform extraction were done as described for full-length SARS-CoV genomic RNA. Concentration of nucleocapsid transcript was determined and adjusted to 2 µg/µL. Nucleocapsid RNA was stored at -70°C.

2.2.2.12 Generation of an RNA standard for quantification of SARS-CoV genomic RNA

The real-time RT-PCR for detection of SARS-CoV genomic RNA amplifies a region within nsp14. In order to absolutely quantify SARS-CoV RNA in cell culture supernatants an RNA standard was generated. A PCR product was amplified using primers T7-SAR-S1, carrying the minimal T7 promoter sequence and E 19031 R. These primers generate an 865 bp amplicon much longer than that generated during real-time PCR, guaranteeing optimal annealing of the real-time primers. The PCR product was purified with Agencourt® AMPure® XP (2.2.2.5) and adjusted to a concentration of 1 µg/8 µL. Uncapped *in vitro* transcript was generated with Ambions MEGAscript® Kit.

The *in vitro* transcription reaction was pipetted on ice according to the following set up:

Reaction set up for uncapped in vitro transcripts

ATP	2 µL
CTP	2 µL
GTP	2 µL
UTP	2 µL
Enzyme Mix	2 µL
10x Reaction Buffer	2 µL
PCR product (1 µg)	8 µL
Total	**20 µL**

The reaction was placed in a thermo mixer and incubated at 37°C for 4 h. After 4 h 1 µL of TURBO DNase was added to the reaction and residual DNA template was degraded at 37°C for 15 min. The *in vitro* transcript was purified using QIAGENs RNeasy® Mini Kit protocol for RNA clean up. Briefly, the *in vitro* transcription reaction was filled up with 80 µL RNase-free water and 350 µL RLT Buffer containing 1% β-mercaptoethanol were added and mixed vigorously. 250 µL 100% ethanol were added and mixed vigorously again. The sample was loaded on an RNeasy® spin column and centrifuged for 15 sec at 8000x g. The flow through was discarded and the column washed twice with 500 µL Buffer RPE. The column was dried by centrifugation at full speed for 1 min. RNA was eluted in 30 µL RNase-free water for 1 min at 8000x g. In order to increase RNA yield, the eluate was used to elute the column again. Afterwards the RNA concentration was determined (2.2.2.9) and RNA copies/µL were calculated using the following equation:

$$\frac{copies}{\mu L} = \frac{(N * c)}{M}$$

N = 6.022x 10^{23}/µL

c = RNA concentration in ng/µL

M = molecular weight of RNA transcript in g/mol

The *in vitro* transcript was immediately diluted 1:10 in AVE buffer (QIAamp® Viral RNA Mini Kit) containing sodium azide as a preservative. Subsequent dilutions were done in nuclease free water containing 10 µg/mL carrier RNA for stabilization of the *in vitro* transcript. The stock and all dilutions were stored at -20°C.

Successful *in vitro* transcription was verified by real-time RT-PCR (2.2.3.3) of a dilution series ranging from 10^8 to 10^3 RNA copies per reaction.

2.2.2.13 Restriction endonuclease digestion and dephosphorylation of DNA

Plasmids and PCR products were digested with New England BioLabs® restriction endonucleases or Fermentas FastDigest® restriction endonucleases according to manufacturer's instructions. Briefly, 6-10 µg of plasmid DNA or PCR product were digested in a total volume of 100-200 µL with up to 50 u of restriction enzyme for 4-8h at optimal temperature for the corresponding enzyme. Successful digestion was verified by agarose gel electrophoresis of 200-300 ng DNA (2.2.2.8). A high amount of template was used in order to compensate loss during ethanol precipitation (2.2.2.7) and gel purification (2.2.2.6). An excess of restriction enzymes and prolonged incubation times were used to assure completeness of restriction. Frequently, templates were digested with two enzymes needing different reaction conditions, which made it necessary to ethanol precipitate the template after the first digestion.

When complete digestion was achieved, the template containing most part of the vector backbone (and/or the resistance gene) was dephosphorylated to avoid religation and creating false positive clones. Dephosphorylation was done with 5 µL Antarctic Phosphatase and 10% Antarctic Phosphatase Buffer in the restriction reaction without prior ethanol precipitation for 15 min at 37°C.

Digested fragments were usually ethanol precipitated prior to immediate downstream applications like separation on preparative agarose gel and subsequent ligation. If storage was necessary, fragments were stored under ethanol and ammonium acetate at -20°C.

2.2.2.14 Ligation of nucleic acid fragments

Ligation of digested DNA fragments was usually done using Roches T4 DNA Ligase according to the following reaction set up:

Ligation reaction set up for T4 ligase

10x Ligation Buffer	1.0 µL
T4 DNA Ligase (5 U/µL)	1.5 µL (1:10 diluted)
Template DNA	7.5 µL
Total	**10.0 µL**

Prior to ligation DNA fragments from restriction reactions were separated on a preparative broad range agarose gel (2.2.2.8). Wanted DNA fragments were excised from the gel using a scalpel and extracted (2.2.2.6). The extracted fragments were quantified (2.2.2.9) and their molecular mass was determined. Ligation of large DNA fragments in the process of assembly the SARS-CoV full-length clone was usually done using equal molecule amounts of each fragment. Small DNA fragments of only several hundred base pairs were applied in a 5-fold excess to vector molecules in the ligation reaction. The molecule concentration was determined using the following equation:

$$\frac{molecules}{\mu L} = \frac{(N * c)}{M}$$

N = 6.022x 10^{23}/µL

c = RNA concentration in ng/µL

M = molecular weight of DNA fragment in g/mol

Ligation reactions were incubated overnight at 14°C and stored at 4°C for short term or at -20°C for long term.

2.2.3 Polymerase chain reaction

Polymerase chain reaction (PCR) is generally used for exponential amplification of DNA fragments using a DNA polymerase and specific forward and reverse primers, which ultimately determine the range of the DNA fragment.

2.2.3.1 Phusion® PCR

DNA amplification for subsequent use in restriction reactions or sequencing was done with Phusion® High-Fidelity DNA Polymerase with the following PCR reaction set up:

Reaction set up for Phusion® PCR

5x Phusion® HF-buffer	5.0 µL
dNTPs (10 mM each)	0.5 µL
Forward primer (10 µM)	0.5 µL
Reverse primer (10 µM)	0.5 µL
Phusion® DNA polymerase	0.25 µL
Template DNA (10-50 ng)	1.0 µL
Ampuwa®	17.25 µL
Total	**25.0 µL**

Cycling was done according to the following temperature profile in an Eppendorf Mastercycler:

Temperature profile for Phusion® PCR

Initial Denaturation	98°C	20 sec	
Denaturation	98°C	10 sec	35x
Annealing	X°C*	20 sec	
Extension	72°C	15 sec/kb	
Storage	4°C	∞	

* primer melting temperature salt adjusted

(Oligo Calc, http://www.basic.northwestern.edu)

2.2.3.1.1 Overlap extension-PCR

Overlap extension-PCRs were used to generate DNA fragments for insertion of mutations of several base pairs in length or the exchange of whole ORFs within SARS-CoV subclones. Phusion® High-Fidelity DNA Polymerase was generally used because of its extremely low error rate and high processivity.
Extensions were done in a 2-step or 3-step approach.

The 2-step approach was used for small insertions. Two partially overlapping PCR products are generated, where the overlapping regions contain the insertion and are introduced via appropriate primers (Fig. 2.3). After ensuring successful amplification by agarose gel electrophoresis (2.2.2.8), the PCR products are purified with Agencourt® AMPure® XP (2.2.2.5) and the actual extension-PCR is done. As primers both outmost primers (F1 and R2) of the preceding PCRs are used. As templates both fragments are mixed in equal volumes and serially diluted 1:10 and 1:100. Dilution of the templates proved to be essential, because high concentrated templates do not necessarily result in optimal extension. After amplification, the PCR product was checked for expected length and absence of undesired amplicons by agarose gel electrophoresis. Distinct PCR products are purified with Agencourt® AMPure® XP and used for downstream application. If the amplicon is contaminated by unspecific PCR products, the PCR reaction is separated on an agarose gel and the desired PCR fragment extracted (2.2.2.6).

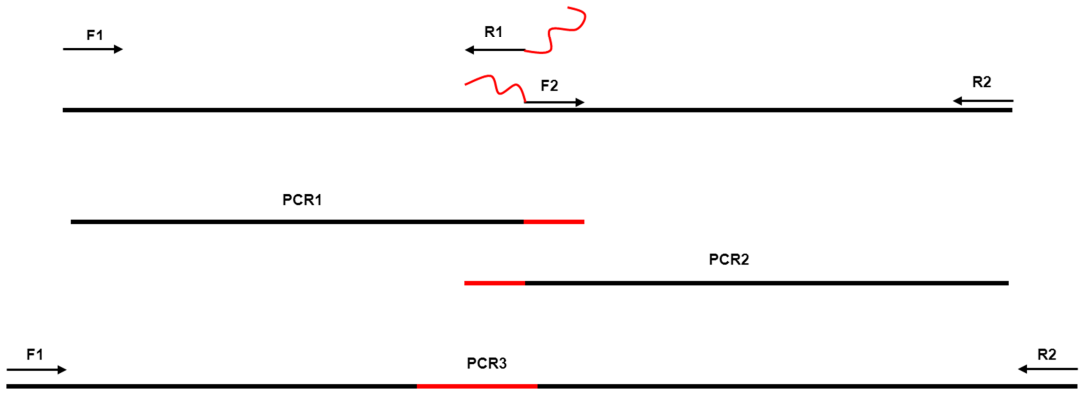

Figure 2.3: 2-step overlap extension PCR.
PCR1 is amplified using primers F1 and R1. PCR2 is generated with primers F2 and R2. Primers R1 and F2 carry the sequence of the insertions and create overlapping ends. During extension PCR using outmost primers F1 and R2 the overlapping region anneals and the template strand is extended.

The 3-step approach was used to exchange whole ORFs by connecting the new ORF with flanking SARS-CoV wild type sequences in order to facilitate introduction into the appropriate SARS-CoV subclone.

In a first PCR (PCR1 in Fig. 2.4) the whole new insert is amplified. Next, the flanking sequences around the position where the new insert should be introduced are amplified (PCR2 and PCR3 in Fig. 2.4). Primer R2 of PCR2 and primer F3 of PCR3 consist of backbone specific sequences and additionally specific sequences of the new insert creating overlapping regions. Extension is done step wise or all at once resulting in 3 possible approaches leading to the final extended PCR product:

- PCR1 + PCR2 = PCR4.1 + PCR3 = PCR5
- PCR1 + PCR3 = PCR4.2 + PCR2 = PCR5
- PCR1 + PCR2 + PCR3 = PCR5

Generally, templates are mixed in equal volumes and subsequently diluted 1:10 and 1:100. The 3 approaches are usually done simultaneously and the method chosen, which leads to success. All PCR products are purified with Agencourt® AMPure® XP (2.2.2.5) or if necessary extracted from an agarose gel (2.2.2.6) prior to the next PCR amplification.

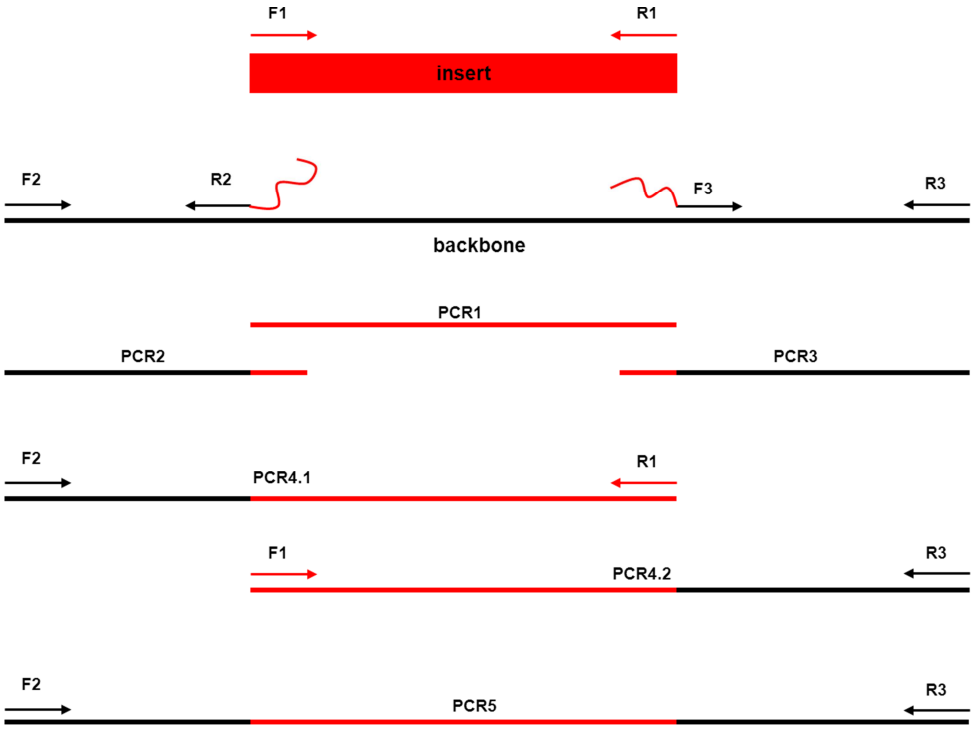

Figure 2.4: 3-step overlap extension PCR.
Three fragments are generated by PCR using primers as indicated. PCR1 (primers F1 and R1) is the sequence to be exchanged in the backbone. PCR2 and PCR3 are tagged with insert specific sequences added by primers R2 and F3, respectively. So, PCR2 and PCR3 contain overlapping sequences to PCR1 which are used in subsequent PCRs for annealing of the template fragments.

2.2.3.2 Real-time RT-PCR for quantification of genomic SARS-CoV RNA

Quantification of genomic SARS-CoV RNA was done by amplifying a region within nsp14 using Invitrogens SuperScript™ III One-Step RT-PCR System with Platinum® *Taq* DNA Polymerase according to the following reaction set up:

Reaction set up for real-time RT-PCR

RNase-free water	3.0 µL
2x Reaction Mix	6.25 µL
BSA (10 µg/mL)	0.5 µL
SuperScript™ III RT/ Platinum® *Taq* Mix	0.5 µL
Forward primer SARS F (10 µM)	0.5 µL
Reverse primer SARS R (10 µM)	0.5 µL
Probe SARS P (10 µM)	0.25 µL
RNA (5 fg-0.5 µg)	1.0 µL
Total	**12.5 µL**

Amplification and detection was done according to the following temperature profile:

Temperature profile for real-time RT-PCR

Reverse transcription	55°C	15 min	
Initial denaturation	95°C	2 min	
Denaturation	95°C	15 sec	45x
Annealing/Extension*	58°C	30 sec	
Cooling	40°C	10 sec	

*Detection

2.2.3.3 Site-Directed Mutagenesis

Small insertions, deletions or point mutations were introduced into plasmids using Finnzymes Phusion™ Site-Directed Mutagenesis Kit according to manufacturer's instructions. Briefly, primers were designed in accordance to the mutation as shown in figure 2.5.

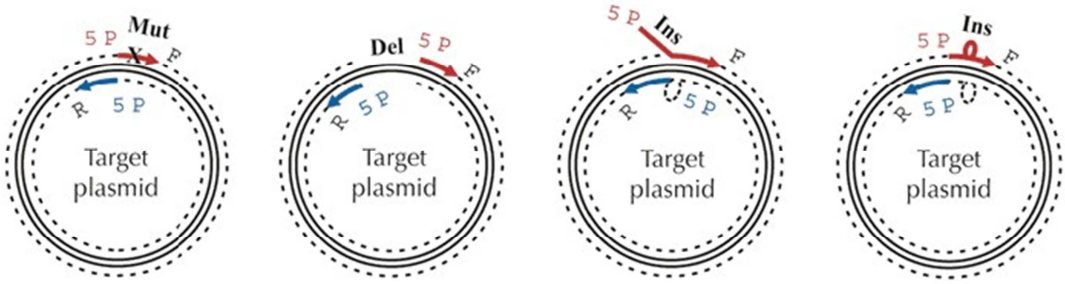

Figure 2.5: Primer design for PhusionTM Site-Directed Mutagenesis

http://www.abgene.com/images/products-fz/fz-1084_1.gif

All primers needed to be phosphorylated at the 5' end and were about 30 nt in length. Due to the length of the primers, their salt adjusted melting temperature usually was about 70°C. The following reaction set up was used for mutagenesis:

Reaction set up for Phusion™ Site-Directed Mutagenesis

5x Phusion™ HF-buffer	5.0 µL
dNTPs (10 mM each)	0.5 µL
Forward primer (10 µM)	0.5 µL
Reverse primer (10 µM)	0.5 µL
Phusion™ Hot Start DNA Polymerase (2 U/µL)	0.25 µL
Template DNA (10 pg-50 ng)	1.0 µL
Ampuwa®	17.25 µL
Total	**25.0 µL**

Cycling conditions for mutagenesis were as follows:

Temperature profile for Site-Directed Mutagenesis PCR

Initial denaturation	98°C	30 sec	
Denaturation	98°C	10 sec	25x
Annealing	X°C *	20 sec	
Extension	72°C	30 sec/kb	
Final Extension†	72°C	10 min	
Storage	4°C	∞	

* Primer melting temperature according to Oligo Calcs (http://www.basic.northwestern.edu) salt adjusted T_M, annealing was done 3°C cooler than melting temperature. If no PCR product could be detected, annealing temperature was lowered to 56°C.
† Final extension was omitted when extension time during cycling exceeded 10 min.

Successful amplification of template DNA was verified by agarose gel electrophoresis (2.2.2.8). If no amplification could be detected, PCR was redone using Finnzymes Phusion® High-Fidelity DNA Polymerase (2.2.3.1).

Circularization of PCR products was done using Quick T4 DNA Ligase without purifying the PCR products prior to ligation. The amount of PCR product used was evaluated from the gel, using 1-5 µL depending on the quantity seen in the agarose gel. Ligation was done according to the following reaction set up:

Ligation reaction set up for Site-Directed Mutagenesis

PCR product	1-5 µL
2x Quick Ligation Buffer	5 µL
Quick T4 DNA Ligase	0.5 µL
Ampuwa®	Add to 10.5 µL

The ligation reaction was incubated for 30 min at room temperature and stored on ice or -20°C until transformation.

The circularized plasmids were transformed into suitable chemically or electrocompetent *E.coli* as described in chapter 2.2.6.

2.2.4 Cloning of PCR products into pEZ™ BAC vector

Lucigens pEZ™ BAC vector is blunt end linearized and dephosphorylated. This allows cloning of PCR products amplified with 5' phosphorylated primers without restriction digestion.
PCR products were generated using Phusion® High-Fidelity Polymerase (2.2.3.1) and amplification was verified by gel electrophoresis (2.2.2.8). The PCR product was purified with AMPure® (2.2.2.5) and the DNA concentration was determined (2.2.2.9). Ligation reaction was set up according to the following protocol:

Ligation reaction set up for cloning into pEZ™ BAC vector

5x Ligation Buffer	2 µL
pEZ™ BAC vector	1 µL
Clone Smart Ligase	1 µL
PCR product (100 ng)	6 µL
Total	**10 µL**

Ligation was done for 2 h at room temperature. Thereafter, the ligation reaction was heat inactivated for 15 min at 70°C and immediately placed on ice.
Transformation of the ligation reaction was done by electroporation into BAC-Optimized Replicator™ v2.0 Electrocompetent Cells. 20 µL electrocompetent cells were transferred to a pre-cooled 1.5 mL reaction and 1 µL ligation reaction was added. The cell-ligation reaction mix was then pipetted into a pre-cooled 1 mm gap cuvette and a pulse was applied. Pulse settings were: 1800 V, 25 µF, 200 Ω. Cells were resuspended in 500 µL recovery medium and incubated for 1 h at 37°C in a shaking incubator. Thereafter, transformed cells were plated on YT-agar plates containing 12.5 µg/mL chloramphenicol and incubated at 37°C overnight.

2.2.5 Production of chemically competent *E.coli*

A 5 mL overnight culture of glycerol stocked One Shot® Stbl3™ was prepared in LB medium. 250 µL of overnight culture were used to inoculate 250 mL LB medium and grown at 37°C in a shaker at 100 rpm. After 1 h a sample was taken and OD600 determined. If OD600 was was not within the range of 0.5-0.7 the culture was further incubated and samples were taken every 30 min. When OD600 reached the correct value the culture was transferred to an ice bath and cooled to 4°C under constant shaking. The culture was then incubated for another 15 min at 4°C. Afterwards the bacteria were pelletized for 15 min at 3000 rpm at 4°C. The supernatant was carefully discarded, the pellet resuspended in 50 mL 80 mM $CaCl_2$ and incubated for 40 min at 4°C. Bacteria were pelletized again for 15 min at 3000 rpm and 4°C. Supernatant was carefully discarded, the pellet resuspended in 5 mL 80 mM $CaCl_2$ + 20% glycerol and aliquoted á 100 µL in pre-cooled 1.5 mL reaction tubes. The bacteria were shock frozen in liquid nitrogen and stored at -70°C.

2.2.6 Transformation of chemically and electrocompetent *E.coli* and preparation of glycerol stocks

Ligation reactions were usually transformed first into chemically competent TOP10 (Invitrogen) or One Shot® Stbl3™ (Invitrogen or self-made) according to manufacturer's instructions. Briefly, 50 µL of bacteria were thawed on ice, mixed gently by stirring with the pipette tip with 8 µL ligation reaction and the transformation reaction was incubated on ice for 30 min. Heat shock was performed at 42°C for 30 sec (TOP10) or 45 sec (One Shot® Stbl3™). After heat shock One Shot® Stbl3™ were placed on ice for 2 min before adding S.O.C. medium, while 250 µL S.O.C. medium were added immediately to TOP10 cells. The bacteria were then incubated at 37°C for 1 h at 300rpm. Cells were spread on LB plates containing the appropriate antibiotic according to the transformed vector (50 µg/mL Ampicillin for pCAGGS, 12.5 µg/mL Chloramphenicol for pBeloBAC11 and pEZ™ BAC) and incubated overnight at 37°C in an incubator.

Ligation reactions yielding no colonies in chemically competent cells were additionally transformed into electrocompetent *E.cloni*® 10G SUPREME or *E.cloni*® 10G ELITE (Lucigen®) according to manufacturer's instructions. Briefly, 1-2 µL ligation reaction were pipetted into a

pre-cooled 1 mm electroporation cuvette and 25 µL *E.cloni*® were added. The cells were electro shocked with one pulse of 10 µF, 600 Ω and 1800 V. 975 µL of Recovery Medium were immediately added to the cuvette, the cells were transferred to a 1.5 mL reaction tube and incubated at 37°C for 1 h at 300 rpm. Thereafter, cells were spread on LB plates containing the appropriate antibiotic according to the transformed vector and incubated overnight at 37°C in an incubator.

Glycerol stocks of sequenced plasmids were produced to conveniently produce high amounts of overnight cultures for plasmid midipreparations. An inoculating loop of bacteria was resuspended in 900 µL LB medium and mixed with 900 µL glycerol. The mixture was aliquoted á 600 µL and stored at -70°C.

2.2.7 Protein biochemical methods and immunodetection assays

2.2.7.1 Protein isolation from eukaryotic cells

Cells were washed thrice with ice cold 1x PBS in order to fixate their current state of protein expression and to remove FBS. The cells were then scraped of in 500 µL 1x PBS, transferred to a 1.5 mL reaction tube and centrifuged for 5 min at 300x g and 4°C. The supernatant was discarded, the pellet resuspended in an appropriate volume of RIPA lysis buffer (25 µL/24-well or 100 µL/6-well) and the lysed cells were incubated on ice for 20 min. Optionally cells were centrifuged for 10 min at full speed and 4°C in order to remove nuclei. The supernatant was then transferred to a fresh 1.5 mL reaction tube. Protein samples were stored at -80°C until use.

2.2.7.2 Sodium dodecyl sulfate polyacrylamide gel electrophoresis (SDS-PAGE)

Prior to Western blot analysis protein samples were separated according to their mass by denaturating SDS-PAGE. SDS-PAGE gels were prepared depending on the mass of the proteins to be analyzed between 12 and 14% acrylamide (table 2.17).

Composition of SDS-polyacrylamide gels

2 mini gels	Separation gel		Stacking gel
	12%	14%	
30% Acrylamide	4.00 mL	4.67 mL	0.50 mL
1.875 mM Tris (pH8.8)	2.00 mL	2.00 mL	
0.6 M Tris (pH6.8)			0.60 mL
Water	3.85 mL	3.18 mL	1.85 mL
10% SDS	0.10 mL	0.10 mL	0.03 mL
10% APS	0.05 mL	0.05 mL	0.015 mL
TEMED	0.01 mL	0.01 mL	0.003 mL

After complete polymerization of the gel it was placed into the Mini-PROTEAN electrophoresis module (Bio-Rad) and the module was filled with 1x SDS-PAGE running buffer. Gel slots were rinsed vigorously by pipetting running buffer in order to remove gel residuals. Protein samples were mixed with 4x NuPAGE® LDS Sample Buffer (Invitrogen) and boiled for 5 min at 95°C if necessary prior to loading the gel. 8 µL of Fermentas PageRuler™ Prestained Protein Ladder were used as mass reference. Separation was achieved by applying 100 V.

2.2.7.3 Western blot analysis

Following separation of protein samples by SDS-PAGE proteins can be visualized on polyvinylidenfluorid (PVDF) membranes. Therefore, proteins are transferred from an SDS gel onto the membrane via application of electric current in a semi-dry blotting system. Transferred proteins are then specifically detected by a primary antibody which again is detected by a secondary antibody that is coupled to horse radish peroxidase (HRP). Detection is done by conversion of a chemiluminescent substrate and pictured in Peqlabs FUSION FX7™ imaging system.

6 Whatman papers were equilibrated in 1x transfer buffer and the PVDF membrane was activated by short incubation in 100% methanol. Afterwards the PVDF membrane is rinsed in water and transferred to 1x transfer buffer to avoid drying-out. The electrode of the blotting system was assembled with 3 Whatman paper, activated PVDF membrane, SDS gel and again 3

Whatman paper. Air bubbles were smoothed out, the second electrode placed on top and the proteins were transferred applying 150 mA per blot for 1.5 h. After successful protein transfer the membrane was blocked with 5% dry milk in PBS-Tween for 1 h at room temperature or overnight at 4°C. Following blocking and 3 times washing with PBS-Tween for 5 min the membrane was incubated for 1 h at room temperature with the primary antibody diluted in 1% dry milk in PBS-Tween. Afterwards the membrane was again washed thrice with PBS-Tween and incubated for 1 h at room temperature with the secondary antibody diluted 1:20,000 in 1% dry milk in PBS-Tween. Finally, the membrane was washed 6 times with PBS-Tween and detection was done with SuperSignal® West Pico or Femto Chemiluminescent Substrate.

When a second protein needed to be detected on a membrane (e.g. β-actin as loading control), already bound primary and secondary antibody had to be removed first. Therefore, the membrane was incubated in Re-Blot Plus-Strong solution (diluted 1:10 in water) for 20 min at room temperature. The membrane was washed 3 times with PBS-Tween and was then ready for incubation with new antibodies.

2.2.7.4 Immunofluorescence assay (IF)

For visualization of overexpressed proteins within cells the immunofluorescence assay was used. A cell monolayer is fixed with paraformaldehyde maintaining cell structures and protein epitopes. Fixed cells are then incubated with a primary antibody directed against the protein of interest and a secondary antibody coupled to a fluorescent dye. Detection is done by fluorescence microscopy.

Cells were seeded according to their size and speed of growth between 1x 10^5 and 3x 10^5 cells on round glass cover slips in 24-wells. Cells were then transfected as described in chapter 2.2.1.2. Usually 24h after transfection supernatant was removed and the cells were washed once with ice cold 1x PBS. The cells were fixed with 500 µL Roti®-Histofix per 24-well for 20 min at room temperature. Thereafter, cells were washed twice with PBS-Tween and cell membranes were permeabilized with 200 µL freshly made 0.1% Trition® X-100 in PBS-Tween for 10 min at room temperature. After washing twice with PBS-Tween cells were incubated with the primary antibody diluted in EUROIMMUN sample buffer for 1 h at 37°C in a wet chamber. Next, cells were washed again twice with PBS-Tween and incubated with the secondary antibody diluted in 1x PBS for 30 min at 37°C in a wet chamber. After washing the cells twice with PBS-Tween cell nuclei were stained with 4',6-diamidino-2-phenylindole (DAPI) diluted 1:1000 in 1x PBS for

2 min in the dark at room temperature. Cells were finally washed twice with 1x PBS and once with water. Cover slips were then placed with the cell layer facing down onto microscope slides and the cover slips were sealed with Dako Fluorescence Mounting Medium. After drying of the mounting medium for at least 8h at 4°C cells were ready for microscopy.

2.2.8 RVFV-Renilla bioassay

In order to determine cell line-specific pan-species IFN effective concentrations (EC) an RVFV-Ren bioassay was performed. Here a genetically modified Rift Valley fever virus is used that carries a *Renilla* luciferase (RVFV-Ren) instead of its IFN antagonist NSs making it highly sensitive to IFN treatment. *Renilla* luciferase expressed in infected cells can be measured with Promegas *Renilla* luciferase assay system and gives a direct correlation between virus growth and biologically active IFN.

For determination of pan-species IFN EC values 100 µL/96-well of a cell suspension with a concentration of $6x10^5$ cells/mL were seeded and cultivated overnight. Medium was removed and replaced by 100 µL/well of pan-species IFN diluted in DMEM. Cells were further incubated for 7 h. Thereafter, IFN containing medium was removed and cells were infected with 100 µL RVFV-Ren at an MOI of 0.01. Virus containing supernatant was not taken off during infection. For each assay 2 controls were needed. A positive control, were cells were not incubated with IFN but infected with virus, resembling maximal virus growth/luciferase expression. A negative control, were cells were neither incubated with IFN nor infected with virus, for determination of background signal. 16 h post infection the supernatant was removed completely and cells lysed in 50 µL passive lysis buffer per well by shaking at room temperature in the dark. Cell lysis was controlled by microscopy. Incompletely detached cells were scraped off. 10 µL cell lysate were transferred to one well of a read-out plate, the plate was covered with aluminium foil until read-out was performed. Luciferase activity was determined as relative light units (RLU) after addition of 50 µL luciferase substrate per well by a luminescent reader.

3 Results

3.1 Technical preliminary work

3.1.1 Generation of recombinant SARS-CoVs

3.1.1.1 SARS-CoV reverse genetics system

In order to investigate the influence of mutations of the SARS-CoV genome on the virus' phenotype, a reverse genetic system was established in our working group [49]. The full-length SARS-CoV genome was split into 6 overlapping parts (A-F) of about 4.4 to 6.9 kb in length and cloned into high copy vectors (Fig. 3.1). Within these vectors silent mutations were inserted into the genome to delete restriction sites and to create a cloning strategy that made it possible to re-assemble the whole genome stepwise. Fragment A and B were ligated to subclone pAB (14,415 bp), B, C and D were combined to subclone pBCD (16,245 bp), D and E were fused to pDE (15,900 bp) and E and F to subclone pEF (15,376 bp). Due to instability of large fragments in high copy vectors, the vector backbone was changed during assembly of the subclones to the low copy bacterial artificial chromosome (BAC) vector pBeloBAC11. The 5'-half of the full-length genome was then assembled after restriction of pAB and pBCD with restriction enzymes PspOMI, cutting within the vector backbone and Bsu36I, cutting within nsp3 of the SARS-CoV genome, resulting in the half-clone pABCD (22,807 bp).

Subclone pEF and half-clone pDEF carried the 3'-end of the SARS-CoV genome including all accessory genes. Since the focus of this thesis was the characterization of the accessory genes ORF6 and ORF8 the subclones pEF and pDEF were used to introduce mutations and deletions. Assembly of pDEF from pDE and pEF and the subsequent assembly of the full-length SARS-CoV clone are described in more detail below.

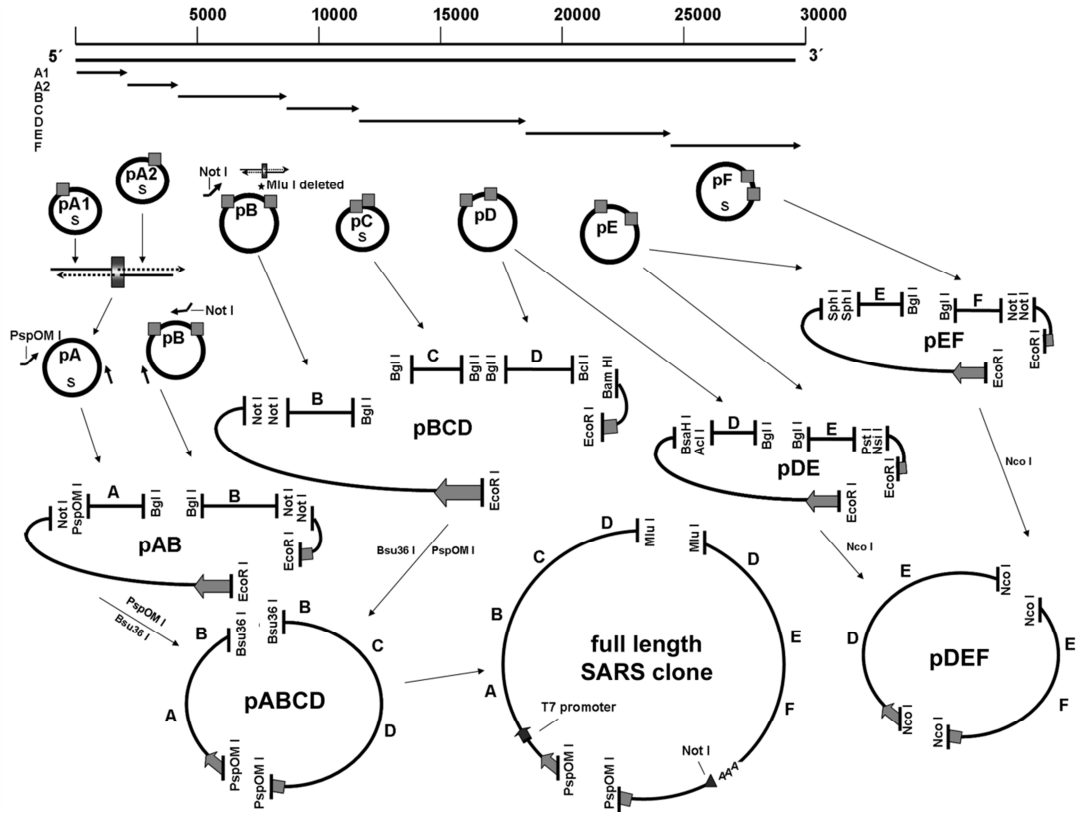

Figure 3.1 Assembly of the full-length SARS-CoV clone.
After cloning of SARS-CoV genome fragments A-F into high copy vectors, a stepwise assembly and a change of the vector backbone to pBeloBAC11 was done. Fragment A was cut out of its vector with BglI and PspOMI. Fragment B was excised using BglI and NotI. The new vector backbone pBeloBAC11 was cut in two by NotI and EcoRI. All four fragments were ligated at once to create subclone pAB. NotI and PspOMI produce compatible ends, ligation thus deletes both restriction sites. For assembly of subclone pBCD, fragment B was cut out using NotI and BglI, C was excised by BglI and D using BglI and BclI. Vector pBeloBAC11 was digested by NotI, EcoRI and BamHI. All four fragments were ligated at once. BclI and BamHI create compatible ends; upon ligation both restriction sites are consequently deleted. Fragment D was cut out with AclI and BglI, while E was excised using BglI and PstI for assembly of pDE. PBeloBAC11 was cut in two by BsaHI, EcoRI and NsiI. The four fragments were ligated. BsaHI and AscI as well as PstI and NsiI create compatible ends. Ligation results in deletion of the restriction sites. Subclone pEF was built up of fragment E, cut with SphI and BglI and fragment F, cut with BglI and NotI. The vector backbone was digested with SphI, EcoRI and NotI. Plasmids pAB and pBCD were digested with Bsu36I and PspOMI to create pABCD. To create pDEF subclone pDE and pEF were digested with NcoI only. The full-length SARS clone was finally assembled by ligation of fragments ABCD and DEF, which were cut using PspOMI and MluI. Figure taken from Pfefferle et al., 2009 [49]

3.1.1.2 Assembly of half-clone pDEF

Subclone pEF contained all structural and accessory genes of the SARS-CoV genome and the 3'-terminal 227 bp of nsp16 (Fig. 3.2A). The complete clone comprised 15.4 kb with an insert of 8.5 kb. One possibility to mutate single ORFs was the generation of mutated PCR amplicons by overlap extension PCR (2.2.3.2) and subsequent introduction of the fragment into pEF via restriction sites SwaI or BamHI and NotI. All three enzymes cut only once within the subclone, as indicated in Fig. 3.2A. Due to its relatively small size pEF could be used for site-directed mutagenesis (2.2.3.4). This technique allowed introducing mutations by primers followed by the complete amplification of the plasmid by PCR.

Subclone pDE contained 99% of the RNA polymerase (nsp12) sequence, nsp13 to nsp16 and a small part of the ORF coding for the spike protein including the NcoI site for assembly with pEF (Fig. 3.3A).

Assembly of half-clone pDEF was achieved by a single digestion of pDE and pEF with NcoI. As indicated in the vector maps in Fig. 3.2A pDE and pEF shared an overlapping region within the 5'-end of the spike ORF including the naturally occurring NcoI site, which was used to fuse the SARS-CoV genome sequence. Digestion of pDE with NcoI resulted in the fragmentation of the plasmid into two fragments of 9,630 bp and 6,270 bp in length. The difference in fragment length was sufficient to distinguish both fragments on an agarose gel and enabled efficient excision from a preparative gel (Fig. 3.2B). Digestion of pEF with restriction enzyme NcoI cut the plasmid into two fragments of 13,753 bp and 1,623 bp in length (Fig. 3.2B). Of each subclone only the large fragments were needed for ligation.

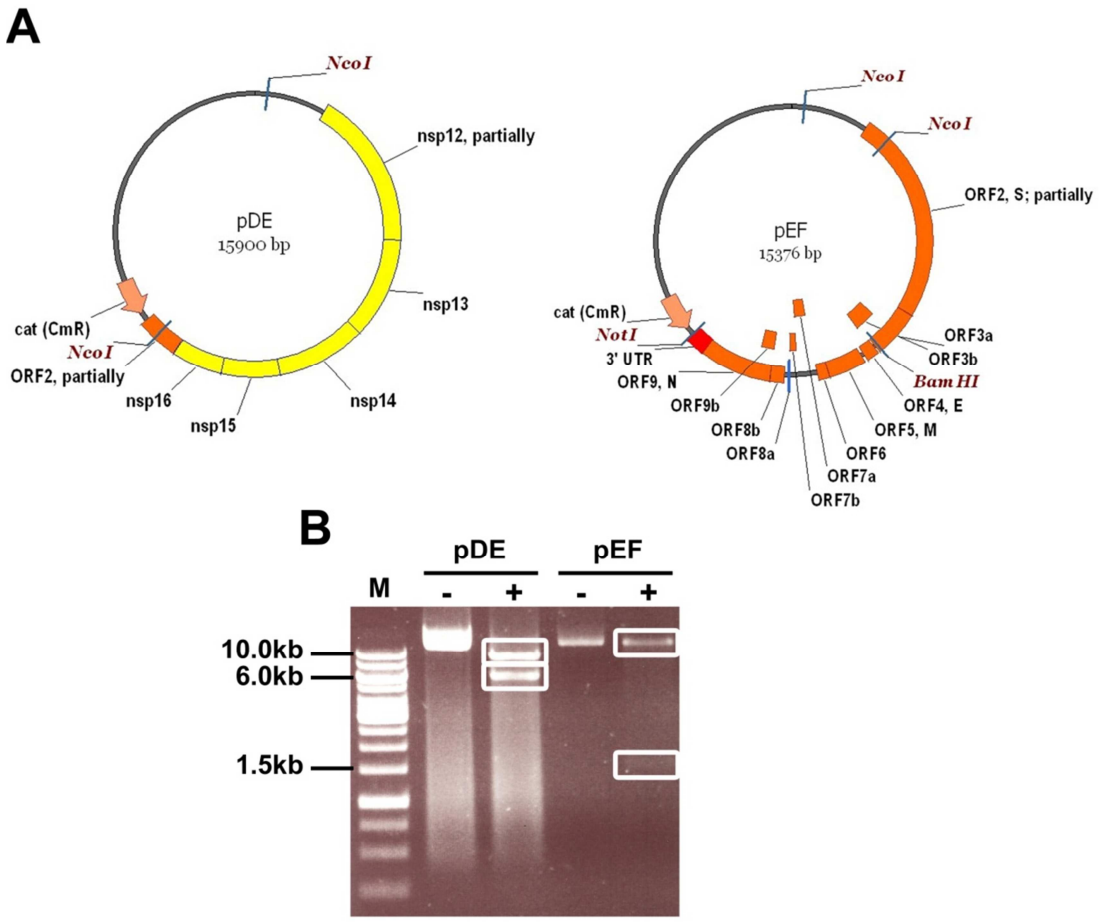

Figure 3.2: NcoI digestion of pDE and pEF for assembly of pDEF.
(A) Vector maps of subclones pDE and pEF, restriction sites of NcoI are indicated. (B) Digestion of pDE with NcoI yielded fragments of 9,630 bp and 6,270 bp, while pEF was cut into fragments of 13,753 bp and 1,623 bp. M = 1 kb DNA ladder; "-" indicates uncut plasmid; "+" indicates digestion with NcoI. 200 ng of plasmid were applied per lane.

The fragment of pEF used for ligation contained the major part of the pBeloBAC11 vector backbone including the chloramphenicol resistance gene. Dephosphorylation of this fragment was necessary in order to minimize religation and growth of false positive colonies (2.2.2.13). After dephosphorylation, both restriction reactions were applied on a preparative agarose gel (2.2.2.8). The desired DNA fragments were extracted from an agarose gel and ligated as described (2.2.2.6; 2.2.2.14). Chemically competent *E. coli* cells were transformed with the ligation reaction (2.2.6). Grown colonies were picked and plated on LB agar for small scale plasmid preparations (2.2.2.4). Plasmids were applied on an agarose gel and their sizes determined in comparison to a supercoiled DNA marker. Plasmids with a size of about 23 kb were first screened for correct orientation of the ligation product. Since pDE and pEF were only cut with

one restriction enzyme, there were two possibilities of ligation. Incorrect ligation resulted in a discontinuous SARS-CoV genome fragment that could not be used for further cloning. In order to prove correct cloning a subset of sequencing PCR reactions was done covering the complete construct (Table 2.2). PCR No. 3 amplified a region of the insert carrying the naturally occurring NcoI site within the SARS-CoV genome. Amplification could only be achieved when the ligation was successful and in the correct orientation. An amplification product (amplicon 3) proved right ligation, while an indistinct PCR product indicates incorrect ligation.

After successful generation of amplicon 3 and verification of an intact NcoI restriction site by sequencing with primer E 21452 F, all remaining sequencing PCRs (see table 2.2 for primer pairs and cycling conditions) were done using the standard reaction set up for Phusion® High-Fidelity Polymerase (2.2.3.1). PCR products were controlled by gel electrophoresis, purified and sequenced with suitable sequencing primers as listed in table 2.2 (2.2.2.5; 2.2.2.10). When the complete DEF insert was sequenced and no undesired mutations were detected, the plasmid was prepared in midi-scale for use in assembly of the full-length clone.

3.1.1.3 Assembly of the full-length SARS-CoV clone

In this working step half-clone pDEF had to be fused to half-clone pABCD, containing the 5'-half of the SARS-CoV genome, in order to obtain a full-length continuous SARS-CoV genome. The non-structural proteins nsp1-10 and 80% of the RNA polymerase (nsp12) were included in pABCD (Fig. 3.3A). The inserts ABCD and DEF overlapped in nsp12, where the naturally occurring MluI site was located. This MluI site was used to fuse both inserts and generate the complete genome. A second MluI site, present in nsp3 of the SARS-CoV genome, was deleted by introduction of a silent mutation in subclone pB as indicated in Fig. 3.1.

First, both half-clones, pABCD and pDEF, were linearized with restriction enzyme PspOMI, which cut within the vector backbone as indicated in Fig. 3.3A. Successful linearization was indicated by reduction of two bands, representing supercoiled and open circle forms of the plasmid (Fig. 3.4B), to only one band, representing a linear DNA fragment. A typical agarose gel of a supercoiled plasmid in comparison to its linearized form is shown in Fig. 3.5A. Digestion of half-clone pABCD with the second restriction enzyme MluI resulted in two fragments of 15,130 bp and 7,677 bp in length. The half-clone pDEF was cut with the same enzyme in

fragments of 21,567 bp and 1,816 bp. The typical fragmentation pattern of the plasmids after digestion with PspOMI and MluI is shown in Fig. 3.3B.

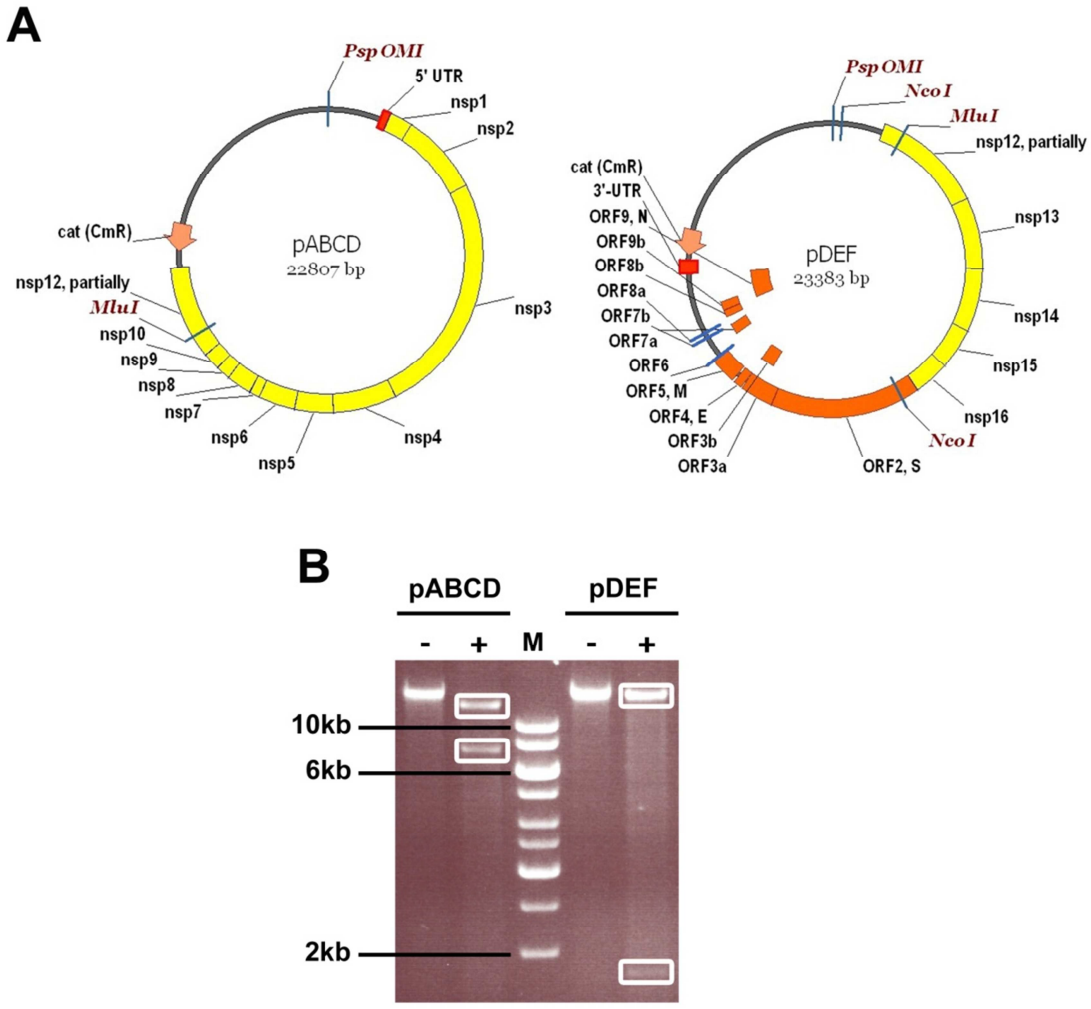

Figure 3.3: Digestion of pABCD and pDEF for assembly of full-length SARS-CoV clone.
(A) Vector maps of pABCD and pDEF, restriction sites of PspOMI and MluI needed for restriction and assembly of the full-length clone are indicated. (B) Digestion of pABCD with PspOMI and MluI yielded fragments of 15,130 bp and 7,677 bp, while pDEF was cut into fragments of 21,567 bp and 1,816 bp. M = 1 kb DNA ladder; "-" indicates undigested plasmid; "+" indicates digestion with both enzymes. 200 ng plasmid were applied per lane of a 0.8% agarose gel.

Only the large fragments of each half-clone were needed for ligation. The large fragment of pDEF contained most of the pBeloBAC11 vector backbone including the chloramphenicol resistance gene and was therefore dephosphorylated (2.2.2.13). The fragments needed for ligation were extracted from a preparative gel (2.2.2.8; 2.2.2.6). Ligation was done with equal amounts of

each fragment (2.2.2.14). *E. coli* cells were chemically transformed with the ligation reaction and resulting colonies were picked and used for plasmid minipreparations (2.2.6; 2.2.2.4). Plasmids were screened for correct size by agarose gel electrophoresis in comparison to a supercoiled DNA marker. Plasmids with sizes of about 37 kb (Fig. 3.4B) were first screened with PCR No. 5 as listed in table 2.3. PCR 5 amplified a fragment containing the MluI site, which was only generated by successful ligation.

Integrity of the MluI site was then verified by sequencing of the PCR product with primer D 13700 F. After confirmation of the integrity of the MluI site, all remaining sequencing PCRs were done using the standard Phusion® High-Fidelity Polymerase reaction set up (2.2.3.1; see table 2.3 for primer pairs and cycling conditions). PCR products were controlled by agarose gel electrophoresis, purified and sequenced with the appropriate primers listed in table 2.3 (2.2.2.8; 2.2.2.10). After ruling out mutations, the plasmid was prepared in midi-scale (2.2.2.4). The resulting full-length SARS-CoV clone is depicted in Fig. 3.4A. A minimal T7 promoter sequence was inserted directly upstream of the genome for *in vitro* transcription into infectious full-length genomic RNA (2.2.2.11). A NotI site located directly downstream of the poly-A tail and was used to linearize the full-length clone making it accessible to the T7 polymerase.

The generated SARS-CoV full-length clone was then used for the rescue of recombinant SARS coronavirus (rSCV) as described in the following (3.2.1.4).

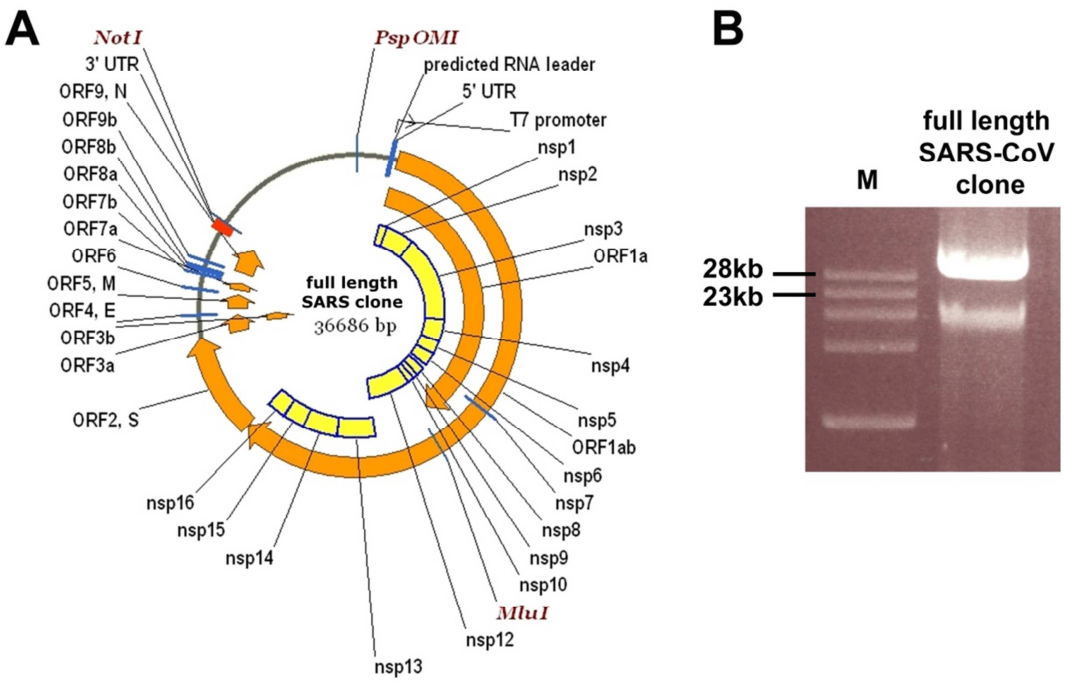

Figure 3.4: Full-length SARS-CoV clone.
(A) Vector map of the full-length SARS-CoV clone. (B) Separation characteristics of the full-length SARS-CoV clone on a 0.8% GTQ agarose gel. M = Supercoiled DNA marker set. The upper band represents the supercoiled form of the plasmid.

3.1.1.4 Rescue of recombinant SARS-CoVs

The full-length SARS-CoV clone served as a template for the generation of infectious viral RNA. Since T7 polymerase needs linear DNA templates for *in vitro* transcription the plasmid was first linearized by digestion with NotI (2.2.2.11). The restriction site was located downstream of the genome's poly-A tail as shown on the vector map of the plasmid in Fig. 3.4A. Complete linearization of the plasmid was checked by agarose gel electrophoresis (2.2.2.8). The differences in migration patterns of linearized full-length plasmid in comparison to supercoiled plasmid in the gel are shown in Fig. 3.5A. The linearized plasmid was then purified by phenol-chloroform extraction and ethanol precipitation in order to generate highly pure template for *in vitro* transcription (2.2.2.7). *In vitro* transcription of full-length genomic RNA was then done as described in chapter 2.2.2.11. The resulting *in vitro* transcript was again phenol-chloroform extracted and ethanol precipitated to yield highly pure RNA. Replication of coronaviruses initiated from pure genomic RNA proved to be enhanced by co-electroporation of capped nucleocapsid RNA [96]. Therefore, the nucleocapsid sequence of SARS-CoV was amplified from subclone pEF using a forward primer that binds to the nucleocapsid's start codon and contains the minimal SP6 promoter sequence adding it to the PCR amplicon (2.2.3.1). The reverse primer bound within the 3'-end of the 3'-UTR of the SARS-CoV genome and contained a poly-A tail. The modified PCR product (Fig. 3.5B) could be used for the *in vitro* transcription (2.2.2.11) of capped and poly-A tailed RNA that is directly translated in the cytoplasm of electroporated cells.

Capped viral genomic RNA and capped nucleocapsid were electroporated into BHK-J cells (2.2.1.3). BHK-J cells are not susceptible to SARS-CoV, because they lack the SARS-CoV receptor hACE2. However, they can be efficiently electroporated and produce viable viruses that are released into the cell culture supernatant. Therefore, virus-containing supernatant was harvested 24h post electroporation and was transferred to the SARS-CoV-susceptible primate cell line, VeroFM. Virus replication was documented as the increase of viral RNA in the cell culture supernatant by real-time RT-PCR (2.2.3.3). A typical growth kinetic of recombinant virus is shown in Fig. 3.5C.

Production of virus stock was generally terminated after 3d, because it was experimentally shown that virus replication was optimal at this time point. Further incubation yielded only a small additional increase in viral RNA but led to a decreased yield in infectious virus particles (data not shown).

Aliquoted virus stock was quantified for the presence of viable, infectious particles by plaque titration (2.2.1.6). In addition, the morphology of plaques was analyzed (Fig. 3.5D). Generally, a virus titer of 10^6 PFU/mL was achieved.

In order to verify that the virus stock contained recombinant SARS-CoV and was not produced by contamination from a patient isolate, the marker mutation deleting the second MluI site within nsp3 was sequenced. While the MluI site was present in the patient's isolate, it was not detectable in the newly generated virus stock (Fig. 3.5E). All recombinant viruses used in the present thesis were characterized in this manner.

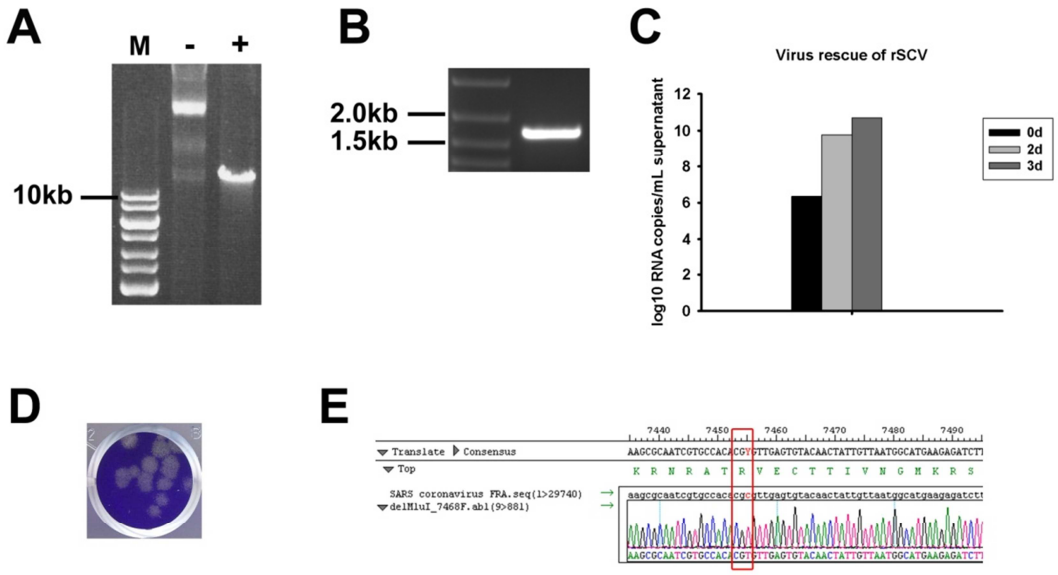

Figure 3.5: Rescue of recombinant SARS-CoVs.
Linearized full-length SARS-CoV plasmid (A) and a PCR amplicon of SARS-CoVs nucleocapsid (B) were *in vitro* transcribed into capped and poly-A tailed RNA. Both RNAs were co-electroporated into BHK-J cells. 24h post electroporation, cell culture supernatant was transferred to susceptible VeroFM cells and virus replication was monitored by real-time RT-PCR (C). The produced virus stock was quantified by plaque titration (D) and an introduced marker mutation, deleting an MluI site within nsp3, was sequenced to verify the origin of the virus stock being the SARS-CoV full-length clone.

3.1.2 Generation of a SARS-CoV-susceptible bat cell line

Horseshoe bats (*Rhinolophus sp.*) have been described as the putative reservoir of SARS-related coronaviruses [10, 72]. To date there are only two bat cell lines commercially available, Tb1-Lu derived from *Tadaria brasiliensis* and Mvi/It derived from *Myotis velifer incautus* [104], both of which do not belong to the SARS-related CoVs reservoir genus. Because the full-length genome of the SARS-related bat-CoV from Bulgaria was sequenced from bat feces sampled from *Rhinolophus blasii*, a cell line from this genus was chosen to be generated. Primary cell cultures from *Rhinolophus landeri* embryonic lungs (RhiLu) were prepared and cells were immortalized by lentiviral transduction of the simian virus 40 large T-antigen as previously described [105, 106]. However, this cell line was not susceptible to human SARS-CoV (data not shown), presumably because it lacked the SARS-CoV receptor hACE2. In the course of the Bachelor project of Hanna Roth, the immortalized cell line was made susceptible to SARS-CoV infection by lentiviral transduction of *hACE2* [103].

The VSV-G pseudotyped lentiviruses used for transduction of RhiLu cells with *hACE2* were kindly provided by Alexander Pfeifer (Institute of Pharmacology and Toxicology, University of Bonn). Transduction of RhiLu cells was done as described in chapter 2.2.1.7.2. During expansion of the newly generated cell line, samples were taken and analyzed for genomic integration of *hACE2* and expression of hACE2.

Genomic integration of *hACE2* was verified by PCR (2.2.3.1). Genomic DNA was extracted (2.2.2.3) and PCR performed with a forward primer binding within the *hACE* gene and a reverse primer binding within the puromycin resistance gene, yielding a 1.9 kb amplicon (Fig. 3.6B). The pCR4® vector containing the *hACE2*-puromycin resistance gene construct was used as a PCR positive control.

Expression of hACE2 was confirmed by SDS-PAGE and Western blot analysis (2.2.7.2; 2.2.7.3) as shown in Fig. 3.6C. No expression of hACE2 was detected in native, immortalized RhiLu cells. However, RhiLu-hACE2 cells showed expression of the transgene with similar amounts as in the naturally hACE2-expressing MA104 cells. β-actin was additionally detected to ensure that similar amounts of each sample were applied. It is noteworthy that the β-actin antibody used here was, in addition to other species reactivity specified by the manufacturer, also cross-reactive with bat β-actin.

Finally, the newly generated RhiLu-hACE2 cells were tested for susceptibility to SARS-CoV infection in comparison to MA104 cells. Cells were infected with SARS-CoV Frankfurt-1 at two different MOIs (2.2.1.5) and virus replication was determined at different time points p.i. by plaque titration of the supernatant (2.2.1.6). RhiLu-hACE2 cells clearly supported SARS-CoV replication, although not as efficiently as MA104 cells (Fig. 3.6D).

With the generation of this cell line, a valuable tool to study SARS-CoV in the context of its natural reservoir was established. Together with the genetic information obtained from the full genome sequence of the SARS-related bat-CoV it was now possible to compare human and bat coronaviral proteins in their respective hosts.

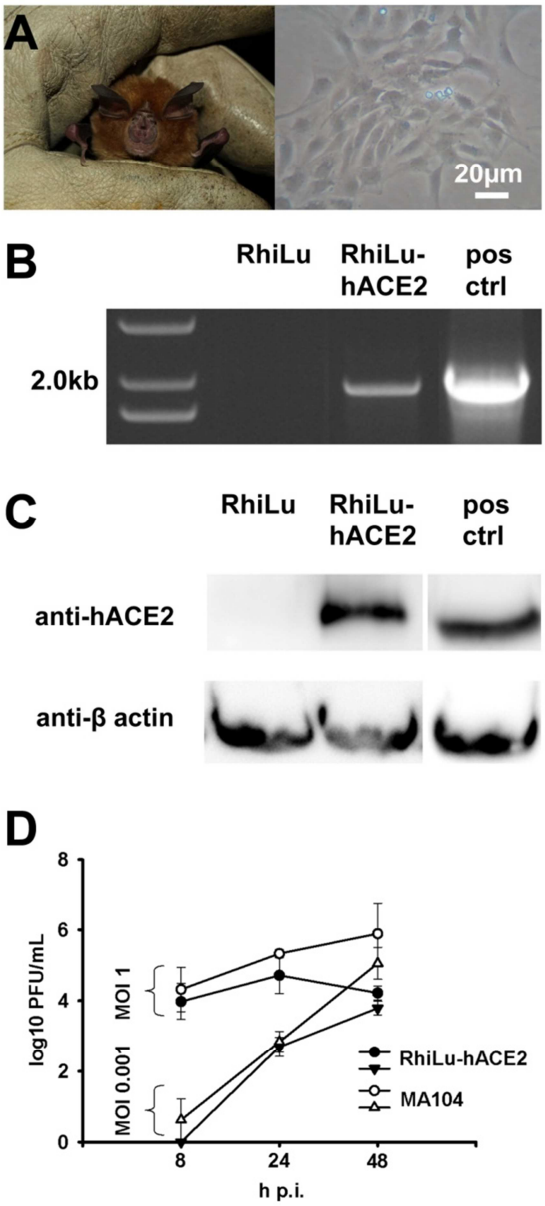

Figure 3.6: Generation of a SARS-CoV susceptible bat cell line.
(A) Primary cell culture and immortalization of *Rhinolophus landeri* embryonic lung cells was done as previously described [105, 106]. Immortalized cells were transduced with *hACE2* by lentiviruses. (B) Integration of *hACE2* into the genome of the cells was verified by PCR. The vector containing the hACE2-puromycin resistance gene construct was used as a PCR positive control. (C) Expression of hACE2 was confirmed by Western blot analysis using mouse-anti-hACE2 (1:1000). In addition, β-actin was detected using mouse-anti-β-actin (1:2000) to ensure that similar protein amounts were applied. MA104 cells, expressing hACE2 naturally, served as positive control. (D) Susceptibility to SARS-CoV of the newly generated cell line was confirmed by infection of RhiLu-hACE2 in comparison to MA104 with SARS-CoV Frankfurt-1 at MOIs 1 and 0.001. At 8, 24 and 48h p.i. supernatants were sampled and virus titers determined by plaque titration.

3.1.3 Determination of pan-species IFN EC_{50} on primate and bat cell culture

In order to investigate the ability of a virus to cope with intracellular countermeasures, an antiviral state was induced in the cells before infection. This antiviral state is a result of the upregulation of IFN-stimulated genes (ISGs) caused by pretreatment with IFN. The species-specific IFN receptor is a limiting factor in this case. SARS-CoV was shown to be highly sensitive to IFN [107], however, the responsible ISGs or other underlying factors have not yet been identified [108-110]. A comparison of SARS-CoV mutants in primate and bat cell cultures was to be done in this thesis. This included IFN treatment of cells to characterize host-specific interactions with the respective mutants. Therefore it was necessary to identify the particular amount of a pan-species universal IFN to induce a comparable antiviral state in the different primate and bat cell cultures.

In order to test the bat cell line RhiLu-hACE2 along with the primate cell lines VeroFM and MA104, the universal type I IFN (pan-species IFN) was used on all cell lines. It was expected that the ability of this pan-species IFN to induce an antiviral state differed among the three cell lines. In order to quantify this difference, the IFN concentration required to reduce viral replication of a Rift Valley fever virus (RFVF) to 50% (EC_{50}) was determined for each cell line. The RVFV (RVFV-Ren) is a mutant expressing *Renilla* luciferase instead of its IFN antagonist, the non-structural protein NSs, making it highly IFN-sensitive [111]. Expression of *Renilla* luciferase was measured with a luciferase assay and was consistent with virus replication patterns [111].

VeroFM, MA104 and RhiLu-hACE2 cells were seeded, preincubated with different concentrations of pan-species IFN and infected with RVFV-Ren as described in chapter 2.2.8. Thereafter, cells were lysed and expression of luciferase was determined in relative light units (RLU).

To determine the EC_{50} values, IFN concentrations in log10 U/mL were plotted against the percentages of emitted RLU (Fig. 3.7). Background signals (cells treated with neither IFN nor virus) were subtracted from all values. The maximal signal of the positive control (cells not preincubated with IFN but infected with RVFV-Ren) was normalized to 100%. A linear equation was calculated based on the exponential progression of the plotted curve. Cell specific EC_{50} values were set at 50% RLU.

Cell line-specific pan-species IFN EC_{50} values were 31.8, 8.5 and 5.6 U/mL for VeroFM, MA104 and RhiLu-hACE2, respectively.

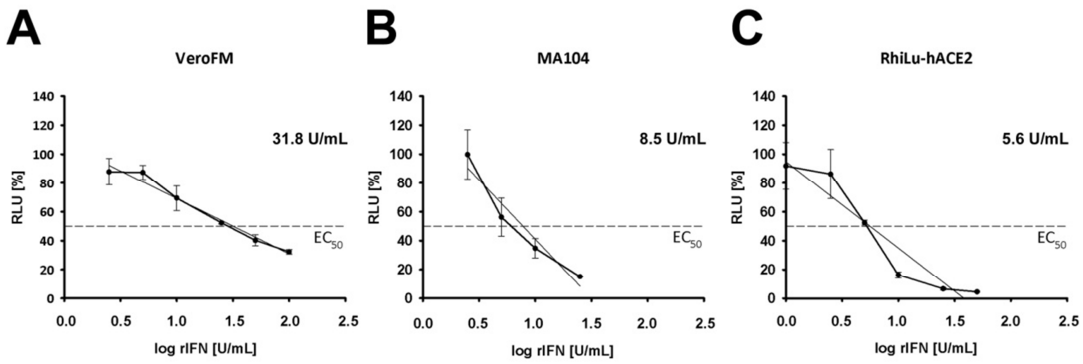

Figure 3.7: Determination of cell line-specific pan-species IFN EC_{50}.
VeroFM (A), MA104 (B), and RhiLu-hACE2 (C) were seeded in 96-well plates, incubated with pan-species IFN concentrations between 0 and 100 U/mL for 7h, and then infected with a *Renilla* luciferase expressing Rift Valley fever virus (RVFV-Ren) at an MOI of 0.01 for 16 h. Cells were lyzed and luciferase expression measured with a luciferase assay in relative light units (RLU). RLU in % were plotted against log rIFN concentrations and EC_{50} values determined at 50% RLU. rIFN = recombinant pan-species IFN.

3.2 Assessment of putative virulence factors of SARS-CoV and SARS-related bat-CoV

The SARS-related bat-CoV Bt-CoV/BM48-31 (BG-CoV) was identified by our working group in *Rhinolophus* bats from Bulgaria, thereby providing valuable genome sequence information on a SARS-related CoV in its natural host and leading to the imminent question of whether this virus poses a threat to humans [88]. Initially BG-CoV and human SARS-CoV Tor2 were compared on genomic level by alignments. As shown in Fig. 3.8 the nucleic acid identity exceeded 90% in most parts of the genome. Major differences were found in genes encoding IFN antagonists, like ORF6 coding for p6. Strikingly, ORF8 was entirely absent.

An amino acid alignment of SARS-CoV p6 (SA-p6) and BG-CoV p6 (BG-p6) shown in Fig. 3.9 revealed that both proteins shared 50% amino acid identity and 78.1% amino acid similarity.

Screening of more bats of the genus *Rhinolophus* from other countries revealed that none of the European SARS-related bat-CoVs carry an ORF8 [Drexler et al., unpublished data], while all SARS-CoVs isolated from Chinese animals (civets and bats) carry the full-length ORF8 [10, 72, 78].

ORF6 and ORF8 were chosen for detailed investigations on their potential to serve as putative virulence factors that might play a role in interspecies transmission. Therefore, overexpression analysis and studies addressing the function of these proteins in the context of the virus replication cycle were conducted.

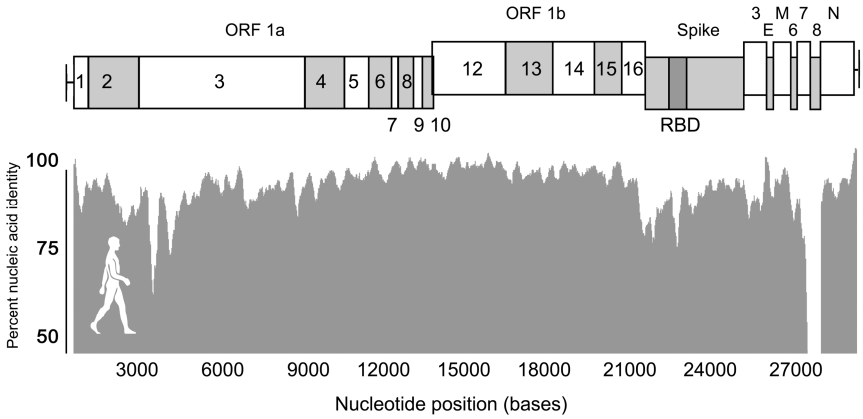

Figure 3.8: Nucleic acid percent identity plot. The genome of the the SARS-related bat CoV BtCoV/BM48-31 was aligned with the human SARS-CoV Tor2 and the percentage of identical nucleic acids were plotted against their genome position.

3.2.1 Characterization of SARS-CoV and SARS-related bat-CoV p6

The mechanism by which SA-p6 inhibits the transport of STAT1 into the nucleus and thus the transcriptional initiation of IFN-stimulated genes was already described by Frieman et al. [59]. The C-terminal 10 amino acids of p6 directly interact with KPNA2, retaining it at the rough ER/Golgi apparatus, which in turn binds to KPNB1, thus depleting the pool of free KPNB1 that is necessary for the transport of the ISGF3:KPNA1 complex into the nucleus [59]. As shown in Fig. 3.9A the C-terminal region of p6 is exposed to the cytosol thus allowing the binding of KPNA2. The amino acid alignment of SA-p6 and BG-p6 in Fig. 3.9B shows that the C-terminal 10 amino acids of both proteins are highly similar. Therefore, BG-p6 might be able to bind human KPNA2. This hypothesis was first investigated in overexpression systems.

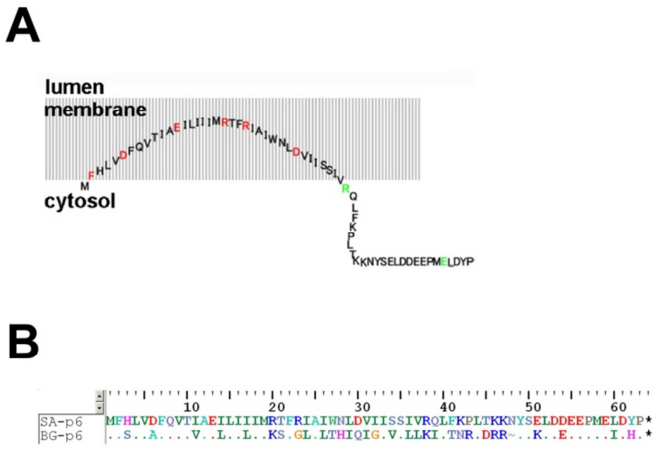

Figure 3.9: SARS-CoV p6 putative conformation and amino acid alignment with bat-CoV p6.
(A) Schematic diagram of the putative conformation of p6 relative to intracellular membranes as described by Zhou et al. [56]. The C-terminus, responsible for the interaction with KPNA2 is exposed to the cytosol, while the N-terminal region, inducing membrane rearrangements is embedded in the membrane. (B) Amino acid alignment of p6 of SARS-CoV and p6 of the SARS-related bat-CoV found in European *Rhinolophus*.

3.2.1.1 Cloning of SARS-CoV and SARS-related bat-CoV ORF6 into expression vector pCAGGS

In order to compare SA-p6 to BG-p6 the corresponding ORF6 were cloned into the pCAGGS expression vector. Both ORF6 were PCR amplified (2.2.3.1) using gene specific primers listed in chapter 2.1.11.1. Each forward primer included an HA-tag, the Kozak consensus sequence and an EcoRI restriction site, while the reverse primers included the NotI restriction site (Fig. 3.10A). The generated PCR product and the expression vector pCAGGS were digested with NotI and EcoRI (2.2.2.13). Digested pCAGGS was dephosphorylated in order to minimize vector religation. All restriction reactions were applied on a preparative agarose gel from which the desired fragments were excised and purified (2.2.2.8; 2.2.2.6). Ligation was done with a 5-fold excess of insert molecules as compared to the vector (2.2.2.14). Transformation of the ligation reaction and plasmid preparations of selected and subcultured colonies was done as described (2.2.6; 2.2.2.4). The size of prepared plasmids was compared to empty pCAGGS vector on an agarose gel (2.2.2.8). Plasmids larger than the empty vector were directly sequenced with specific vector primers (2.1.11.5) for a correct insert. Correct insertion of ORF6 including Kozak sequence and HA-tag is exemplarily shown for SARS-CoV ORF6 in Fig. 3.10A. For each construct of C-terminally HA-tagged ORF6, one plasmid was picked and prepared in midi-scale

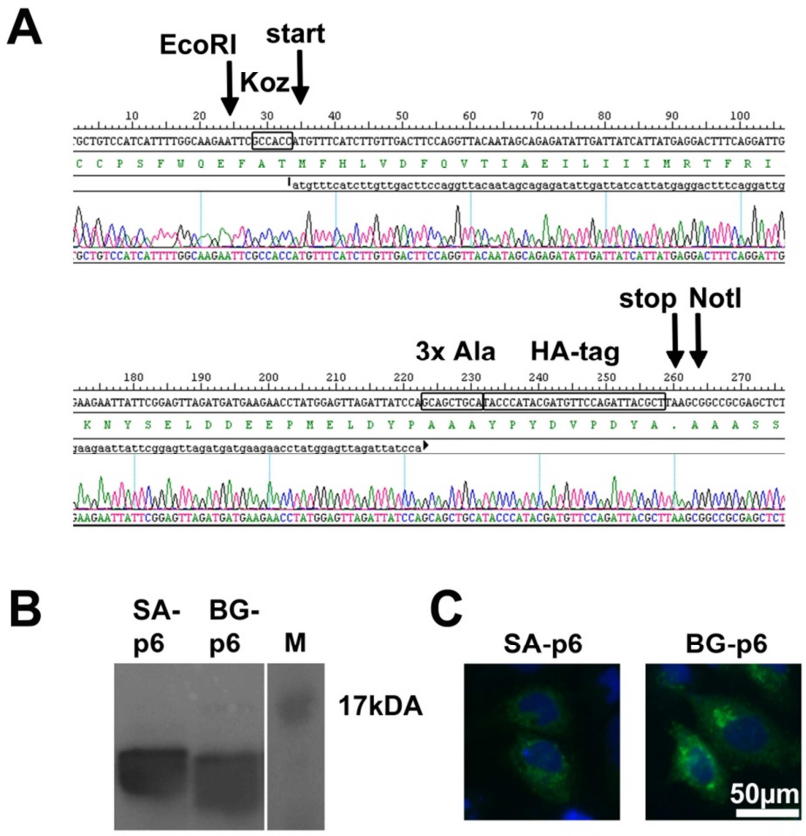

Figure 3.10: Generation and validation of ORF6 expression vector constructs.
Restriction sites EcoRI and NotI as well as the Kozak consensus sequence (Koz) and an HA-tag sequence were added to the ORF6 sequences of SARS-CoV and BG-CoV by PCR. After cloning of the PCR products into pCAGGS vector the constructs were sequenced for correct insertion. The partial chromatogram of the SARS-CoV ORF6 construct is shown (A). Successful expression of SA-p6 and BG-p6 was verified by Western blot analysis (B) and immunofluorescence (C). (B) 293T cells were transfected with 3 µg of either ORF6 expression vector constructs at a 1:2 ratio of FugeneHD. Cells were harvested 24h post transfection and protein expression was detected by Western blot using rabbit-anti-HA primary antibody (1:5000). M = PageRuler™ Prestained Protein Ladder (C) Huh7 cells were seeded on cover glass slips and transfected with 500 ng SAO6- or BGO6-pCAGGS at a 1:3 ratio of FugeneHD. P6 expression was visualized with primary rabbit-anti-HA antibody (1:100) and secondary goat-anti-rabbit-Cy2 antibody (1:200). Nuclei were stained with DAPI (1:1000).

(SARS-CoV ORF6 vector construct "SAO6-pCAGGS" and BG-CoV ORF6 vector construct "BGO6-pCAGGS").

Expression and cellular localization of tagged proteins might be altered by the tag in comparison to the untagged proteins. Successful C-terminal HA-tagging of SARS-CoV p6 has already been described [59] but was verified again for the constructs produced here. SAO6- and BGO6-pCAGGS were therefore chemically transfected into 293T and Huh7 cells (2.2.1.2). 293T cells

were used for Western blot analysis because of their high transfection efficiency. The predicted molecular masses of SA-p6 and BG-p6 are 8.6 and 8.4 kDa, respectively. Both proteins were detected by Western blot analysis though at masses lower than 17 kDa but higher than 10 kDa when compared to the protein marker. Proteins detected at masses other than predicted is a common phenomenon and is frequently due to the fact that protein markers only provide approximate protein masses. Huh7 cells were used for IF due to their relatively large size, which facilitates the visualization of expressed proteins. As shown in Fig. 3.10C both p6 were strongly expressed in the cytoplasm of transfected cells.

After verification of the functionality of the plasmids SA-p6 and BG-p6 could be compared in different overexpression experiments.

3.2.1.2 Cellular localization of SA-p6 and BG-p6 in human and bat cells

SA-p6 is known to localize at the endoplasmatic reticulum/Golgi membrane of primate cells [59]. In order to determine if this is also true for BG-p6 a subcellular colocalization study was performed by IF assay in human cells. In addition, bat cells were included to investigate differences in subcellular localizations. Human hepatocarcinoma (Huh7) cells and RhiLu-hACE2 cells were transfected with SAO6- and BGO6-pCAGGS as described in chapter 2.2.1.2 and prepared for IF (2.2.7.4) 24h post transfection.

Both proteins SA-p6 and BG-p6 were expressed in the cytoplasm of transfected human and bat cells as shown in Fig 3.11. The Golgi apparatus of Huh7 cells was visualized by co-staining with a Golgi protein marker antibody showing a characteristic perinuclear distribution. SA-p6 and BG-p6 partially overlapped with the Golgi staining. In RhiLu-hACE2 cells proteins SA-p6 and BG-p6 appeared to localize more clearly to single regions which could be co-stained with the Golgi marker. However, it was shown that both proteins partially colocalize with a Golgi marker in Huh7 and RhiLu-hACE2 cells. Because both proteins showed a similar expression pattern in human cells and because sequence data on bat cellular proteins were lacking, further overexpression studies on SA-p6 and BG-p6 were done in primate cells only.

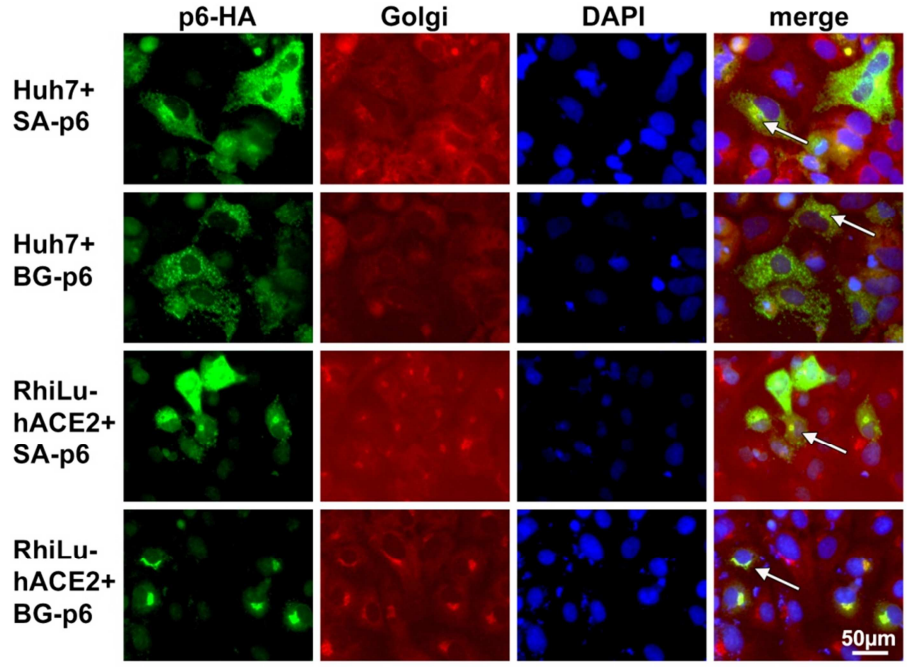

Figure 3.11: Colocalization of SA-p6 and BG-p6 with the Golgi apparatus of human and bat cells. To investigate the subcellular distribution of SA-p6 and BG-p6 in human Huh7 cells in comparison to bat RhiLu-hACE2 both cell lines were transfected with 500 ng of each HA-tagged O6 plasmid at a 1:3 ratio of FugeneHD. 24h post transfection, cells were fixed and labeled with primary rabbit-anti-HA antibody (1:100) and secondary goat-anti-rabbit-Cy2 antibody (1:200) for localization of p6 and mouse-anti-Golgi (1:100) and goat-anti-mouse_Cy3 (1:200) for visualization of the Golgi apparatus. Nuclei were stained with DAPI (1:1000).

3.2.1.3 Colocalization of SA-p6 and BG-p6 with human karyopherins

It has been described that SA-p6 binds directly to cellular KPNA2 thus inhibiting the nuclear import of ISGF3 [59]. In the following experiment the question was addressed, of whether BG-p6 also retains KPNA2 at the ER/Golgi. The cell line was changed to primate kidney cells (VeroFM) as follow-up studies with recombinant SARS-CoV (3.2.2) would be done in those highly susceptible cells. VeroFM cells were cotransfected with either SAO6- or BGO6-pCAGGS in addition to FLAG-tagged KPNA1- or KPNA2-pCAGGS (a kind gift from Megan Shaw, Mount Sinai Medical Center, New York) as described in chapter 2.2.1.2.

As expected, KPNA2 was retained in the cytoplasm of the cell in presence of SA-p6 (second row of Fig. 3.12). According to published data, KPNA1 had a nuclear distribution (Fig. 3.12 first row). In fact, BG-p6 was similarly able to inhibit the nuclear translocation of human KPNA2 (Fig. 3.12 third row), but not of KPNA1 (Fig. 3.12 fourth row).

These results indicate that p6 derived from a bat CoV is able to interfere with the same human transport protein as its hCoV counterpart, suggesting a potentially similar mechanism in antagonizing the cellular IFN signaling pathway.

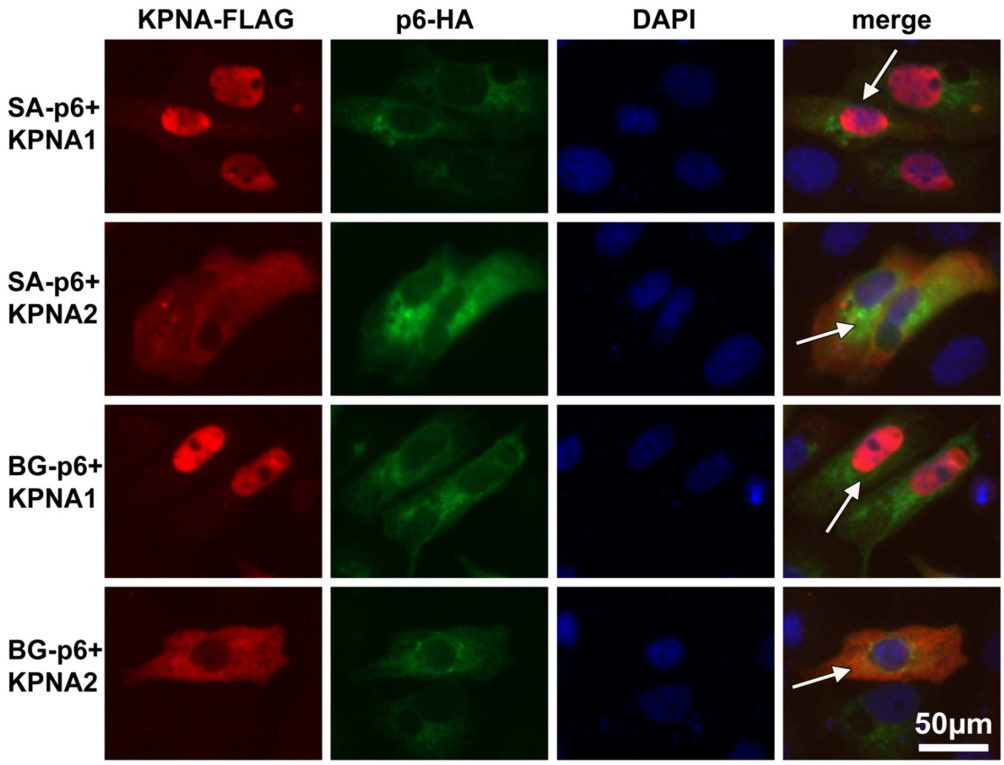

Figure 3.12: Colocalization of SA-p6 and BGp6 with KPNA2.
For colocalization of p6 with human karyopherins VeroFM cells were transfected with 250 ng HA-tagged SAO6 or BGO6 plasmid and 250 ng FLAG-tagged KPNA1 or KPNA2 plasmid with FugeneHD at a ratio of 1:3. 24h post transfection, cells were fixed in 4% PFA and labeled with rabbit-anti-HA (1:100) and mouse-anti-FLAG (1:100). Anti-HA antibody was visualized with goat-anti-rabbit-Cy2 (1:200) secondary antibody. Anti-FLAG antibody was visualized with goat-anti-mouse-Cy3 antibody (1:200) secondary antibody. Nuclei were stained with DAPI (1:1000).

3.2.1.4 Inhibition of STAT1 nuclear translocation upon IFN stimulation by SA-p6 and BG-p6 in primate cells

In order to quantify and compare the IFN-antagonistic abilities of SA-p6 and BG-p6 a STAT1-translocation assay was performed. STAT1 is part of the ISGF3 complex and is rapidly transferred to the nucleus upon IFN stimulation. In this assay the capability of SA-p6 and BG-p6 to inhibit this STAT1 translocation after IFN stimulation was determined. VeroFM cells were transfected with SAO6-, BGO6-, or empty pCAGGS vector together with GFP-tagged STAT1 (2.2.1.2). 24h post transfection cells were stimulated with pan-species IFN or left untreated as a negative control. As shown in Fig. 3.13A STAT1 was evenly distributed in the cytoplasm and nucleus of IFN-untreated cells in the absence of either types of p6. Upon IFN treatment STAT1 was more concentrated within the nucleus. In the presence of SA-p6 and BG-p6 STAT1 was clearly retained in the cytoplasm. In order to quantify this effect three IF pictures were taken randomly from each setting at low magnification. A total of 50 positively transfected cells per picture were counted and analyzed for STAT1 translocation. Cells where STAT1 was found evenly distributed between nucleus and cytoplasm were defined as "STAT1 translocated". Cells where STAT1 was found only in the cytoplasm were defined as "no STAT1 translocation". The percentage of cells without STAT1 translocation was calculated and compared for each setting (Fig. 3.13B). After IFN stimulation almost all cells showed a translocation of STAT1 into the nucleus. In the presence of either protein STAT1 translocation after IFN stimulation was greatly reduced. It appeared that BG-p6 was slightly more efficient than SA-p6 in inhibiting the transport of STAT1. These results further support the previous finding that the bat CoV-derived BG-p6 is equally functional in primate cells as its hCoV counterpart SA-p6.

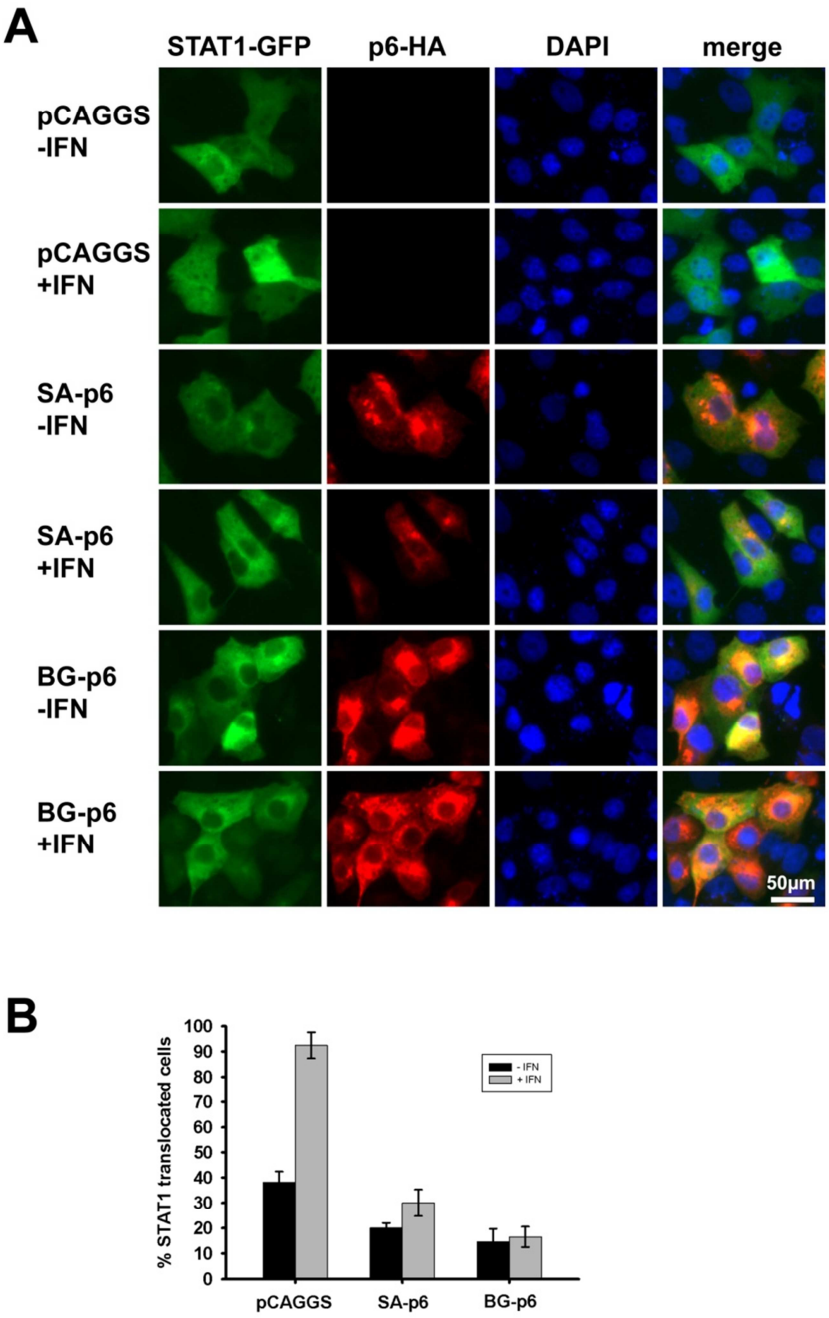

Figure 3.13: Inhibition of nuclear translocation of STAT1-GFP by SA-p6 and BG-p6.
(A) VeroFM cells were transfected with 250 ng SAO6, BGO6, or empty pCAGGS plasmid in addition to 250 ng STAT1-GFP plasmid with X-tremeGENE transfection reagent at a ratio of 1:3. 24h post transfection, cells were treated with 1000 U/mL pan-species IFN for 1 h. Cells were then fixed in 4% PFA and labeled with rabbit-anti-HA (1:100) primary antibody and goat-anti-rabbit-Cy3 (1:200) secondary antibody. Nuclei were stained with DAPI (1:1000). (B) Pictures were taken from three sections of each setting, a total of 50 cells per picture were counted for translocation of STAT1-GFP into the nucleus.

3.2.2 Characterization of BG-p6 in the full virus context

In overexpression analysis BG-p6 exhibited similar functions as its counterpart SA-p6. With the help of the SARS-CoV reverse genetics system a chimeric recombinant SARS-CoV carrying ORF6 from the SARS-related bat-CoV was generated next, BGO6-rSCV. In addition, a recombinant SARS-CoV lacking ORF6 was constructed to serve as a control virus. This was done to give evidence that observed effects can be allocated exclusively to ORF6.

3.2.2.1 Generation of an rSCV carrying the SARS-related bat CoV ORF6

SARS-CoV ORF6 is located within subclone pEF as shown in Fig. 3.14B. To exchange SARS-CoV ORF6 with its homologue from the SARS related bat-CoV an overlap extension PCR was designed. The generated amplicon consisted of the BG-CoV ORF6 and flanking SARS-CoV wild type sequences. This new chimeric sequence was introduced into subclone pEF via two unique restriction sites (BamHI and NotI). The strategy of the overlap extension PCR is depicted in Fig. 3.14A. Primers used in these PCRs are listed in chapter 2.1.11.1. Fig. 3.14B shows the vector map of subclone pEF and the unique restriction sites of BamHI and NotI for introduction of the PCR product.

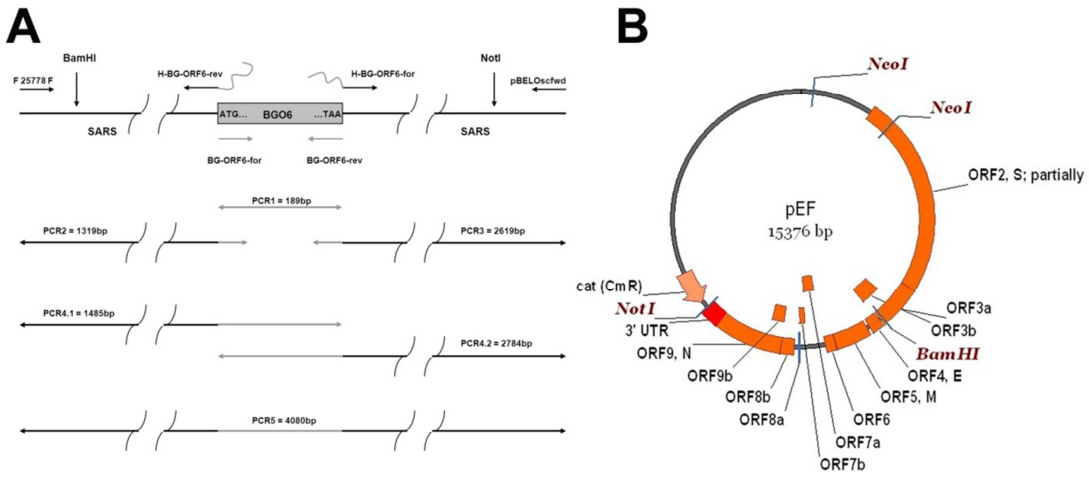

Figure 3.14: BGO6-rSCV cloning strategy.
(A) Overview of the BGO6 cloning strategy. PCR1 amplified the complete BGO6, while PCR2 and PCR3 were done with primers that added additional BG specific sequences to the 3' and 5' ends of the amplicons. Amplicons from PCR4.1 and PCR4.2 could be amplified using products of PCR1 and PCR2 or PCR1 and PCR3. PCR5 amplicons were generated with either PCR4.1 and PCR3 or PCR4.2 and PCR2. (B) Vector map of subclone pEF with single cutters NotI and BamHI for introduction of the overlap extension PCR product.

For cloning of the BG-CoV ORF6 the ORF6 sequence was required to be generated from bat feces. Therefore, viral RNA was extracted from bat feces stored in RNA later and cDNA was synthesized with a specific RT primer binding 55 nts downstream of the ORF6 stop codon (2.2.2.1; 2.2.2.2). The cDNA was used for amplification of the entire ORF6 represented by amplicon PCR1 from the overlap extension PCR shown in Fig. 3.14A (2.2.3.1). The flanking sequences were amplified directly from subclone pEF. Amplicon PCR2, upstream of SARS-CoV ORF6, was generated with a SARS-CoV specific reverse primer that added BG-CoV ORF6 sequence to the 3'-end of the PCR product. Amplicon PCR3, which lay downstream of SARS-CoV ORF6, was generated with a SARS-CoV specific forward primer that added BG-CoV ORF6 sequence to the 5'-end of the PCR product. These newly added BG-CoV ORF6 sequences created overlapping regions to the PCR1 that were used for binding in the subsequent overlap extension PCRs. Template amplicons for the overlap extension PCRs are shown in Fig. 3.15A.
Three different amplicons should be generated in the first round of overlap extension PCR. Amplicon PCR4.1 should be generated with templates PCR1 and PCR2. Amplicon PCR4.2 was to be produced with PCR1 and PCR3 as templates. In addition, it was attempted to create amplicon PCR5 by directly fusing PCR1, PCR2 and PCR3. As described in chapter 2.2.3.1.1 templates were combined and serially diluted. Primers for the corresponding amplicons were used as depicted in the cloning strategy in Fig. 3.14A. The results of the extension PCRs are

shown in Fig. 3.15B. PCR4.1 was successfully amplified without the generation of non-specific fragments. PCR4.2 was only generated in minor amounts and a by-product of about 300 bp appeared in relatively large quantities. A direct amplification of PCR5 was not achieved. Therefore, PCR4.1 was used for the second round of overlap extension PCR.

PCR4.1 and PCR3 were combined, serially diluted and subjected to PCR amplification. Amplicons are shown in Fig. 3.15C. The amplicon PCR5 was successfully generated. The yield of the desired amplicon and the reduction of non-specific PCR products were optimal when the templates were diluted 1:10. This PCR setup was used to generate high amounts of PCR5 for enzymatic digestion.

Amplicon PCR5 and subclone pEF were digested with BamHI and NotI (2.2.2.13). In the case of amplicon PCR5 this led to fragments with predicted lengths of 3,702 bp, 267 bp and 111 bp. Subclone pEF was cut into fragments of 11,671 bp and 3,705 bp in length. Successful digestion was verified by gel electrophoresis (2.2.2.8) shown in Fig. 3.15D. The 11.7 kb fragment of pEF contained the entire pBeloBAC11 backbone including the resistance gene. To avoid false positive clones due to relegation, the backbone was dephosphorylated (2.2.2.13). The BG-CoV ORF6 is one codon shorter than that of SARS-CoV ORF6. Therefore the insert from PCR5 comprised only 3,702 bp, while the fragment cut out from pEF was 3,705 bp in length. Both restriction reactions were separated on a preparative agarose gel and the correct fragments for ligation were excised and extracted (2.2.2.6; 2.2.2.14). Colonies grown after transformation were prepared for plasmid isolation in mini-scale (2.2.6; 2.2.2.4). Plasmids were analyzed for their size on an agarose gel in comparison to subclone pEF. All analyzed plasmids showed the same length as pEF (data not shown) but eventually only one plasmid was chosen for sequencing (sequencing PCRs, PCR conditions and sequencing primers are listed in table 2.1). Special attention was paid to the region between BamHI and NotI. The introduced fragment was exclusively generated by PCR and was therefore subjected to several amplification cycles. The probability of PCR-based mutations was thereby increased. The selected plasmid "BGO6-pEF-K1" showed no undesired mutations and was prepared in midi-scale for the assembly of a full-length clone as described in chapters 3.1.1.2 and 3.1.1.3.

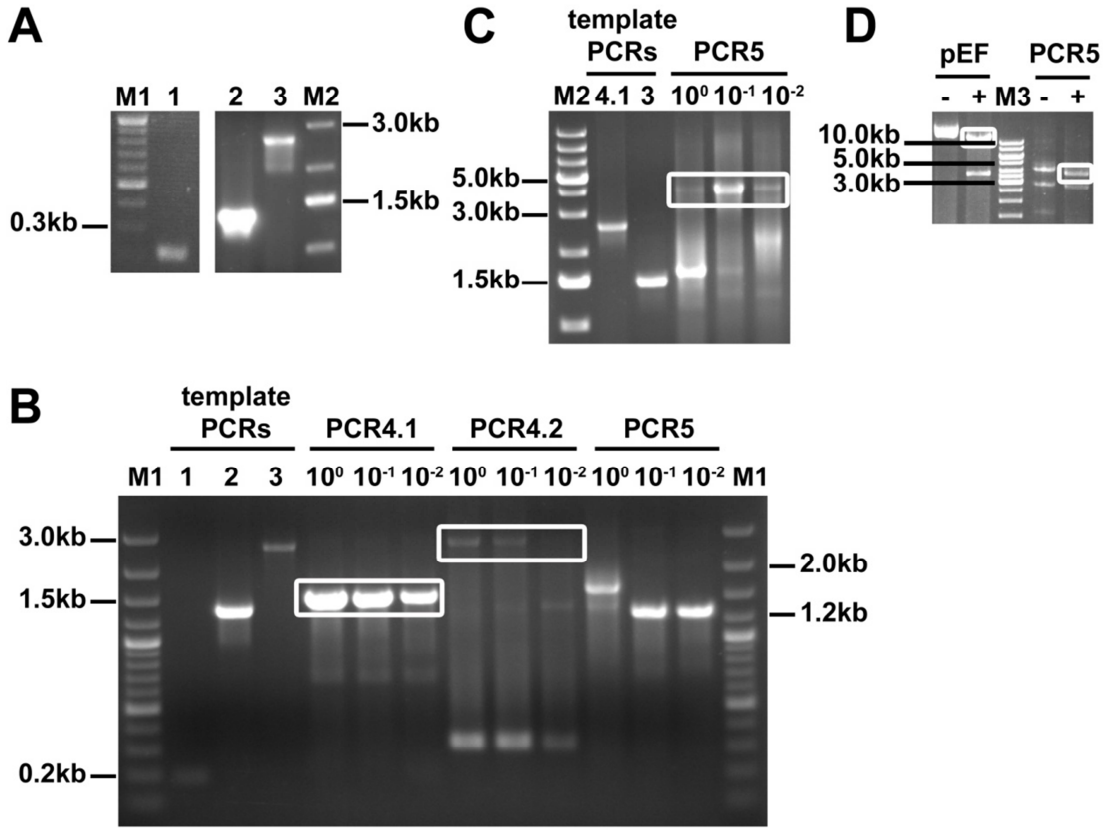

Figure 3.15: Overlap extension PCRs and restriction digests for the cloning of BGO6 into subclone pEF.

(A) Generation of templates for overlap extension PCR. PCR1 (189 bp) was amplified using BGO6 specific primers. Template cDNA was synthesized from viral RNA isolated out of bat feces. PCR2 (1.3 kb) and PCR3 (2.6 kb) were directly amplified from subclone pEF. (B) First round extension PCR. PCR1 and PCR2 were mixed 1+1 and serially diluted 10^{-1} and 10^{-2} to serve as template in the extension PCR generating PCR4.1 (1.5 kb). PCR1 and PCR3 were used as templates for PCR4.2 (2.8 kb) and PCR1+PCR2+PCR3 were used as templates for PCR5 (4.1 kb). (C) Second round extension PCR: PCR4.1 and PCR3 were mixed 1+1 and serially diluted 10^{-1} and 10^{-2} to serve as template in the second round extension PCR generating PCR5 (4.1 kb). (D) Digestion of pEF and PCR5 for introduction of BGO6 into subclone pEF. PCR5 and pEF were digested with BamHI and NotI. The 11.7 kb fragment of pEF and the 3.7 kb fragment of PCR5 were used for subsequent ligation. "-" = undigested DNA; "+" = double digested DNA. Generally, 5 µL PCR product or 200 ng plasmid DNA were applied on one lane of a 0.8% agarose gel. M1 = 100 bp DNA ladder plus; M2 = 1 kb DNA ladder plus; M3 = 1 kb DNA ladder.

3.2.2.2 Generation of an rSCV with a deleted ORF6

It was shown for CoVs that up- and downstream elements of the TRS are important for virus replication and transcription [24, 112]. In particular the generation of subgenomic mRNAs relies on a correct genomic context. By deleting a complete ORF the transcription of subgenomic mRNAs of neighboring ORFs might be ablated. In case of ORF6, transcription regulation of the membrane coding ORF5 and ORF7 might be altered by deleting the ORF6 sequence.

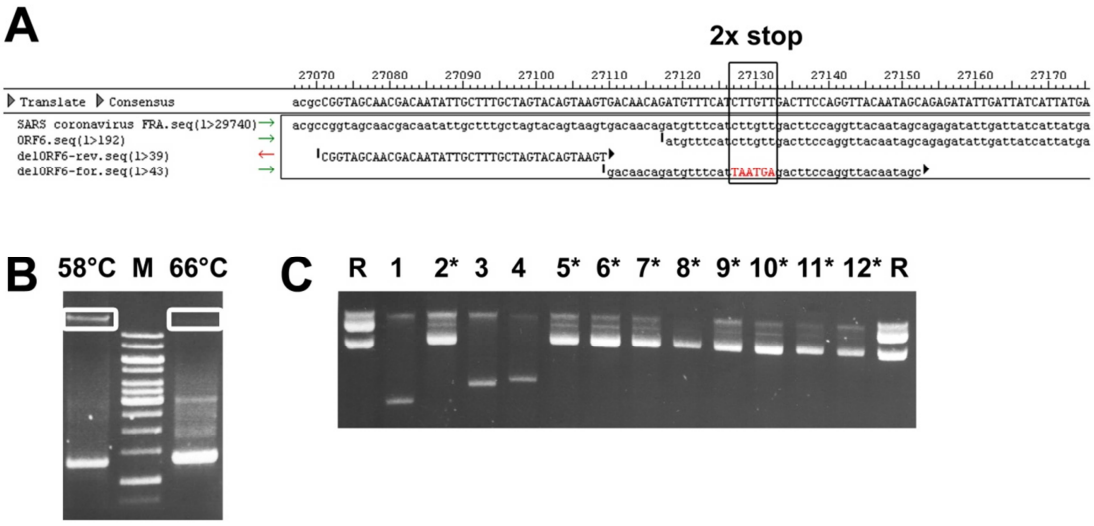

Figure 3.16: Deletion of ORF6 within subclone pEF by site-directed mutagenesis PCR.
(A) Codons 4 and 5 of SARS-CoV ORF6 were exchanged by a double stop codon via site-directed mutagenesis to prevent translation of protein 6, thus generating an ORF6 deletion mutant. (B) 5' phosphorylated primers, of which the forward primer carried the double-stop codon, were used for amplification of the entire pEF yielding an amplicon of 15.4 kb. Annealing temperatures of 58°C and 66°C were compared in order to minimize non-specific PCR products. (C) Ligation of the PCR product yielded a high number of plasmids with the same size as the reference plasmid (R) pEF. Plasmids of correct size are marked with "*".

Therefore ORF6 was not completely deleted but provided with a double stop codon at amino acid positions 5 and 6 as shown in Fig. 3.16A, leading to the translation of a shortened non-sense peptide.

The double-stop codon was introduced into subclone pEF by site-directed mutagenesis (2.2.3.3). Mutation primers were designed as shown in Fig. 3.16A. The 5' phosphorylated forward primer contained the double-stop codon in the middle of its 43nt sequence. It was essential that the forward and reverse primers were placed end-to-end in correspondence with the template strand. Nucleotide gaps between both primers would result in deletion mutations. Using this primer

design the whole pEF was amplified. Primer annealing temperatures of 58°C and 66°C were compared. It was expected that a higher annealing temperature would result in more specific primer binding and therefore less non-specific PCR products. Conversely, at the low temperature the PCR product of 15,376 bp was generated more efficiently and with lesser non-specific products (Fig. 3.16B). It was assumed that the non-specific product did not contain enough sequence information to give rise to false positive colonies. The amplicon was therefore not purified. Ligation of the unpurified amplicon was done as described (2.2.3.3). Plasmids of selected and subcultured colonies were screened for correct size in comparison to pEF. As shown in Fig. 3.16C, the yield of plasmids with the correct size was reasonably high. Prepared plasmids were first screened for the presence of the double-stop codon with PCR2 from the sequencing PCRs listed in table 2.1 and primer F 26918 F binding upstream of ORF6. Only one plasmid carried the mutation.

This was most likely due to the presence of pEF in the PCR reaction, since it had not been purified and therefore probably contained some residual amount of pEF. It is also possible that the primer design was not optimal, resulting in the double-stop codon only being incorporated into a small number of amplicons. Due to the high probability of PCR-based undesired mutations within the 15.4 kb amplicon, the whole plasmid was sequenced. No additional mutations were detected and the plasmid (delO6-pEF-K12) was prepared in midi-scale for assembly of the corresponding full-length clone as described in chapters 3.1.1.2 and 3.1.1.3.

3.2.2.3 Rescue and quantification of ORF6 mutant rSCVs

Both ORF6 mutant rSCVs, BGO6-rSCV and delO6-rSCV, were rescued as described in chapter 3.1.1.4. Virus growth was monitored by real-time RT-PCR quantification of viral RNA (2.2.2.1; 2.2.3.2) in a VeroFM cell culture infected with supernatant of electroporated BHK-J cells. The increase of viral RNA over three days of infection is shown in Fig. 3.17A.

Both virus stocks were sequenced for correct mutations. The cDNA was synthesized from viral RNA (2.2.2.2) with a SARS-CoV specific reverse primer and was used as template for a PCR amplifying the genome region around ORF6 (2.2.3.1). Finally, the amplicons were sequenced with primer F 26918 F. Both virus stocks contained recombinant virus with the desired mutation.

Following verification of correct mutations, the newly generated virus stocks were quantified by plaque titration (2.2.1.6). Although both stocks contained equal amounts of viral RNA

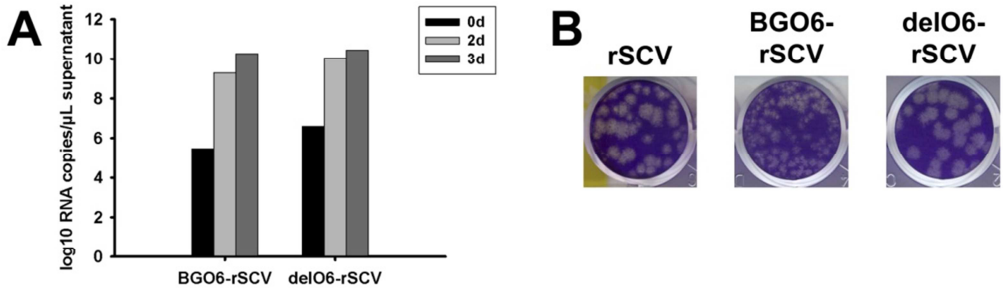

Figure 3.17: Rescue of ORF6 mutant viruses.
(A) Supernatant of BHK-J cells electroporated with *in vitro* transcribed RNA of ORF6 mutated viral genomes was transferred to VeroFM cells for rescue of recombinant virus. Virus growth was measured by real-time RT-PCR. (B) Plaque morphology of BGO6- and delO6-rSCV was compared to rSCV.

(Fig. 3.17A), the quantity of infectious particles of BGO6-rSCV was increased by 10-fold in comparison to delO6-rSCV (data not shown). Genotypically different viruses could give rise to altered plaque morphologies on account of a different phenotype. As shown in Fig. 3.17B plaques produced by BGO6-rSCV were considerably smaller than that of wild type rSCV. On the contrary, plaques of delO6-rSCV were slightly enlarged in comparison to plaques of rSCV. These initial findings on the varying plaque morphology of the ORF6 mutant viruses indicated that the viruses may display further altered phenotypic characteristics. Therefore, both mutant viruses were compared to wild type rSCV for replication differences in a growth kinetic.

3.2.2.4 Growth kinetics of ORF6 mutant viruses

Yount et al. showed that an rSCV lacking ORF6 had no replication disadvantages as compared to wild type rSCV after infection at a high MOI of 1 [60]. On the contrary Zhao et al. reported that the absence of p6 results in decreased virus growth when infection is done at a low MOI of 0.01 [54]. In the present study an MOI of 0.001 was chosen in order to emphasize replication differences between the three ORF6 variants more clearly than previous studies. In addition, this scenario was expected to imitate the early phase of an infection and/or the first animal to human transmission, where virus concentrations would still be low. This scenario was considered representative for the characterization of potential zoonotic risk markers.

VeroFM cells were infected with rSCV, BGO6-rSCV and delO6-rSCV (2.2.1.5). Supernatant was sampled at indicated time points and plaque titrated (2.2.1.6). Results of plaque titration are shown in Fig. 3.18. At 8 and 24h p.i. all three viruses grew to almost identical titers of 2-5x

10^2 PFU/mL and 1x 10^5 PFU/mL, respectively. At 48h p.i. BGO6-rSCV exhibited a 6.5-fold increase of infectious particles as compared to wild type rSCV. At 72 h p.i. replication differences between the three viruses had leveled out.

These results suggested a replication advantage of the recombinant virus expressing p6 of the SARS-related bat-CoV.

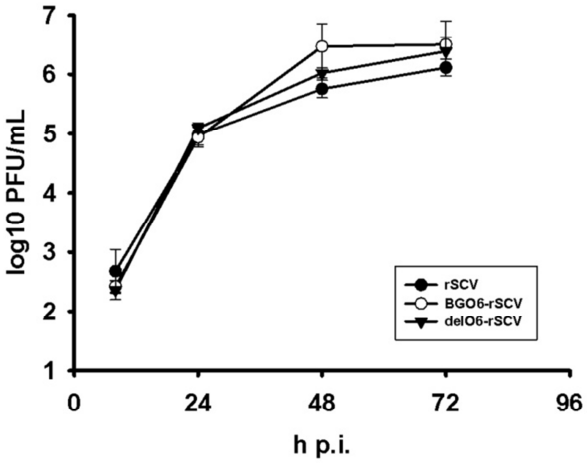

Figure 3.18: Growth kinetics of ORF6 mutant viruses.
VeroFM cells were infected with rSCV, BGO6-rSCV, and delO6-rSCV at an MOI of 0.001. Supernatant was sampled at 8, 24, 48, and 72 h p.i. and virus titers were determined by plaque titration.

3.2.2.5 Growth of ORF6 mutant viruses in primate and bat cells in an anti-viral state

An influence on replication of viruses mutated within the IFN antagonist expressing ORF6 was expected to be seen best in IFN-competent cells put into an anti-viral state by IFN stimulation. VeroFM cells do not secrete IFN but still have functional type I IFN receptors and therefore respond normally to externally applied IFN [113]. MA104 cells possess an intact IFN system [114]. So VeroFM and MA104 cells were chosen as representative primate cell lines. In addition to comparing the three ORF6 variants on primate cells, each virus was compared for its ability to replicate in a bat cell line in comparison to the primate cells. For this purpose the SARS-CoV susceptible and IFN-competent bat cell line RhiLu-hACE2 (3.1.2) was included in the following experiment.

In order to induce an anti-viral state cultures were incubated with their cell line-specific pan-species IFN concentrations. Previous experiments showed that MA104 cells preincubated with 600 U/mL pan-species IFN allowed virus growth which was clearly reduced as compared to untreated cells (data not shown). The corresponding cell line-specific pan-species IFN concentrations for VeroFM and RhiLu-hACE2 cells were calculated with the help of the determined EC_{50} values (3.1.3). The EC_{50} value of VeroFM cells is 3.7-fold higher, while the EC50 value of RhiLu-hACE2 cells is 1.5-fold lower than that of MA104 cells. Therefore, VeroFM cells were treated with 2245 U/mL and RhiLu-hACE2 cells with 395 U/mL pan-species IFN.

The above-described growth kinetic done in VeroFM cells exhibited replication differences at 48h p.i. Kinetics done by other groups rather found differences at earlier time points p.i. This might be due to higher MOIs used in these experiments. However, in order not to bypass the optimal time point, samples were taken at 24 and 48h p.i.

The supernatants sampled at 48h p.i. were first analyzed by real-time RT-PCR (2.2.3.2). The results presented in Fig. 3.19 show that IFN-induced reduction of virus replication had already leveled out in VeroFM and MA104 cells. However, differences in viral RNA load were still obvious on RhiLu-hACE2 cells. Based on these findings supernatants sampled 24h p.i. were plaque titrated for quantification of infectious virus particles 2.2.1.6).

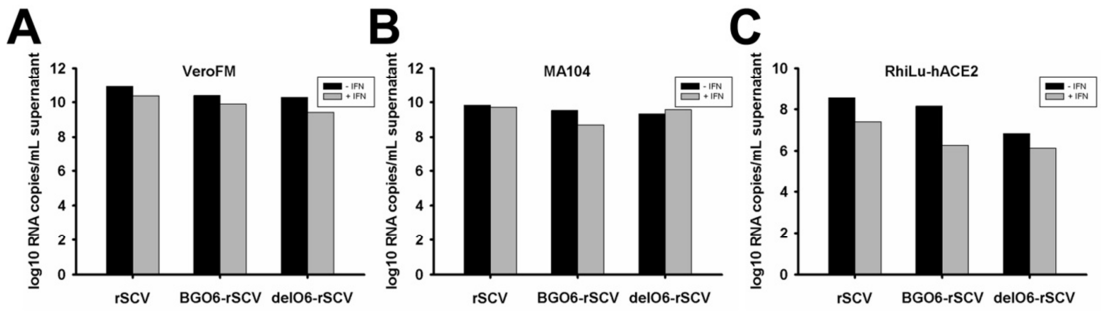

Figure 3.19: Viral RNA load of ORF6 mutant viruses 48h p.i on VeroFM, MA104 and RhiLu-hACE2.
(A) VeroFM, (B) MA104 and (C) RhiLu-hACE2 were infected at an MOI of 0.001 with rSCV, BGO6-rSCV and delO6-rSCV. Viral RNA was extracted from supernatants at 48h p.i. Replication differences of the ORF6 mutant viruses had already disappeared.

Plaque titration, as shown in Fig. 3.20, revealed different overall levels of virus replication in the three cell lines. Virus titers were highest in VeroFM cells, while titers of the same virus in MA104 cells were 10 to 100-fold lower. Virus titers obtained from RhiLu-hACE2 cells were up to 1000-fold lower than from VeroFM cells. Reduced virus growth in MA104 cells as compared to VeroFM cells might be explained by their intact IFN system. Although SARS-CoV is known to antagonize the type I IFN pathway, type III IFNs which use a distinct signaling pathway were found to play a critical role in managing virus replication [115]. A possible explanation could be that MA104 cells with intact type I and III IFN pathways reduced SARS-CoV replication more efficiently than VeroFM cells having only an intact type III IFN system [116]. Reduced overall virus replication in RhiLu-hACE2 cells was already observed during the course of their generation. It is most likely that differences in the cellular processing machinery between bat cells and primate cells could be the cause of inefficient post-translational modifications of viral proteins and virus maturation of a virus that is adapted to primate cells.

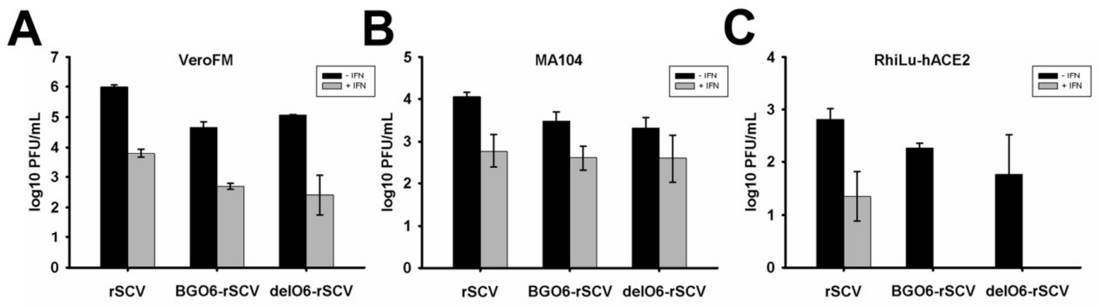

Figure 3.20: Virus growth of ORF6 mutant viruses on primate and bat cells.
VeroFM (A), MA104 (B) and RhiLu-hACE2 (C) were preincubated with cell line-specific pan-species IFN concentrations or medium only for 16 h and infected with rSCV, BGO6-rSCV and delO6-rSCV at an MOI of 0.001 for 24h. Supernatants were plaque titrated for determination of virus titers. Wild type rSCV grew to highest titers on all three cell lines.

Notably, in all three cell lines wild type rSCV grew to higher titers than BGO6-rSCV and delO6-rSCV. BGO6-rSCV and delO6-rSCV grew to similar titers in both primate cell lines. Interestingly, in RhiLu-hACE2 cells delO6-rSCV grew to lower titers than BGO6-rSCV. This replication pattern could be seen even more distinctly at 48h p.i. as shown in Fig. 3.21.

Preincubation of VeroFM cells with pan-species IFN led to a 150- and 100-fold decreased virus growth of rSCV and BGO6-rSCV, respectively. DelO6-rSCV replication was even 260-fold lower. IFN stimulated MA104 cells yielded reduced virus replication of rSCV, BGO6-rSCV and

delO6-rSCV by 15-, 7- and 3-fold, respectively, as compared to un-stimulated cells. This clearly showed that the influence of externally applied IFN on reduction of virus replication was more distinct in IFN-deficient VeroFM cells than in IFN-competent MA104 cells. It was likely that the already reduced virus replication in MA104 cells could only be slightly reduced by additional IFN. Consequently, in VeroFM cells, having a supposedly diminished IFN response to virus infection, the presence of external IFN resulted in a strong response and therefore had a comparably high impact on virus replication.

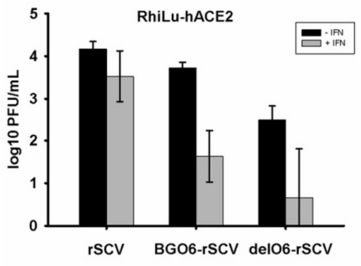

Figure 3.21: Virus replication of ORF6 mutants on RhiLu-hACE2 cells 48h p.i.
RhiLu-hACE2 cells were preincubated with their cell line-specific pan-species IFN concentration and infected with the three ORF6 mutant viruses as described above. Supernatants were sampled 48h p.i. and plaque titrated. 48h p.i. wild type rSCV grew to the highest titer, while delO6-rSCV replicated the least efficiently.

The impact of IFN treatment prior to infection was the highest in VeroFM cells, but in this scenario not relevant because viruses were to be compared within one cell line and not between different cell lines.

In summary, growth of the three viruses was equally inhibited in VeroFM cells by IFN pretreatment. In MA104 cells replication of rSCV was reduced to a greater extent than that of BGO6-rSCV and delO6-rSCV. However, pretreatment with IFN of RhiLu-hACE2 cells led to a drastic inhibition of BGO6-rSCV replication as compared to wild type rSCV, which could be seen best 48h p.i (Fig. 3.21). Replication of delO6-rSCV was inhibited more efficiently than rSCV but to a lesser extent than BGO6-rSCV. These data suggest a general attenuating effect when the BG-p6 was expressed in the context of viral replication.

3.2.3 Impact of ORF8 integrity on virus replication

The most obvious difference in genome organization between Asian SARS-related bat-CoVs, the human pandemic SARS-CoV and the Bulgarian SARS-related bat-CoV (Bt-CoV/BM48-31) sequenced by our group is the integrity of ORF8 [88]. While Asian bat-CoVs and early human isolates carry one single full-length ORF8, ORF8 isolated during the human pandemic adapted a 29nt-deletion thereby splitting it into two separate open reading frames, ORF8a and 8b [10, 72, 78]. In the Bulgarian bat-CoV ORF8 is entirely absent. Sampling of more *Rhinolophus* bats from Spain, Italy and Slovenia revealed that ORF8 was missing in all European SARS-related bat-CoVs (Fig. 3.22, unpublished data).

A gene and its respective protein, undergoing such drastic mutations might serve as a virulence factor and was therefore studied in the context of viral replication. With the help of the SARS-CoV reverse genetics system, two ORF8 mutants were generated. O8full-rSCV carried the untruncated ORF8 without the 29nt-deletion while delO8-rSCV lacked the entire ORF8 sequence.

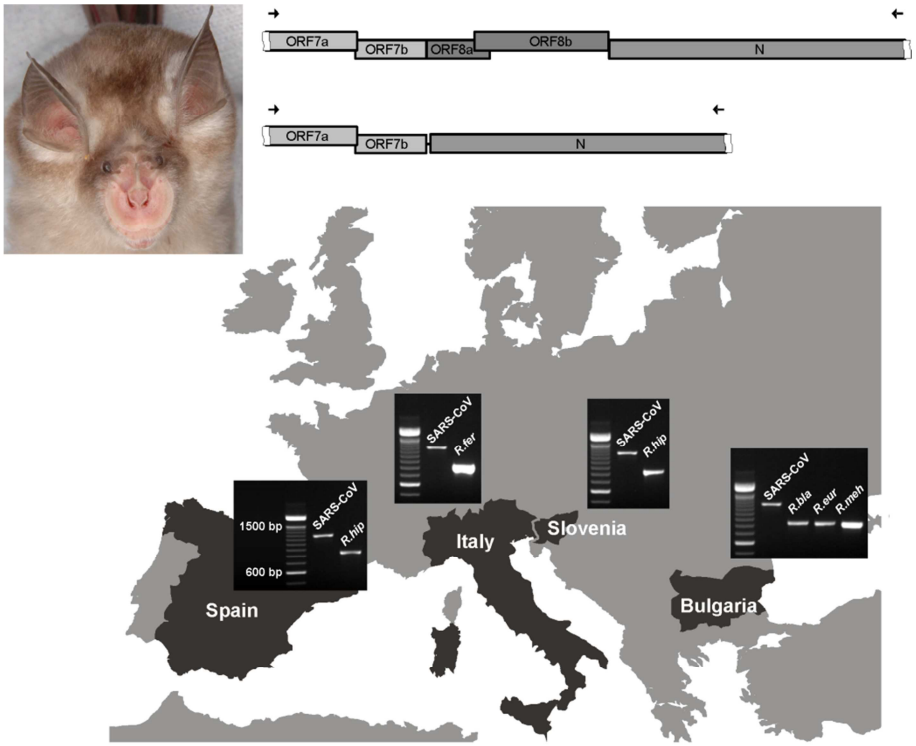

Figure 3.22: ORF8 integrity of European SARS-related bat-CoVs. Feces from *Rhinolophus* bats from Spain, Italy, Slovenia and Bulgaria were sampled. PCR amplification of the ORF8 region revealed that all SARS-related bat-CoVs lack ORF8. R.hip = *Rhinolophus hipposideros*, R.fer = *Rhinolophus ferrumequinum*, R.bla = *Rhinolophus blasii*, R.eur = *Rhinolophus euryale*.

3.2.3.1 Completion of ORF8 for the generation of O8full-rSCV

The missing 29nts that reconstitute SARS-CoVs ORF8a and ORF8b to a single ORF8 were introduced by a two-step overlap extension PCR (2.2.3.1.1) as depicted in the cloning strategy in Fig. 3.23A. The reverse primer of PCR1 and the forward primer of PCR2 contain the additional 29nts which partially overlap for annealing in the subsequent extension PCR (Fig. 3.23B). The extended PCR product covered the region between restriction sites BamHI and NotI enabling

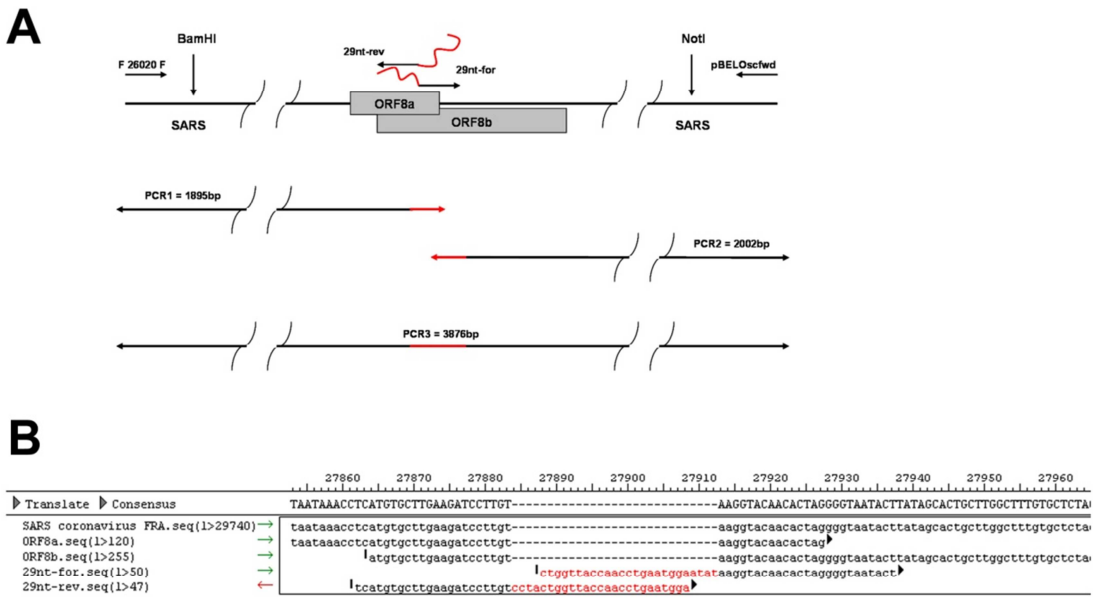

Figure 3.23: Cloning strategy for generation O8full.
(A) The 29 nucleotides (nt), fusing SARS-CoVs ORF8a and 8b to one single full-length ORF8, were introduced by overlap extension PCR. PCR1 amplicon was generated using primer F 26020 F and the reverse primer 29nt-rev, which carried 24 of the 29nts. PCR2 amplicon was generated with the forward primer 29nt-for, which carried 25 of the 29nts, and pBELOscfwd. The overlapping region of 21 nt was used for annealing of PCR1 and PCR2 in the subsequent extension PCR. Introduction of the mutated fragment into subclone pEF was done via restriction sites BamHI and NotI. (B) The alignment illustrates the primer design for the O8full cloning strategy.

the introduction of the mutated SARS-CoV sequence into subclone pEF as described for BGO6-pEF in chapter 3.3.1.

Amplicons PCR1 and PCR2, shown in Fig. 3.24A, were generated from subclone pEF. The forward primer of PCR1 and the reverse primer of PCR2 were 5' phosphorylated for subsequent cloning of the extension PCR product into pEZ^{TM} BAC as described in chapter 2.2.4. For the fusion of amplicons PCR1 and PCR2 to amplicon PCR3, both template PCRs were combined in equal amounts and serially diluted before performing PCR amplification. Generation of

amplicon PCR3 was successful in each dilution as shown in Fig. 3.24B. Subclone pEF served as a PCR positive control. Amplicon PCR3 obtained from the template PCR 10^{-2} dilution was used for cloning into pEZ™ BAC vector (2.2.4). The vector insert was sequenced (2.2.2.10) and the plasmid "O8full-pEZ-K1" prepared in midi-scale (2.2.2.4) for introduction of the full-length ORF8 into subclone pEF. Therefore, plasmids O8full-pEZ-K1 and pEF were successively digested with BamHI and NotI as shown in Fig. 3.24C (2.2.2.13). The pEZ vector contained one additional BamHI site and two additional NotI sites up- and downstream of its multiple cloning site. The digestion with BamHI had already released the complete insert from the vector because

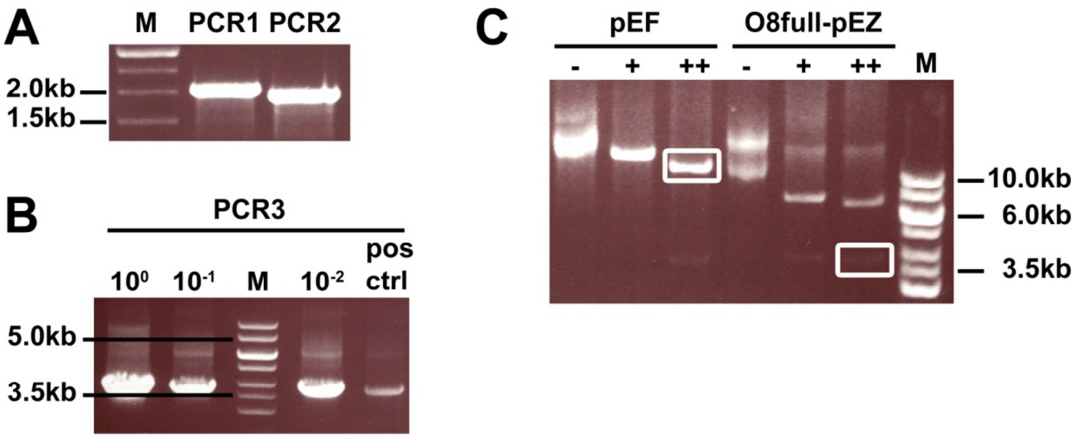

Figure 3.24: O8full extension PCR and cloning into pEZ-BAC.
(A) PCR1 (1.9 kb) and PCR2 (2.0 kb) were combined in equal amounts and serially diluted 10^{-1} and 10^{-2} to serve as templates to generate extension PCR product PCR3 of 3.9 kb (B). Subclone pEF served as PCR positive control. 5 µL of each PCR product were applied per lane on a 0.8% agarose gel to verify successful amplification. (C) PCR3 was first cloned into pEZ™-BAC. Thereafter, the mutated insert was cut out with restriction enzymes BamHI and NotI and inserted into pEF. "+" indicates digestion with BamHI; "++" indicates additional digestion with NotI; M = 1 kb DNA ladder.

the vector-included restriction site is positioned only 46 bp downstream of the insert. This fragment comprising 3,891 bp is shown in the control gel in Fig. 3.24C. After restriction with NotI subclone pEF was dephosphorylated. The 11.7 kb fragment of pEF and the 3.7 kb fragment of O8full-pEZ were excised from a preparative gel, extracted and ligated (2.2.2.8; 2.2.2.6; 2.2.2.14). Colonies selected after transformation were prepared for plasmid isolation in mini-scale (2.2.6; 2.2.2.4). Plasmids were analyzed for their size on an agarose gel in comparison to subclone pEF. Plasmids of the same size as pEF were used as templates for sequencing PCR2 in table 2.1. The PCR products were sequenced for correct mutation of ORF8. All plasmids carried the introduced 29nts within ORF8. One plasmid, O8full-pEF-K1, was fully sequenced

using sequencing PCRs and sequencing primers listed in table 2.1. No undesired mutations were found and the plasmid was prepared in midi-scale (2.2.2.4) and used for assembly of the full-length clone as described in chapters 3.1.1.2 and 3.1.1.3.

3.2.3.2 Deletion of ORF8 for the generation of delO8-rSCV

ORF8a and 8b were deleted from the SARS-CoV genome in two different ways. In the first approach both reading frames were cut out from ORF8as ATG to ORF8bs TAA (variant delO8-1). In the second approach both ORFs were exchanged by the sequence AATAA according to the sequence around the missing ORF8 in the BtCoV/BM48-31 genome (variant delO8-2). The mutations were introduced into a suitable subclone by site-directed mutagenesis as generally described in chapter 2.2.3.3. 5' phosphorylated primers were designed in a way that the forward primers (delORF8-1-for and delORF8-2-for) bound directly downstream of ORF8bs TAA and the reverse primers (delORF8-1-rev and delORF8-2-rev) hybridized directly upstream of ORF8as ATG, amplifying the complete subclone except ORFs 8a and 8b (see Fig. 3.25A).
In order to minimize cloning steps after deletion of ORF8a/b, site directed mutagenesis was done with subclone pDEF and the full-length SARS-CoV clone instead of pEF. In addition, Phusion™ Hot Start DNA Polymerase was compared to Phusion® High-Fidelity DNA Polymerase concerning the enzymes processivities. Therefore, reactions were set up as described in chapter 2.2.3.1 and 2.2.3.3 for the corresponding enzymes. PCR products were applied on an agarose gel shown in Fig. 3.25B. Phusion™ Hot Start DNA Polymerase was not able to amplify any of the templates; while Phusion® High-Fidelity DNA Polymerase yielded distinct amplicons of pDEF (see Fig. 3.25B). Although the hot start DNA polymerase is part of the site-directed mutagenesis kit, its processivity was reduced as compared to the high-fidelity polymerase. When mutating large plasmids it is therefore recommended to switch enzymes. PCR products from template pDEF of both ORF8 deletion variants were used for ligation as per the manufacturer's recommendations in the site-directed mutagenesis kit.

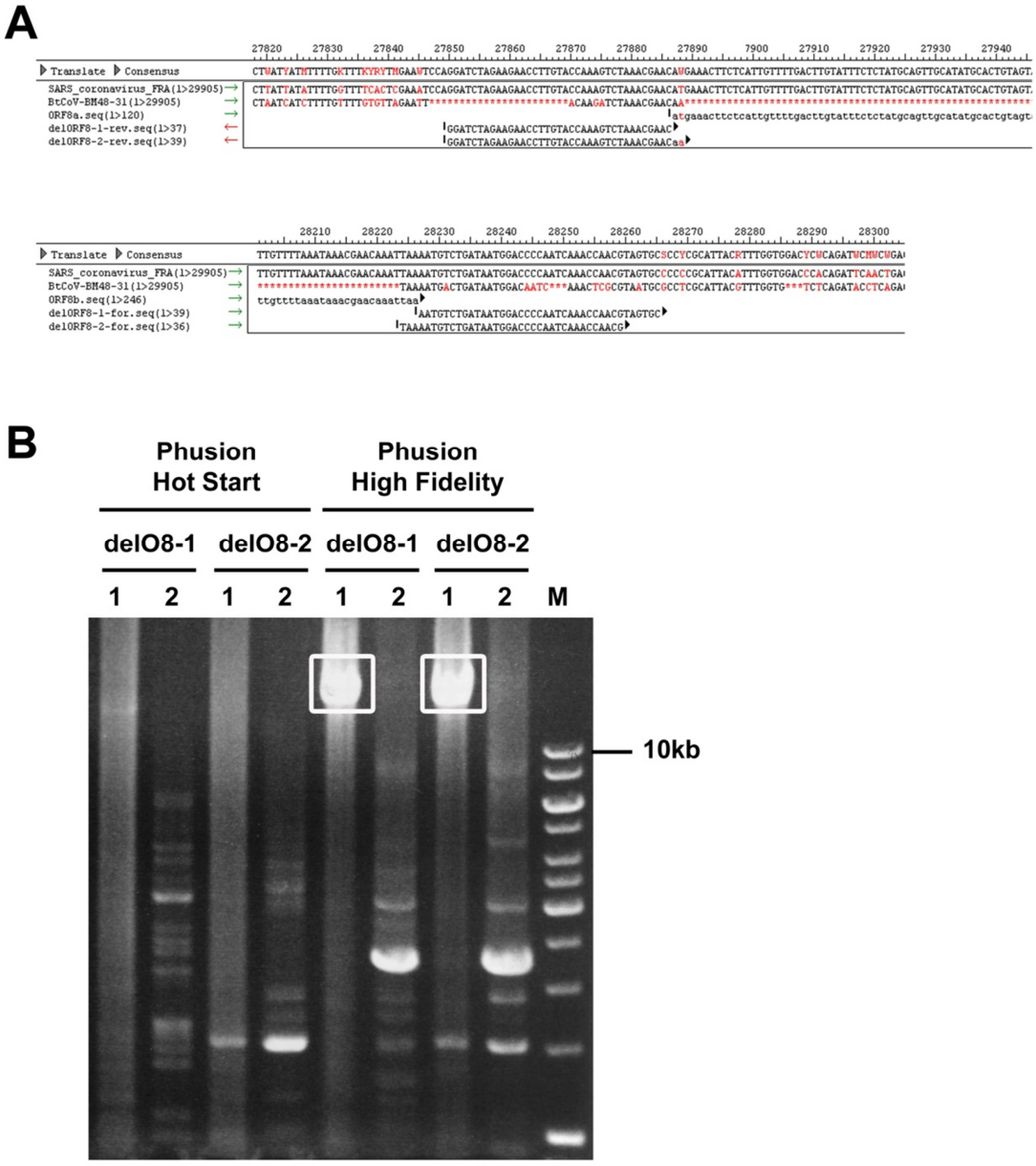

Figure 3.25: DelO8 cloning strategy and mutagenesis PCR.
(A) Alignment of ORF8a/b from SARS-CoV strain Frankfurt-1 with the SARS-related bat-CoV BtCoV-BM48-31. Primers illustrate the two different cloning strategies for the deletion of ORF8a/b. Site-directed mutagenesis PCR with primer pair delORF8-1 entirely deletes ORF8a/b, while primer pair delORF8-2 exchanges ORF8a/b with the sequence "AATAA". (B) Site-directed mutagenesis PCRs with primer pairs delORF8-1 (delO8-1) and delORF8-2 (delO8-2). Mutagenesis PCRs were done on subclone pDEF (1) and the full-length SARS-CoV clone (2). Comparatively, Phusion Hot Start and High Fidelity polymerase were used for amplification. Only the high fidelity polymerase was able to generate PCR amplicons. M = 1 kb DNA ladder.

Transformation of the ligation reactions into in-house produced stbl3 cells (2.2.6) yielded only 5 colonies for the delO8-1 variant and 3 colonies for the delO8-2 variant. This was likely due to the low competence of self-made bacteria but probably also reflects the difficulty of handling of

large DNA fragments. Here, ligation of the PCR product might not have been efficient. All 8 colonies were picked and their plasmids prepared in mini-scale (2.2.2.4). Gel electrophoresis, as shown in Fig. 3.26A, revealed that only 3 colonies of the del-O8-1 variant and 1 colony of the delO8-2 variant carried plasmids of the same size as the pDEF reference plasmid. The shorter plasmids were most likely a result of the ligation of shortened PCR products generated during mutagenesis. One way to circumvent the generation of false positive colonies would be the purification of the mutated PCR product from an agarose gel. This was not done because it was assumed that non-specific PCR products would not contain enough vector sequence for propagation in bacteria.

Plasmids of the correct size were screened by PCR with appropriate primers amplifying the genome region around ORF8. Amplicons would be 5,417 bp for wild type sequence or 5,077 bp and 5,082 bp for delO8-1 and delO8-2, respectively. Two of three delO8-1 plasmids and the single delO8-2 plasmid yielded shortened PCR products as compared to the amplicon from wild type subclone pDEF (Fig. 3.26B). Sequencing of the shortened PCR products revealed that all plasmids were correctly deleted of ORF8. Plasmids "delO8-1-pDEF-K3" and "delO8-2-pDEF-K3" were sequenced using sequencing PCRs and primers as listed in table 2.1. Both plasmids were free of PCR-based undesired mutations and thus prepared in midi-scale (2.2.2.4) for the assembly of the full-length clones as described in chapter 3.1.1.3.

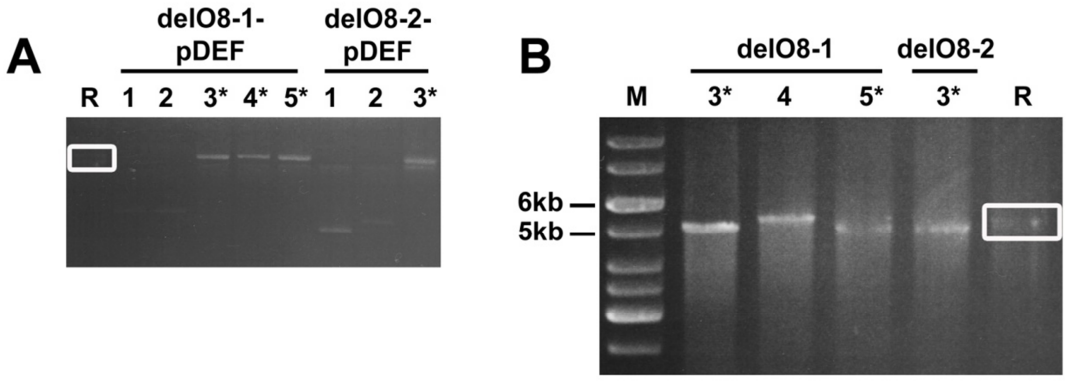

Figure 3.26: DelO8-pDEF plasmid minipreparations and screening PCRs.
(A) Ligation and transformation of the two mutagenesis PCR products yielded only a total of 8 colonies. All colonies were picked and prepared for plasmid minipreparations. 200 ng of each plasmid were applied on one lane of a 0.8% agarose gel and sizes were compared to unmutated pDEF (R). Mutated plasmids of the same size as pDEF are marked "*". (B) These four plasmids were screened in a PCR amplifying the ORF8a/b region. Amplicons would be about 5.1 kb in length when ORF8a/b was deleted successfully and would comprise 5.4 kb when the wild type sequence was used as template (R). Two plasmids of delO8-1 and the single delO8-2 plasmid yielded shortened amplicons (marked "*"). M = 1 kb DNA ladder.

3.2.3.3 Rescue and quantification of ORF8 mutant rSCVs

All ORF8 mutants, O8full-rSCV, delO8-1-rSCV and delO8-2-rSCV, were rescued as described in chapter 3.1.1.4. Virus growth was confirmed by real-time RT-PCR quantification of viral RNA (2.2.2.1; 2.2.3.2). The increase of viral RNA after infection of VeroFM cells with supernatant of electroporated BHK-J cells is shown in Fig. 3.27A. Most interestingly, virus growth of delO8-1-rSCV was greatly delayed as compared to the other viruses. Infection was therefore extended for 1 day. Nonetheless, the amount of viral RNA was still lower as compared to the second ORF8 deletion variant delO8-2-rSCV.

For sequencing of the virus stocks cDNA was synthesized from viral RNA (2.2.2.2) using a specific reverse primer binding downstream of ORF8. The produced cDNA was used in a PCR with a forward primer binding at the downstream end of ORF7a and a reverse primer binding within ORF9 as depicted in Fig. 3.27C. The generated amplicons already provided evidence for either the presence or absence of the correct mutation. As shown in Fig. 3.27C the length of the PCR product was determined by the corresponding ORF8 mutation. Amplicons generated from the respective virus stocks (Fig. 3.27D) were of correct size and their sequence was verified.

Quantification of the newly generated virus stocks was done by plaque titration (2.2.1.6). Morphologies of O8full-rSCV and wild type rSCV plaques were similar as shown in the upper panel of Fig. 3.27B. Notably, the deletion of ORF8 greatly altered the plaque morphology of the rSCVs. As shown in Fig. 3.27B plaques of delO8-1-rSCV are much smaller than those of wild type rSCV. In addition, the discrepancy between viral RNA and infectious particles was considerably higher. Typically, the amount of viral RNA/mL is 10^4-fold higher than PFU/mL. Correspondingly, the first countable amount of plaques of delO8-1-rSCV was expected at a dilution of 10^{-4} but was in fact determined at a dilution of 10^{-2}. Plaques of delO8-2-rSCV were also smaller in size as compared to wild type rSCV but not as small as delO8-1-rSCV plaques. Moreover, the discrepancy between viral RNA and PFU was similar to that of wild type rSCV. These findings strongly suggested that the sequence context around an ORF is of considerable importance to the viability and fitness of SARS-CoV. The virus with a simple deletion of ORF8a/b displayed an impaired growth. But the virus, designed according to the genome organization of the bat-related SARS-CoV, where ORF8a/b was replaced by a short context sequence, exhibited robust virus growth.

Because of the better fitness and the more profound genome organization, further cell culture experiments were only done with delO8-2-rSCV, which is in the following text only referred to as delO8-rSCV.

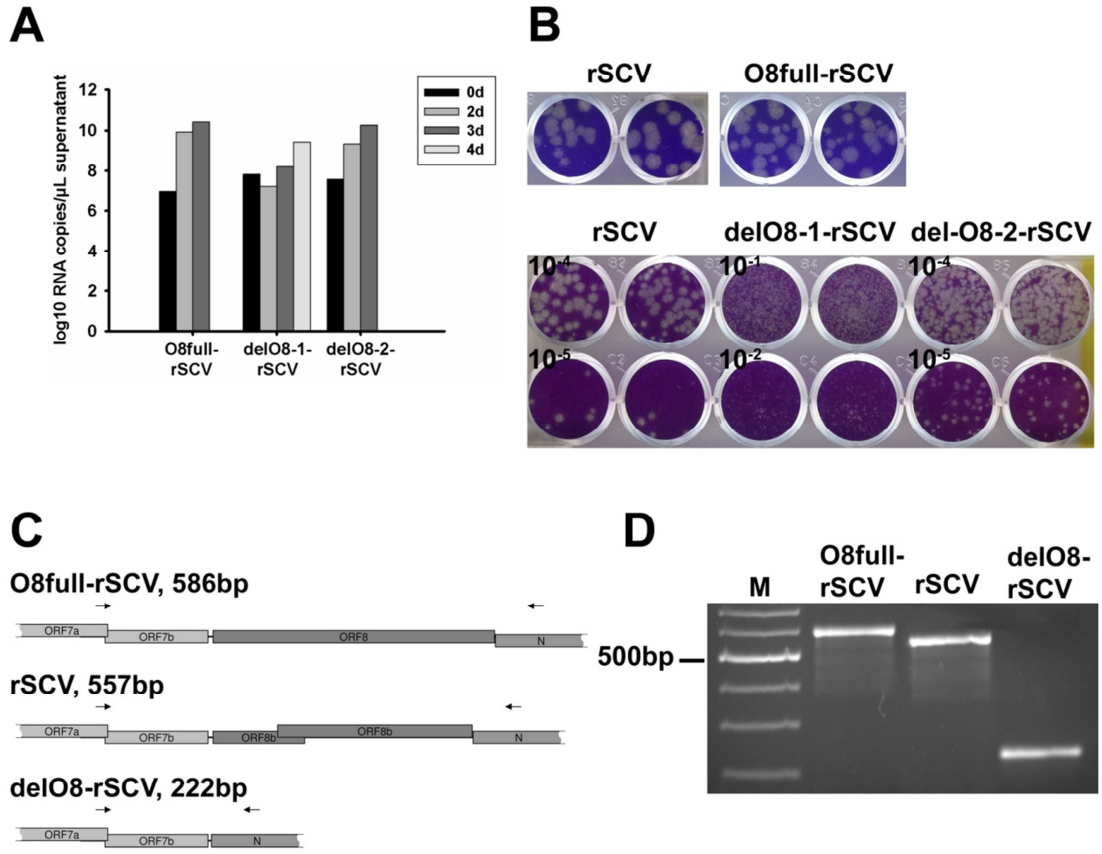

Figure 3.27: Rescue of ORF8 mutant rSCVs.
VeroFM cells were infected with supernatant of BHK-J cells electroporated with the *in vitro* transcribed full-length RNA of the three different ORF8 mutants. Virus growth was monitored by real-time RT-PCR (A). Plaque morphology of the newly generated ORF8 mutant viruses were determined (B) and the genomic region around ORF8 was PCR amplified and sequenced for correct mutation. M = 100 bp Plus DNA Ladder.

3.2.3.4 Comparative growth kinetics of ORF8 variants

Differences in ORF8 mutant virus plaque morphology were already observed during virus rescue (3.2.3.3). In further experiments the influence of the integrity of ORF8 on virus replication was investigated. VeroFM cells were infected at a very low MOI of 0.001 and virus replication was determined by plaque titration of cell culture supernatant. A low MOI was chosen because this would magnify small replication differences and would best resemble the early phase of a zoonotic transmission event. As shown in Fig. 3.28 already at 8h p.i. O8full-rSCV grew to higher titers than rSCV and delO8-rSCV. At 24h p.i. this replication pattern had noticeably developed. Virus titers decreased with reduced integrity of ORF8. O8full-rSCV, with a single full-length ORF8, yielded highest titers. The wild type rSCV, with a truncated ORF8a and a potentially nonfunctional ORF8b, grew to intermediate titers, while delO8-rSCV, entirely lacking ORF8, yielded the lowest titers. Replication differences disappeared by 48h p.i., by which time the replication plateau of all three viruses was reached.

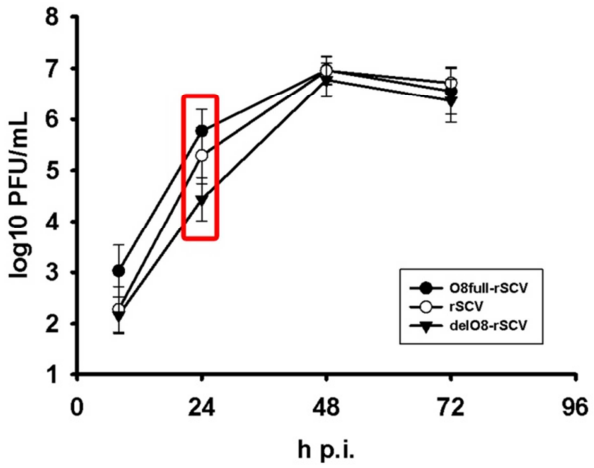

Figure 3.28: Virus growth of ORF8 variants on VeroFM cells.
VeroFM cells were infected with the three ORF8 variants, O8full-rSCV, rSCV, and delO8-rSCV, at an MOI of 0.001. Supernatants were sampled at 8, 24, 48, and 72 h p.i. and virus titers were determined by plaque titration. 24h p.i. O8full-rSCV grew to highest titers, while delO8-rSCV displayed delayed virus growth.

These results confirmed that infections at low MOIs show replication differences of the ORF8 variants, which could not be seen after infections at high MOIs [60].

3.2.3.5 Replication of ORF8 mutant viruses on IFN stimulated primate and bat cell lines

In addition to a second primate cell line, virus replication was again analyzed on the bat cell line RhiLu-hACE2. The virus variant delO8-rSCV was detected in samples from European *Rhinolophus* bats. The truncated version of ORF8 was exclusively found in the human pandemic virus. The single full-length ORF8 was identified in Asian *Rhinolophus* bats, amplifying hosts and human isolates from the early phase of the pandemic. For these reasons the question arose of whether ORF8 influenced the adaptation to a new host and served as a virulence factor. According to the results from the previous experiments (3.2.2.4), cells were infected at a low MOI and supernatants sampled 24h p.i. were plaque titrated. In addition to comparing virus growth on different cell lines, a potential antagonism with the IFN signaling pathway should be investigated. Therefore, cells were preincubated with their cell line-specific pan-species IFN concentrations prior to infection as described for the ORF6 mutant viruses in chapter 3.3.5.

In all three cell lines the same replication pattern as found in the previous experiment was identified (Fig. 3.29). Virus titers decreased with reduced integrity of ORF8. Especially distinct were the growth differences between O8full-rSCV and delO8-rSCV. Virus titers were 25- to 272-fold increased when the virus encoded the full-length ORF8 depending on the cell line used. Furthermore, as already seen in ORF6 mutant experiments, similar virus replication differences between the analyzed cell lines were detected (3.2.2.5). Generally, virus titers obtained in VeroFM cells were higher than those obtained in MA104 cells. Release of infectious particles from RhiLu-hACE2 cells was lower as compared to primate cells.

Preincubation of the cells with IFN reduced the general replication level of all three viruses. This suggested an IFN-independent mechanism of ORF8 influenced virus replication.

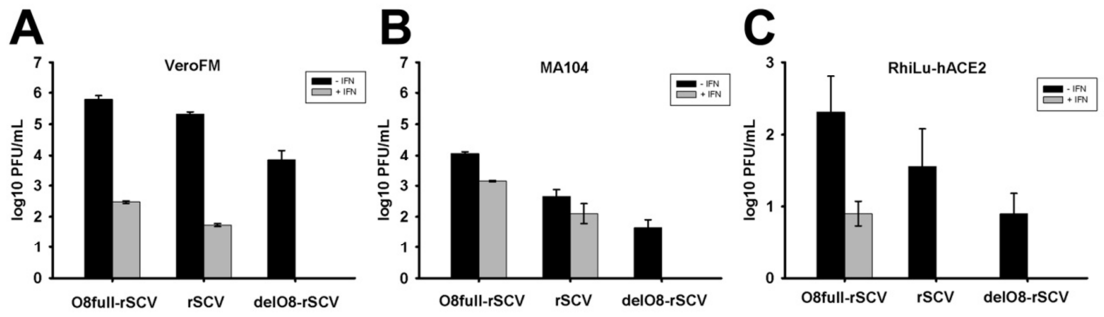

Figure 3.29: Replication of ORF8 variants on IFN stimulated cells.
VeroFM (A), MA104 (B), and RhiLu-hACE2 (C) were preincubated with cell line-specific pan-species IFN concentrations or medium as a control 16 h prior to infection with O8full-rSCV, rSCV, and delO8-rSCV at an MOI of 0.001. Supernatants were sampled 24h p.i. and virus titers were determined by plaque titration.

3.2.3.6 Trans-complementation of ORF8 variants

To verify that the observed differences in virus replication were due to expression of the ORF8-encoded protein (p8) only, a trans-complementation assay was performed. Cells overexpressing p8 were infected with delO8-rSCV in order to determine if replication efficiency can be enhanced by the presence of the protein. Lentiviral transduction was chosen as the optimal method for gene transfer since it guarantees high protein expression levels in most cell lines (2.2.1.7). In this experiment a transient expression of the protein was sufficient. Therefore, cells were not subjected to selection pressure as done in the course of generating the bat cell line RhiLu-hACE2 (3.2.2).

Cells were transduced with lentiviruses carrying either the full-length ORF8 (O8full) or ORF8a. Overexpression of p8b was left out as it is most likely not expressed during virus infection [26, 63].

VeroFM, MA104 and RhiLu-hACE2 cells were transduced as described in chapter 2.2.1.7.2. Infection with delO8-rSCV was done 48h post transduction since expression of the transgenes was shown to reach highest expression levels at that time point (data not shown). Cells were infected with an MOI of 0.001. Samples were taken 24h p.i. Supernatants were plaque titrated for the determination of infectious particles. Cells were lysed for quantification of protein expression in Western blot analysis (2.2.7) and used in an IF (2.2.7.4) for localization of the expressed proteins. Proteins p8full and p8a were FLAG-tagged for detection.

As shown in Fig. 3.30A expression of p8full and p8a was especially strong in MA104 cells. VeroFM cells also expressed both proteins but to a considerably reduced extent. For unknown reasons RhiLu-hACE2 cells did not express either of the proteins. A transduction failure due to lack of entry of VSV-G pseudotyped lentiviruses can be ruled out as RhiLu-hACE2 cells were made hACE2-transgenic by the same method (3.2.2). However, to exclude this possibility, the expression plasmids were transfected transiently (2.2.1.2). Again both proteins were not expressed (data not shown). This suggests either a malfunction of the CMV promoter in bat cells or that the proteins might have been prone to degradation as already shown in case of p8b [67]. Because of the lack of p8full and p8a in RhiLu-hACE2 cells in Western blot analysis, bat cell samples were not further analyzed.

The IF revealed a different distribution of p8full as compared to p8a (Fig. 3.30C). In VeroFM cells as well as in MA104 cells p8full was evenly distributed throughout the whole cytoplasm. In contrast p8a formed small granules in both cell lines. These differences between p8full and p8a expression have already been described by Keng, et al. and are thought to be a result of different protein conformations [63].

Plaque titration of the supernatants revealed that expression of p8full and p8a was able to enhance replication of delO8-rSCV (Fig. 3.30B). Expression of p8a in MA104 cells was especially strong and enhanced virus replication by 10-fold as compared to cells not expressing any p8. It was assumed that p8full overexpression would reconstitute virus replication most efficiently. This effect was not observed but was most likely due to the low expression level of p8full. Nevertheless, even a low expression level of p8full resulted in a 3-fold enhanced virus replication on MA104 cells. The same trans-complementation effects were observed in VeroFM cells, although to a lesser extent. This was most likely caused by the considerable lower expression level of p8full and p8a in VeroFM as compared to MA104 cells.

In conclusion, virus growth of delO8-rSCV could be enhanced in correspondence to the expressed p8 amounts. This clearly demonstrated that the absence of p8 was responsible for the impaired replication efficiency of delO8-rSCV.

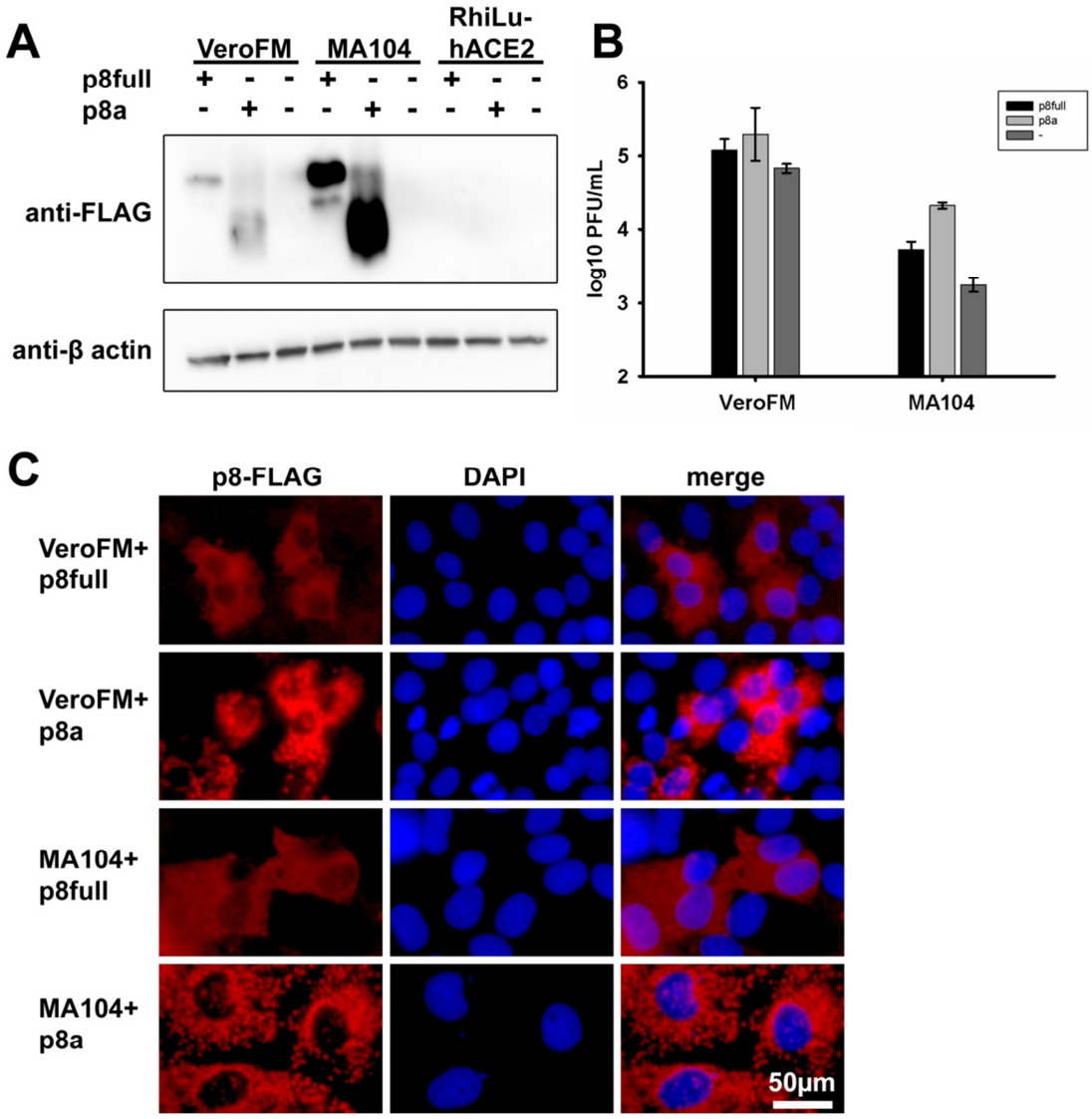

Figure 3.30: Trans-complementation of p8full and p8a in delO8-rSCV infected cells.
VeroFM, MA104, and RhiLu-hACE2 cells were transfected with O8full and O8a by lentiviral transduction 48h prior to infection with delO8-rSCV for 24h. Expression of the proteins p8full and p8a was confirmed by Western blot analysis (A) using rabbit-anti-FLAG primary antibody (1:5000). As a loading control β-actin was detected with a mouse-anti-β-actin primary antibody (1:2000). In addition, expression and localization of p8full and p8a were visualized by immunofluorescence assay (C). Cells were fixed in 4% PFA and p8full and p8a were stained with mouse-anti-FLAG (1:100) and goat-anti-mouse-Cy3 (1:200). Infection of the cells was confirmed using a human-anti-SARS-CoV serum (1:100) and goat-anti-human-Cy2 (1:200) for secondary detection. Nuclei were stained with DAPI (1:1000). Virus replication was determined by plaque titration of cell culture supernatants (B). Virus growth of delO8-rSCV was enhanced in correspondence to the amount of expressed p8.

4 Discussion

4.1 Reverse genetics

Reverse genetic systems are highly valuable tools to study viral gene functions in the context of viral replication. Designing and successfully handling a full-length cDNA clone of one of the largest viral RNA genomes has proven to be immensely challenging. In this study the reverse genetic system established by our group was used to generate the investigated SARS-CoV mutants [49]. In this system the full-length SARS-CoV cDNA genome is cloned into a BAC vector. Large DNA fragments cloned into BAC vectors and then maintained in bacteria are subjected to various mutations, like deletions and insertions [99]. Nevertheless, in the course of generating subclones and full-length clones described here, the disintegration of an insert occurred only once. When expanding the bacteria carrying the full-length genome of delO6-rSCV for a plasmid midipreparation, which was used for RNA *in vitro* transcription and subsequently an attempt to rescue recombinant virus, the complete degradation of the full-length plasmid occurred. Unfortunately, degradation was not observed by agarose gel electrophoresis of the plasmid, but degradation could be rapidly detected by screening the plasmid using the PCRs which are routinely generated for sequencing. Moreover, resolution of plasmids of 20-30 kb on agarose gels would not expose other modifications like deletions or insertions of a few hundred base pairs. However, this could be achieved by performing a range of PCRs spanning the entire genomic insert. In order to prevent the use of disintegrated plasmids it is therefore suggested to screen and fully sequence the midipreparations (not minipreparations), which are either used for further assembly or *in vitro* RNA transcription. In addition, the use of One Shot® Stbl3™ competent cells should be discontinued in favor One Shot® TOP10 competent cells. In contrast to TOP10 Stbl3™ still express *E. coli* cells primary endonuclease (endA) which degrades plasmid DNA [117].

One demand on reverse genetics is the rapid generation of recombinant viruses. Here the system described by Baric's group probably provides the quickest solution [98]. The SARS-CoV genome is segmented into six fragments, which are maintained in conventional vectors. In order to generate the full-length cDNA genome, the fragments are released from the vector and ligated in a single step. These inserts of about 5 kb can be easily mutated and the assembly of the whole cDNA genome into one vector backbone is not required. Assembly of the full-length genome in

a BAC vector is absolutely necessary in the system used in this work. The use of Phusion® High-Fidelity DNA Polymerase greatly reduced the time needed to generate a full-length clone. According to the manufacturer (Fermentas) Phusion® polymerase possess and error rate of 4.4x 10^{-7}, which is 50-fold less than *Taq* polymerase and a processivity 10-fold higher than *Pfu* polymerase. In addition, site-directed mutagenesis is possible on plasmids of up to 23.4 kb in length (deletion of ORF8 in subclone pDEF, described in chapter 3.1.7). The yield of colonies after PCR-based mutation is rather low, e.g. only one of three plasmids had the correct size in case of delO8-2-pDEF. Nevertheless, the polymerase's extremely low error rate almost guarantees for correct sequences. Furthermore, overlap extension-PCR is possible, thereby fusing long DNA fragments without introducing undesired mutations. Especially when performing a three-step overlap extension-PCR the single fragments undergo unusually many amplification cycles, raising the probability of PCR based mutations. If a PCR-based mutation would be introduced into the amplicon during the first cycles of amplification, all subsequent extended PCR products would carry this mutation. Without the low error rate of Phusion® polymerase overlap extension-PCR of large fragments would very likely be less successful. A new timesaving approach to mutate large DNA fragments maintained in BAC vectors is the two-step Red recombination system [118]. This method allows for recombination based mutagenesis of plasmids within an engineered *E.coli* strain. Plasmid preparations and standard cloning procedures, like restriction digestions and ligations, are unnecessary. This system was already successfully used for the generation and mutagenesis of a recombinant cow pox virus [119]. The adaptation of this mutagenesis method to the BAC vector based SARS-CoV reverse genetic system of our group will greatly improve the generation of mutated recombinant viruses.

4.2 Transgenic bat cells

All *in vitro* studies conducted on the importance of SARS-CoVs accessory proteins to date were done on primate cells. Most of these studies conclude that the actual relevance of accessory proteins can only be seen in the reservoir host of the virus [53, 120, 121]. Only two bat cell lines have been available before this study, but neither resembles the reservoir host of SARS-related CoVs [104]. With the establishment of the SARS-CoV-susceptible immortalized *Rhinolophus* cell line RhiLu-hACE2 a major step has been taken for SARS-CoV studies.

In the present study it was shown that SARS-CoV replicated efficiently in the new bat cell line. As SARS-CoV is highly sensitive to IFN [107] it was important to clarify if the IFN response was functional in RhiLu-hACE2. In particular, as the RhiLu cell culture was first immortalized and then provided with *hACE2* both by lentiviral transduction (3.1.2). The stable integration of transgenes into the cellular genome can heavily influence signal transduction pathways [122-124]. The IFN response can be triggered by different methods mostly involving double-stranded RNA intermediates that are sensed by cellular RIG-like helicases or Toll-like receptors [125-127]. It has already been shown that bat cell cultures respond to polyinosinic polycytidylic acid (poly I:C) stimulation or virus infection by the upregulation of genes involved in the IFN response pathway and the secretion of biologically active IFN [105, 128-130]. Poly I:C is structurally similar to double-stranded RNA, which is present during virus replication (e.g. of SARS-CoV) and routinely used to induce type I IFN response [131]. A functional IFN response of RhiLu-hACE2 was proven on different levels as described in detail in the Bachelor thesis of Hanna Roth [103]. IFN induction was verified by upregulated ISGs upon transfection of poly I:C. In addition, secretion of biologically active IFN was confirmed with the RVFV-Ren bioassay. Determination of the pan-species IFN concentration that reduces viral replication of RVFV-Ren up to 50% gave additional indication of an intact IFN response. RhiLu-hACE2 cells could be put into an antiviral state upon IFN treatment and virus replication was reduced in an IFN concentration-dependent manner (3.1.2). Successful replication of SARS-CoV was determined by measuring the increase of viral RNA in real-time RT-PCR and production of infectious particles by plaque titration in the course of characterizing the newly established cell line. Notably, the overall replication efficiency on RhiLu-hACE2 was clearly reduced as compared to primate cells like VeroFM or MA104. This was most likely due to differences between bat and primate cellular processing machinery. As described above, many viral proteins are involved in establishing a virus replication-friendly environment in the infected cells. This is done, for example, by induction of

membrane rearrangements to induce the formation of replication complexes [23, 56, 132]. It could also be possible that human-adapted SARS-CoV proteins interact less efficiently with bat cellular proteins. In addition, maturation of the virions takes place in the ERGIC [23, 27]. Differences in protein processing between bat and primate cells might lead to the assembly of defective, non-infectious virus particles. Reduced production of infectious virus particles might also be a mechanism used to establish a persistent infection. Another noticeable characteristic of RhiLu-hACE2 cells was that the transfection/transduction of ORF8 was not possible. Firstly, the precursor cell line RhiLu was already successfully transduced with hACE2. Secondly, lentiviral vectors are pseudotyped with the G protein of VSV. The G protein mediates viral entry by endocytosis and therefore makes a broad range of cell lines accessible to the lentiviral vector [133]. Possibly, RhiLu cells immediately degrade expressed p8, which could be why the SARS-related bat-CoV found in European *Rhinolophus* has lost ORF8. But the fact that SARS-related bat-CoVs found in Asian *Rhinolophus* bats carry the full-length ORF8 objects to this explanation [10, 77, 134]. It might also be possible that transcription of ORF8 is inhibited. The undirected integration of hACE2 into the RhiLu cells genome could also have destroyed some essential cellular functions for transcription or translation of certain genes. To rule out the production of artifacts on RhiLu-hACE2 cells, resulting from the disruption of important cellular genes, cells were not cloned. This measure created a heterologous cell population in which heavily degenerated cells would not considerably influence experimental outcomes.

It is commonly known that cell culture models are only a substitute for animal models. In most parts of the world bats are protected species and the breeding of bat colonies for experimental studies is limited to very few laboratories. Therefore, the bat cell line described here is a unique tool for simulating reservoir host conditions for a variety of viruses found in bats of the genus *Rhinolophus*, especially SARS-CoV.

4.3 The potential of accessory proteins to serve as risk markers

Bats carry a large diversity of SARS-related CoVs, which demands predictions of epidemic and pathogenic potential of these viruses [72-76]. Features that discriminate high- and low-risk variants have to be identified to achieve this goal. Two accessory proteins of SARS-CoV were chosen as potential risk markers. The ORF6 encoded p6 is a very well characterized IFN antagonist [59]. With the sequence information obtained from the first full-length genome sequence of a European SARS-related bat-CoV a comparative study on SARS-CoV p6 and a reservoir-borne SARS-related CoV p6 was possible [88]. ORF8 displayed a striking genetic variation in geographically distant reservoir hosts. SARS-related CoVs detected in Asian *Rhinolophus* bats carry an intact full-length ORF8 [10, 72], while *Rhinolophus* bats sampled in Southern and Western Europe exclusively carry SARS-related CoVs without an ORF8 gene [88]. The human pandemic strain of SARS-CoV is characterized by a 29nt-deletion within ORF8 that splits it in two separate ORFs, 8a and 8b [61].

Generally, protein functions are first characterized in overexpression systems. These settings are rather error-prone and might produce artifacts, because proteins are expressed at very high levels that are most likely not achieved during virus infection. With increasing advances in reverse genetics systems, proteins should additionally be studied in full virus context, which are usually conducted in primate cells. However, especially in the case of SARS-CoV and related viruses, which were found to have their reservoir in bats of the genus *Rhinolophus* [10, 72], additional cell culture models are needed. The establishment of an immortalized SARS-CoV susceptible *Rhinolophus* cell line specifically fulfills this need. This allowed for comparative studies on the above-mentioned proteins in their respective hosts.

4.3.1 Protein 6

Proteins SA-p6 and BG-p6 were expressed in human and bat cells to investigate their distribution patterns. While both proteins were evenly distributed in the cytoplasm of human cells, they localize in punctuate structures within close proximity of the nucleus in bat cells. No protein-specific differences in cellular localizations were observed. Therefore, the punctuated localization of p6 in RhiLu-hACE2 might be specific for bat cells. As described by Frieman et al. SA-p6 is

able to retain the transport protein KPNA2 at the ER/Golgi and thus inhibits IFN signaling [59]. An inhibition of KPNA2 nuclear translocation by SA-p6 could be reproduced. Interestingly, the bat-CoV derived BG-p6 also inhibited KPNA2 translocation into the nucleus but allowed KPNA1 to translocate. Furthermore, translocation of STAT1 into the nucleus of primate cells was blocked efficiently by both p6 upon IFN treatment. These findings strongly suggest that both proteins, sharing an amino acid similarity of 78.1%, interfere with the IFN signaling by the same mechanism. The C-terminal 10 amino acids of SA-p6 (amino acids 54-63) are responsible for efficient binding to KPNA2 and thereby the blocking of STAT1 nuclear translocation [59]. SA-p6 and BG-p6 differ in only 3 of the last 10 amino acids. In two of these three changes the amino acid maintains its properties. At amino acid position 54 the asparagine of SA-p6 is changed into a glutamine in BG-p6, both amino acids are acidic. Leucine was changed into an Isoleucine at position 60, with both amino acids being non-polar and hydrophobic. These "silent" amino acid changes are most likely the reason why BG-p6 exhibits functions similar to SA-p6. The highly conserved C-terminus is the first implication that p6 has a similar IFN antagonistic function in bats. Mutagenesis studies on BG-p6 and studies on p6 of other European SARS-related bat-CoVs will follow. In addition, detailed functional studies in bat cells are needed including for example protein-protein interactions with bat-derived homologous proteins. These studies were not done during the course of this work due to the lack of bat genome sequence information. Sequencing of bat homolog genes coding for bat-karyopherins and bat-STAT1 is in progress and will greatly increase understanding of SARS-CoV protein interaction with the bat specific IFN response pathway.

The greatest challenge when comparing homologous viral proteins in the context of viral replication is to know when to define a replication difference as relevant and significant. There is obviously no general agreement and the literature is contradictory [54, 60]. BGO6-rSCV grew to titers 20-fold lower than that of rSCV on VeroFM cells, while delO6-rSCV showed an 8.3-fold reduction in virus growth as compared to the wild type rSCV. Yount et al. described an ORF6 deleted rSCV to "grow as efficiently as (the) wild type virus", when they observed a 3-fold reduction in virus titers [60]. In contrast, Zhao et al. found that their ORF6 deleted rSCV after infection of Vero E6 cells at an MOI of 0.01 grew to titers 3 to4-fold lower than wild type virus and described it as "to grow more slowly and to lower titers" compared to the wild type virus [54]. For example in the case of influenza A, differences of virus growth between mutant and wild type viruses of 5-10-fold were found to be significant [135]. The replication differences found by Yount et al. and Zhou et al. could be confirmed by our experimental setup. Moreover,

this replication pattern was reproduced in another primate and one bat cell line. The fact that replication differences, even though small, were found for rSCV and delO6-rSCV independently by three different groups, strongly suggests that even small differences are reproducible and therefore valid. Nevertheless, the focus of this study was not the deletion of p6 but the comparison of SA-p6 and BG-p6 their influence on virus replication in their respective hosts. In all three tested cell lines BGO6-rSCV grew to lower titers as compared to rSCV. This suggested an attenuating effect of the bat-CoV p6 when introduced into the genome of the pathogenic SARS-CoV. Interestingly, the attenuating effect of BG-p6 was also seen in bat cells. This rejects the initial assumption that BGO6-rSCV would be able to replicate more efficiently than rSCV in RhiLu-hACE2 because it possess the IFN antagonist matching the cell line. Correspondingly, rSCV was expected to exhibit replication advantages on primate cells as compared to BGO6-rSCV. However, the results obtained here rather suggest a general attenuating effect of BG-p6. This is consistent with previous findings, where p6 was described as a virulence factor that was able to fundamentally influence the pathogenicity of a murine CoV [53]. Zhao et al. postulate that the presence of ORF6 has no influence on the IFN sensitivity of rSCV [54]. The results shown here indicate that IFN-pretreatment of primate cells reduces the growth of BGO6-rSCV less efficiently than rSCV, while the growth of BGO6-rSCV is inhibited more than the growth of rSCV on IFN pretreated bat cells. This indicates that primate cells might have better tools to counteract the IFN antagonist from the human pathogenic virus. Accordingly, bat cells appear rather capable of dealing with the IFN antagonist of the bat derived virus. This implies that the IFN antagonists are host-adapted and virus growth can be reduced in order to save the new host. On the contrary, the dead-end host is inferior to the unknown IFN antagonist and the virus could replicate without hindrance. Nevertheless, the general virus replication is attenuated in the presence of BG-p6. This might suggest that attenuation is not based on the IFN antagonistic feature of p6, but rather on its second function, the N-terminal linked ability to induce membrane rearrangement [56]. The N-terminal region of p6 is not as conserved as the C-terminus. SA-p6 might therefore be more efficiently and universally able to create a replication-friendly environment, e.g. by the induction of replication complex formation, than BG-p6. This is admittedly speculative and further experiments are required to determine the speed of RNA synthesis in the presence of the different p6. As previously shown, viral RNA synthesis is significantly reduced in the absence of p6 [54]. Moreover, it is necessary to clarify cellular architecture and organelle morphology in SARS-CoV infected bat cells. However, it is not yet

known whether membrane rearrangements and the formation of double membrane vesicles as sites of virus replication are also induced in bat cells.

4.3.2 Open reading frame 8

An overrepresentation of mutations within ORF8 in the SARS-CoV genome was already noticed shortly after the epidemic, but these mutations had no apparent effect on the pathogenesis in humans and the encoded protein was said to be functionally irrelevant [61]. Nevertheless, in the following time many studies on the protein's functionality were done [62-65, 68]. In the course of investigating the importance of SARS-CoVs accessory proteins a variety of recombinant viruses lacking different accessory genes were generated [60, 136]. Inexplicably, a virus deleted in ORF8 was never among them. Studies on ORF8 were only conducted in the context of the 29nt-deletion, which distinguishes between early and late phase SARS pandemic isolates. The description of the first SARS-related CoV found in European bats that lacks ORF8 entirely again raised the question of the relevance of ORF8 [88].

Overexpression of p8full and p8a by lentiviral transduction revealed profoundly different cellular distributions of both proteins. P8full is diffused in the cytoplasm while p8a can be found in punctuate vesicle-like structures. This was also found by Keng et al. and emphasizes the proposed difference of both proteins in structure and function, which were also implicated by the very distinct binding profiles of p8full and p8a to other viral proteins [64]

To resolve the detailed functionality of this protein was not an aim of the present study. It was rather to be clarified if ORF8, based on its high susceptibility to mutations, might act as a virulence factor and might therefore be useful as a risk marker assessing newly discovered SARS-related CoVs.

In two primate cell lines and one bat cell line the same replication for the three ORF8 variants could be observed. The replication efficiency decreased with decreasing integrity of the ORF8 gene. Replication differences were similar in primate and bat cells which implied a host-independent mechanism of replication inhibition. IFN pretreatment of infected cells resulted in an overall reduction in virus growth. No ORF8-specific differences were detected, suggesting that the encoded protein does not interfere with the cells' IFN pathway. In addition, overexpression of p8full or p8a resulted in enhanced replication of the ORF8 deleted virus. This proves that decreased virus replication is due to the absence of the ORF8 gene product.

Yount et al. characterized their recombinant SARS-CoV carrying the full-length ORF8 to replicate as efficiently as the wild type virus [60]. In fact, their O8full-rSCV grew to titers 3-fold higher as compared to wild type rSCV. This, admittedly small, growth difference was independently reproducible in all the three cell lines used in this study, and can therefore be regarded as credible. The most pronounced replication differences were those between viruses with an intact full-length ORF8 and the deleted ORF8. The lack or ORF8 led to a 25-270-fold reduction of virus titers depending on the cell line used. This previously undetected genotype is likely to be the reason that the relevance of ORF8 as a virulence factor was overlooked until now.

The closest relatives of SARS-CoV have been found in *Rhinolophus* bats in Asia and Europe [10, 72, 80, 88]. The closest relative of SARS-CoV in Africa was found in a *Chaerephon* bat [86], though both virus and host are only distantly related to SARS-CoV and *Rhinolophus*. Nevertheless, it would be useful to determine the presence of ORF8 in the African SARS-CoV relative. In addition, phylogenetic analyses of the European and Asian SARS-related bat-CoVs might provide valuable information on their common ancestor and their spread through Eurasia.

Taken together the proteins encoded by ORF6 and ORF8 of the SARS-CoV genome can be used to assess the zoonotic potential of newly discovered SARS-CoV-related viruses. The experiments performed on both proteins in this work give profound evidence that SARS-related bat-CoV BtCoV/BM48-31 found in Europe is attenuated. Generally, due to the lack of ORF8 in all European SARS-related bat-CoVs these viruses exhibit a greatly reduced risk potential to initiate another SARS epidemic as compared to the Asian viruses.

5 Summary

The pandemic of the „Severe acute respiratory syndrome“ (SARS) at the end of 2002 caused more than 8000 infections and led to more than 800 deaths. The disease was soon associated with a new zoonotic coronavirus, the SARS-CoV. At first, civet cats were thought to be the natural reservoir of SARS-CoV, but further studies revealed that SARS-related CoVs are present at high diversities in Asian bats of the genus *Rhinolophus*. Emerging viruses are a constant threat to public health and it is of utmost importance to evaluate risk factors that facilitate host transitions.

SARS-CoV encodes several accessory proteins with partially known functions in immune evasion. Minor relevance was assigned to those proteins in cell culture models, but it is generally assumed that they might have important functions in the natural reservoir.

Using the full-length genome sequence of a Bulgarian SARS-related bat-CoV (BG-CoV) identified by us in *Rhinolophus blasii* functionalities of two selected accessory proteins were investigated.

To this end, a *Rhinolophus* bat embryonic lung cell line carrying the human SARS-CoV receptor angiotensin converting enzyme 2 (hACE2) was established (RhiLu-hACE2) to resemble the SARS-CoV reservoir. Type I interferon assays were established for cells from different hosts and extensive reverse genetic studies on SARS-CoV were conducted to project the zoonotic risk of the bat-borne SARS-related CoV.

(i) Protein 6, encoded by open reading frame 6 (ORF6), interacts directly with Karyopherin (KPN) α2 thereby inhibiting interferon (IFN) signaling. BG-CoV protein 6 (BG-p6) shares 78.1% amino acid similarity with human SARS-CoV protein 6 (SA-p6). Overexpressed BG-p6 was able to inhibit nuclear translocation of co-transfected KPN α2 like SA-p6. Moreover, the IFN antagonistic ability of both proteins was determined by the inhibition of nuclear translocation of overexpressed STAT1 due to the effect described above. It was shown that overexpressed BG-p6 inhibited STAT1 translocation as efficiently as SA-p6.

With the help of the SARS-CoV reverse genetics system a chimeric recombinant SARS-CoV carrying the BG-CoV ORF6 (BGO6-rSCV) was generated for studies in a in the context of viral replication in primate and RhiLu-hACE2 cells.

In primate as well as in RhiLu-hACE2 cells BGO6-rSCV replicated less efficiently than wild type rSCV. Interestingly, when cells were preincubated with universal type I IFN BGO6-rSCV exhibited an increased IFN sensitivity on RhiLu-hACE2 cells only. This suggests a host-independent attenuating effect of BG-p6.

(ii) The genomic region around ORF8 was subject to an unusual high mutation rate throughout the SARS pandemic. SARS-related CoVs found in Asian *Rhinolophus* bats, civet cats and early human isolates of SARS-CoV carried a single full-length ORF8. The human pandemic SARS-CoV acquired a 29 nucleotide deletion leading to the disruption of ORF8 into two ORFs, ORF8a and 8b. In the Bulgarian SARS-related bat-CoV we found that ORF8 was entirely missing. Analysis of more *Rhinolophid* bats from Spain, Italy and Slovenia revealed that most likely all European SARS-related bat-CoVs lack ORF8.

The influence of ORF8 integrity on virus replication was investigated with the help of rSCVs carrying these three ORF8 variants. On primate and bat cell culture rSCV carrying the full-length ORF8 grew to the highest titers, while the ORF8 deletion variant grew the worst. IFN pretreatment of the tested cell lines resulted in an overall decrease in virus replication of all ORF8 variants suggesting an IFN-independent mechanism for ORF8 influenced virus replication.

In summary, the present study showed that BG-p6 was able to antagonize type I IFN signaling in primate cells with wild type efficiency. In the full virus context a SARS-CoV expressing BG-p6 was attenuated in primate and bat cell culture. Furthermore, the absence of ORF8 greatly reduced virus replication efficiency. Taken together both findings suggest potentially reduced virulence of the European SARS-related bat-CoVs. For the first time these data indicate a feasible approach to assessing zoonotic risks emanating from bat-borne SARS-related CoVs.

Summary in German/Zusammenfassung

Die Pandemie des „Schweren akuten respiratorischen Syndroms“ (SARS), die Ende 2002 begann, führte weltweit zu über 8000 Infizierten von denen über 800 starben. Die Krankheit wurde schnell mit einem neuartigen, zoonotischen Coronavirus, dem SARS-CoV, assoziiert. Zunächst standen Schleichkatzen unter Verdacht das natürliche Reservoir des SARS-CoV zu sein. In weiteren Studien konnte jedoch gezeigt werden, dass SARS-ähnliche Coronaviren in hoher Diversität in asiatischen Fledermäusen der Gattung *Rhinolophus* zu finden waren. Neu auftretende zoonotische Viren stellen eine konstante Gefährdung für die öffentliche Gesundheit dar. Die Beurteilung von Risikofaktoren, die einen Wirtswechsel ermöglichen, ist von größter Bedeutung.

Das SARS-CoV kodiert für eine für Coronaviren ungewöhnlich hohe Anzahl an akzessorischen Genen. Diesen Genen wird meist eine geringe funktionelle Relevanz in Zellkulturmodellen zugesprochen, aber es wird allgemein angenommen, dass sie wichtige Funktionen im natürlichen Reservoir besitzen.

Mit Hilfe der Vollgenomsequenz eines bulgarischen SARS-ähnlichen Fledermaus-CoV (BG-CoV), welches durch unsere Arbeitsgruppe in *Rhinolophus blasii* gefunden wurde, wurde die Funktionalität zweier ausgewählter akzessorischer Proteine untersucht.

Zu diesem Zweck wurde eine embryonale Lungenzelllinie aus *Rhinolophus* hergestellt, die den humanen SARS-CoV-Rezeptor Angiotensin-konvertierendes Enzym 2 (hACE2) dauerhaft exprimiert, RhiLu-hACE2. Diese Zelllinie sollte dazu dienen, das Reservoir von SARS-CoV im Zellkulturmodell darzustellen. Es wurden Typ-I-Interferonassays für Zellen verschiedener Herkunft etabliert und umfangreiche revers-genetische Studien am SARS-CoV durchgeführt, um das zoonotische Risiko des SARS-ähnlichen Fledermaus-CoV zu beurteilen.

(i) Protein 6, kodiert durch den offenen Leserahmen 6 (ORF6), interagiert direkt mit Karyopherin (KPN) α2 und inhibiert so den Interferon(IFN)-Signalweg. Das BG-CoV Protein 6 (BG-p6) besitzt eine Aminosäureähnlichkeit von 78.1% im Vergleich zum humanen SARS-CoV Protein 6 (SA-p6). Überexprimiertes BG-p6 war wie SA-p6 in der Lage, die nukleäre Translokation von kotransfiziertem KPN α2 zu inhibieren. Die IFN-antagonistische Fähigkeit beider Proteine wurde mit Hilfe der Inhibition der nukleären Translokation von überexprimiertem STAT1, basierend auf den beschriebenen Wechselwirkungen, bestimmt. Überexprimiertes BG-p6 inhibierte die Translokation so effektiv wie SA-p6.

Summary

Mit Hilfe des SARS-CoV reversen Genetiksystems wurde rekombinantes SARS-CoV hergestellt, dass das BG-CoV ORF6 trägt (BGO6-rSCV), um Studien im Vollviruskontext in Primaten- und RhiLu-hACE2-Zellen durchzuführen.

Sowohl in Primaten- als auch in RhiLu-hACE2-Zellen replizierte das BGO6-rSCV weniger effizient als das Wildtyp-rSCV. Wurden die Zellen mit universellem Typ-I-IFN präinkubiert, zeigte BGO6-rSCV nur auf RhiLu-hACE2-Zellen einer erhöhte IFN-Sensitivität. Das weißt auf einen wirtsunabhängigen attenuierenden Effekt durch BG-p6 hin.

(ii) Die Genomregion um ORF8 unterlag während der SARS-Pandemie einer ungewöhnlich hohen Mutationsrate. SARS-ähnliche CoVs aus asiatischen *Rhinolophiden*, sowie SARS-CoV-Isolate aus Larvenrollern und Patienten in der frühen Phase der Pandemie trugen ein einzelnes, vollständiges ORF8. Das humane, pandemische SARS-CoV erwarb eine Deletion von 29 Nukleotiden, die das ORF8 in ORF8a und 8b zweiteilte. Im Genom des bulgarischen SARS-ähnlichen Fledermaus-CoVs fehlte ORF8 vollständig. Untersuchungen von weiteren *Rhinolophiden* aus Spanien, Italien und Slowenien ergab, dass ORF8 sehr wahrscheinlich in alle europäischen SARS-ähnlichen Fledermaus-CoVs fehlt.

Zur Untersuchung des Einflusses der Vollständigkeit von ORF8 auf die Virusreplikation wurden rSCVs konstruiert, die die jeweiligen ORF8-Varianten tragen. In Primaten- und RhiLu-hACE2-Zellen wuchs das rSCV mit dem vollständigen ORF8 am besten. Die ORF8-Deletionsvariante replizierte hingegen am schlechtesten. Eine Behandlung der Zellen mit IFN führte zu einer allgemein verringerten Replikationsrate der Viren, was auf einen IFN-unabhängigen Mechanismus der ORF8-beeinflussten Virusreplikation hindeutet.

Die vorliegende Studie legt nahe, dass das BG-p6 mit Wildtyp-Effizienz den Typ-I-IFN-Signalweg in Primatenzellen antagonisiert. Im Vollviruskontext war das SARS-CoV, was BG-p6 exprimiert, in Primaten- und RhiLu-hACE2-Zellen attenuiert. Zusätzlich trug das Fehlen von ORF8 zu verminderter Virusreplikation bei. Zusammenfassend deuten diese Erkenntnisse darauf hin, dass europäische SARS-ähnliche Fledermaus-CoV vermutlich eine verminderte Virulenz besitzen. Außerdem präsentieren die Daten einen zulässigen Ansatz zur Beurteilung des zoonotischen Risikos durch Fledermaus übertragene SARS-ähnliche CoVs.

6 References

1. Jones, K.E., et al., *Global trends in emerging infectious diseases.* Nature, 2008. **451**(7181): p. 990-3.
2. Parrish, C.R., et al., *Cross-species virus transmission and the emergence of new epidemic diseases.* Microbiol Mol Biol Rev, 2008. **72**(3): p. 457-70.
3. Coker, R., et al., *Towards a conceptual framework to support one-health research for policy on emerging zoonoses.* Lancet Infect Dis, 2011. **11**(4): p. 326-31.
4. Johnson, P.T. and D.W. Thieltges, *Diversity, decoys and the dilution effect: how ecological communities affect disease risk.* J Exp Biol, 2010. **213**(6): p. 961-70.
5. Keesing, F., R.D. Holt, and R.S. Ostfeld, *Effects of species diversity on disease risk.* Ecol Lett, 2006. **9**(4): p. 485-98.
6. Wolfe, N.D., C.P. Dunavan, and J. Diamond, *Origins of major human infectious diseases.* Nature, 2007. **447**(7142): p. 279-83.
7. Hengel, H., U.H. Koszinowski, and K.K. Conzelmann, *Viruses know it all: new insights into IFN networks.* Trends Immunol, 2005. **26**(7): p. 396-401.
8. Garcia-Sastre, A. and C.A. Biron, *Type 1 interferons and the virus-host relationship: a lesson in detente.* Science, 2006. **312**(5775): p. 879-82.
9. Sheahan, T., et al., *Pathways of cross-species transmission of synthetically reconstructed zoonotic severe acute respiratory syndrome coronavirus.* J Virol, 2008. **82**(17): p. 8721-32.
10. Li, W., et al., *Bats are natural reservoirs of SARS-like coronaviruses.* Science, 2005. **310**(5748): p. 676-9.
11. Drake, J.W. and J.J. Holland, *Mutation rates among RNA viruses.* Proc Natl Acad Sci U S A, 1999. **96**(24): p. 13910-3.
12. Denison, M.R., et al., *Coronaviruses: an RNA proofreading machine regulates replication fidelity and diversity.* RNA Biol, 2011. **8**(2): p. 270-9.
13. Hamre, D. and J.J. Procknow, *A new virus isolated from the human respiratory tract.* Proc Soc Exp Biol Med, 1966. **121**(1): p. 190-3.
14. van der Hoek, L., et al., *Identification of a new human coronavirus.* Nat Med, 2004. **10**(4): p. 368-73.
15. McIntosh, K., W.B. Becker, and R.M. Chanock, *Growth in suckling-mouse brain of "IBV-like" viruses from patients with upper respiratory tract disease.* Proc Natl Acad Sci U S A, 1967. **58**(6): p. 2268-73.
16. Rota, P.A., et al., *Characterization of a novel coronavirus associated with severe acute respiratory syndrome.* Science, 2003. **300**(5624): p. 1394-9.
17. Drosten, C., et al., *Identification of a novel coronavirus in patients with severe acute respiratory syndrome.* N Engl J Med, 2003. **348**(20): p. 1967-76.
18. Woo, P.C., et al., *Characterization and complete genome sequence of a novel coronavirus, coronavirus HKU1, from patients with pneumonia.* J Virol, 2005. **79**(2): p. 884-95.
19. Peiris, J.S., Y. Guan, and K.Y. Yuen, *Severe acute respiratory syndrome.* Nat Med, 2004. **10**(12 Suppl): p. S88-97.
20. Holmes, K.V. and L. Enjuanes, *Virology. The SARS coronavirus: a postgenomic era.* Science, 2003. **300**(5624): p. 1377-8.
21. Knipe, D.M., P.M. Howley, and D.E. Griffin, *Fields Virology*. 5. ed2007: Lippincott Williams & Wilkins.
22. Modrow, S., et al., *Molekulare Virologie*. 3. ed2010: Spektrum.
23. Perlman, S. and J. Netland, *Coronaviruses post-SARS: update on replication and pathogenesis.* Nat Rev Microbiol, 2009. **7**(6): p. 439-50.

24. Pasternak, A.O., W.J. Spaan, and E.J. Snijder, *Nidovirus transcription: how to make sense...?* J Gen Virol, 2006. **87**(Pt 6): p. 1403-21.
25. Sawicki, S.G., D.L. Sawicki, and S.G. Siddell, *A contemporary view of coronavirus transcription.* J Virol, 2007. **81**(1): p. 20-9.
26. Snijder, E.J., et al., *Unique and conserved features of genome and proteome of SARS-coronavirus, an early split-off from the coronavirus group 2 lineage.* J Mol Biol, 2003. **331**(5): p. 991-1004.
27. de Haan, C.A. and P.J. Rottier, *Molecular interactions in the assembly of coronaviruses.* Adv Virus Res, 2005. **64**: p. 165-230.
28. Mortola, E. and P. Roy, *Efficient assembly and release of SARS coronavirus-like particles by a heterologous expression system.* FEBS Lett, 2004. **576**(1-2): p. 174-8.
29. He, R., et al., *Characterization of protein-protein interactions between the nucleocapsid protein and membrane protein of the SARS coronavirus.* Virus Res, 2004. **105**(2): p. 121-5.
30. Bergmann, C.C., T.E. Lane, and S.A. Stohlman, *Coronavirus infection of the central nervous system: host-virus stand-off.* Nat Rev Microbiol, 2006. **4**(2): p. 121-32.
31. Guan, M., et al., *Recombinant protein-based enzyme-linked immunosorbent assay and immunochromatographic tests for detection of immunoglobulin G antibodies to severe acute respiratory syndrome (SARS) coronavirus in SARS patients.* Clin Diagn Lab Immunol, 2004. **11**(2): p. 287-91.
32. Guo, J.P., et al., *SARS corona virus peptides recognized by antibodies in the sera of convalescent cases.* Virology, 2004. **324**(2): p. 251-6.
33. Qiu, M., et al., *Antibody responses to individual proteins of SARS coronavirus and their neutralization activities.* Microbes Infect, 2005. **7**(5-6): p. 882-9.
34. Tan, Y.J., et al., *Profiles of antibody responses against severe acute respiratory syndrome coronavirus recombinant proteins and their potential use as diagnostic markers.* Clin Diagn Lab Immunol, 2004. **11**(2): p. 362-71.
35. Freundt, E.C., et al., *The open reading frame 3a protein of severe acute respiratory syndrome-associated coronavirus promotes membrane rearrangement and cell death.* J Virol, 2010. **84**(2): p. 1097-109.
36. Yu, C.J., et al., *Identification of a novel protein 3a from severe acute respiratory syndrome coronavirus.* FEBS Lett, 2004. **565**(1-3): p. 111-6.
37. Yuan, X., et al., *Subcellular localization and membrane association of SARS-CoV 3a protein.* Virus Res, 2005. **109**(2): p. 191-202.
38. Yuan, X., et al., *Mitochondrial location of severe acute respiratory syndrome coronavirus 3b protein.* Mol Cells, 2006. **21**(2): p. 186-91.
39. Yuan, X., et al., *Nucleolar localization of non-structural protein 3b, a protein specifically encoded by the severe acute respiratory syndrome coronavirus.* Virus Res, 2005. **114**(1-2): p. 70-9.
40. Kopecky-Bromberg, S.A., et al., *Severe acute respiratory syndrome coronavirus open reading frame (ORF) 3b, ORF 6, and nucleocapsid proteins function as interferon antagonists.* J Virol, 2007. **81**(2): p. 548-57.
41. Schaecher, S.R., et al., *Severe acute respiratory syndrome coronavirus gene 7 products contribute to virus-induced apoptosis.* J Virol, 2007. **81**(20): p. 11054-68.
42. Tan, Y.J., et al., *Overexpression of 7a, a protein specifically encoded by the severe acute respiratory syndrome coronavirus, induces apoptosis via a caspase-dependent pathway.* J Virol, 2004. **78**(24): p. 14043-7.
43. Yuan, X., et al., *SARS coronavirus 7a protein blocks cell cycle progression at G0/G1 phase via the cyclin D3/pRb pathway.* Virology, 2006. **346**(1): p. 74-85.
44. Kopecky-Bromberg, S.A., L. Martinez-Sobrido, and P. Palese, *7a protein of severe acute respiratory syndrome coronavirus inhibits cellular protein synthesis and activates p38 mitogen-activated protein kinase.* J Virol, 2006. **80**(2): p. 785-93.

45. Karjee, S., et al., *The 7a accessory protein of severe acute respiratory syndrome coronavirus acts as an RNA silencing suppressor.* J Virol, 2010. **84**(19): p. 10395-401.
46. Huang, C., et al., *Severe acute respiratory syndrome coronavirus 7a accessory protein is a viral structural protein.* J Virol, 2006. **80**(15): p. 7287-94.
47. Schaecher, S.R., J.M. Mackenzie, and A. Pekosz, *The ORF7b protein of severe acute respiratory syndrome coronavirus (SARS-CoV) is expressed in virus-infected cells and incorporated into SARS-CoV particles.* J Virol, 2007. **81**(2): p. 718-31.
48. Schaecher, S.R., M.S. Diamond, and A. Pekosz, *The transmembrane domain of the severe acute respiratory syndrome coronavirus ORF7b protein is necessary and sufficient for its retention in the Golgi complex.* J Virol, 2008. **82**(19): p. 9477-91.
49. Pfefferle, S., et al., *Reverse genetic characterization of the natural genomic deletion in SARS-Coronavirus strain Frankfurt-1 open reading frame 7b reveals an attenuating function of the 7b protein in-vitro and in-vivo.* Virol J, 2009. **6**: p. 131.
50. Meier, C., et al., *The crystal structure of ORF-9b, a lipid binding protein from the SARS coronavirus.* Structure, 2006. **14**(7): p. 1157-65.
51. Sharma, K., et al., *SARS-CoV 9b protein diffuses into nucleus, undergoes active Crm1 mediated nucleocytoplasmic export and triggers apoptosis when retained in the nucleus.* PLoS One, 2011. **6**(5): p. e19436.
52. Geng, H., et al., *The putative protein 6 of the severe acute respiratory syndrome-associated coronavirus: expression and functional characterization.* FEBS Lett, 2005. **579**(30): p. 6763-8.
53. Pewe, L., et al., *A severe acute respiratory syndrome-associated coronavirus-specific protein enhances virulence of an attenuated murine coronavirus.* J Virol, 2005. **79**(17): p. 11335-42.
54. Zhao, J., et al., *Severe acute respiratory syndrome coronavirus protein 6 is required for optimal replication.* J Virol, 2009. **83**(5): p. 2368-73.
55. Kumar, P., et al., *The nonstructural protein 8 (nsp8) of the SARS coronavirus interacts with its ORF6 accessory protein.* Virology, 2007. **366**(2): p. 293-303.
56. Zhou, H., et al., *The N-terminal region of severe acute respiratory syndrome coronavirus protein 6 induces membrane rearrangement and enhances virus replication.* J Virol, 2010. **84**(7): p. 3542-51.
57. Hussain, S. and T. Gallagher, *SARS-coronavirus protein 6 conformations required to impede protein import into the nucleus.* Virus Res, 2010. **153**(2): p. 299-304.
58. Hussain, S., S. Perlman, and T.M. Gallagher, *Severe acute respiratory syndrome coronavirus protein 6 accelerates murine hepatitis virus infections by more than one mechanism.* J Virol, 2008. **82**(14): p. 7212-22.
59. Frieman, M., et al., *Severe acute respiratory syndrome coronavirus ORF6 antagonizes STAT1 function by sequestering nuclear import factors on the rough endoplasmic reticulum/Golgi membrane.* J Virol, 2007. **81**(18): p. 9812-24.
60. Yount, B., et al., *Severe acute respiratory syndrome coronavirus group-specific open reading frames encode nonessential functions for replication in cell cultures and mice.* J Virol, 2005. **79**(23): p. 14909-22.
61. *Molecular evolution of the SARS coronavirus during the course of the SARS epidemic in China.* Science, 2004. **303**(5664): p. 1666-9.
62. Chen, C.Y., et al., *Open reading frame 8a of the human severe acute respiratory syndrome coronavirus not only promotes viral replication but also induces apoptosis.* J Infect Dis, 2007. **196**(3): p. 405-15.
63. Keng, C.T., et al., *SARS coronavirus 8b reduces viral replication by down-regulating E via an ubiquitin-independent proteasome pathway.* Microbes Infect, 2011. **13**(2): p. 179-88.
64. Keng, C.T., et al., *The human severe acute respiratory syndrome coronavirus (SARS-CoV) 8b protein is distinct from its counterpart in animal SARS-CoV and down-regulates the expression of the envelope protein in infected cells.* Virology, 2006. **354**(1): p. 132-42.

65. Law, P.Y., et al., *Expression and functional characterization of the putative protein 8b of the severe acute respiratory syndrome-associated coronavirus.* FEBS Lett, 2006. **580**(15): p. 3643-8.
66. Le, T.M., et al., *Expression, post-translational modification and biochemical characterization of proteins encoded by subgenomic mRNA8 of the severe acute respiratory syndrome coronavirus.* FEBS J, 2007. **274**(16): p. 4211-22.
67. Oostra, M., C.A. de Haan, and P.J. Rottier, *The 29-nucleotide deletion present in human but not in animal severe acute respiratory syndrome coronaviruses disrupts the functional expression of open reading frame 8.* J Virol, 2007. **81**(24): p. 13876-88.
68. Sung, S.C., et al., *The 8ab protein of SARS-CoV is a luminal ER membrane-associated protein and induces the activation of ATF6.* Virology, 2009. **387**(2): p. 402-13.
69. Wu, D., et al., *Civets are equally susceptible to experimental infection by two different severe acute respiratory syndrome coronavirus isolates.* J Virol, 2005. **79**(4): p. 2620-5.
70. Calisher, C.H., et al., *Bats: important reservoir hosts of emerging viruses.* Clin Microbiol Rev, 2006. **19**(3): p. 531-45.
71. Halpin, K., et al., *Isolation of Hendra virus from pteropid bats: a natural reservoir of Hendra virus.* J Gen Virol, 2000. **81**(Pt 8): p. 1927-32.
72. Lau, S.K., et al., *Severe acute respiratory syndrome coronavirus-like virus in Chinese horseshoe bats.* Proc Natl Acad Sci U S A, 2005. **102**(39): p. 14040-5.
73. Leroy, E.M., et al., *Fruit bats as reservoirs of Ebola virus.* Nature, 2005. **438**(7068): p. 575-6.
74. Banyard, A.C., et al., *Bats and lyssaviruses.* Adv Virus Res, 2011. **79**: p. 239-89.
75. Towner, J.S., et al., *Isolation of genetically diverse Marburg viruses from Egyptian fruit bats.* PLoS Pathog, 2009. **5**(7): p. e1000536.
76. Drexler, J.F., et al., *Henipavirus RNA in African bats.* PLoS One, 2009. **4**(7): p. e6367.
77. Wang, L.F., et al., *Review of bats and SARS.* Emerg Infect Dis, 2006. **12**(12): p. 1834-40.
78. Guan, Y., et al., *Isolation and characterization of viruses related to the SARS coronavirus from animals in southern China.* Science, 2003. **302**(5643): p. 276-8.
79. Kan, B., et al., *Molecular evolution analysis and geographic investigation of severe acute respiratory syndrome coronavirus-like virus in palm civets at an animal market and on farms.* J Virol, 2005. **79**(18): p. 11892-900.
80. Poon, L.L., et al., *Identification of a novel coronavirus in bats.* J Virol, 2005. **79**(4): p. 2001-9.
81. Tu, C., et al., *Antibodies to SARS coronavirus in civets.* Emerg Infect Dis, 2004. **10**(12): p. 2244-8.
82. Hudson PJ, R.A., Grenfell BT, Heesterbeek H, Dobson AP, *The ecology of wildlife diseases.* Oxford (UK): Oxford University Press, 2002.
83. Gloza-Rausch, F., et al., *Detection and prevalence patterns of group I coronaviruses in bats, northern Germany.* Emerg Infect Dis, 2008. **14**(4): p. 626-31.
84. Muller, M.A., et al., *Coronavirus antibodies in African bat species.* Emerg Infect Dis, 2007. **13**(9): p. 1367-70.
85. Osborne, C., et al., *Alphacoronaviruses in New World bats: prevalence, persistence, phylogeny, and potential for interaction with humans.* PLoS One, 2011. **6**(5): p. e19156.
86. Pfefferle, S., et al., *Distant relatives of severe acute respiratory syndrome coronavirus and close relatives of human coronavirus 229E in bats, Ghana.* Emerg Infect Dis, 2009. **15**(9): p. 1377-84.
87. Woo, P.C., et al., *Molecular diversity of coronaviruses in bats.* Virology, 2006. **351**(1): p. 180-7.
88. Drexler, J.F., et al., *Genomic characterization of severe acute respiratory syndrome-related coronavirus in European bats and classification of coronaviruses based on partial RNA-dependent RNA polymerase gene sequences.* J Virol, 2010. **84**(21): p. 11336-49.
89. Liang, G., et al., *Laboratory diagnosis of four recent sporadic cases of community-acquired SARS, Guangdong Province, China.* Emerg Infect Dis, 2004. **10**(10): p. 1774-81.

90. Weir, J.P., G. Bajszar, and B. Moss, *Mapping of the vaccinia virus thymidine kinase gene by marker rescue and by cell-free translation of selected mRNA.* Proc Natl Acad Sci U S A, 1982. **79**(4): p. 1210-4.
91. Post, L.E. and B. Roizman, *A generalized technique for deletion of specific genes in large genomes: alpha gene 22 of herpes simplex virus 1 is not essential for growth.* Cell, 1981. **25**(1): p. 227-32.
92. Peden, K.W., et al., *Isolation of mutants of an animal virus in bacteria.* Science, 1980. **209**(4463): p. 1392-6.
93. van Dinten, L.C., et al., *An infectious arterivirus cDNA clone: identification of a replicase point mutation that abolishes discontinuous mRNA transcription.* Proc Natl Acad Sci U S A, 1997. **94**(3): p. 991-6.
94. Rice, C.M., et al., *Production of infectious RNA transcripts from Sindbis virus cDNA clones: mapping of lethal mutations, rescue of a temperature-sensitive marker, and in vitro mutagenesis to generate defined mutants.* J Virol, 1987. **61**(12): p. 3809-19.
95. Racaniello, V.R. and D. Baltimore, *Cloned poliovirus complementary DNA is infectious in mammalian cells.* Science, 1981. **214**(4523): p. 916-9.
96. Yount, B., et al., *Systematic assembly of a full-length infectious cDNA of mouse hepatitis virus strain A59.* J Virol, 2002. **76**(21): p. 11065-78.
97. Yount, B., et al., *Reverse genetics with a full-length infectious cDNA of severe acute respiratory syndrome coronavirus.* Proc Natl Acad Sci U S A, 2003. **100**(22): p. 12995-3000.
98. Yount, B., K.M. Curtis, and R.S. Baric, *Strategy for systematic assembly of large RNA and DNA genomes: transmissible gastroenteritis virus model.* J Virol, 2000. **74**(22): p. 10600-11.
99. Thiel, V., et al., *Infectious RNA transcribed in vitro from a cDNA copy of the human coronavirus genome cloned in vaccinia virus.* J Gen Virol, 2001. **82**(Pt 6): p. 1273-81.
100. Almazan, F., et al., *Engineering the largest RNA virus genome as an infectious bacterial artificial chromosome.* Proc Natl Acad Sci U S A, 2000. **97**(10): p. 5516-21.
101. Almazan, F., et al., *Construction of a severe acute respiratory syndrome coronavirus infectious cDNA clone and a replicon to study coronavirus RNA synthesis.* J Virol, 2006. **80**(21): p. 10900-6.
102. Pfeifer, A. and A. Hofmann, *Lentiviral transgenesis.* Methods Mol Biol, 2009. **530**: p. 391-405.
103. Roth, H., *Establishment and characterization of human angiotensin converting enzyme 2 transgenic bat cell cultures for SARS-Coronavirus infection studies*, 2011, University of Bonn Medical Centre.
104. Crameri, G., et al., *Establishment, immortalisation and characterisation of pteropid bat cell lines.* PLoS One, 2009. **4**(12): p. e8266.
105. Biesold, S.E., et al., *Type I interferon reaction to viral infection in interferon-competent, immortalized cell lines from the African fruit bat Eidolon helvum.* PLoS One, 2011. **6**(11): p. e28131.
106. Kuhl, A., et al., *Comparative analysis of Ebola virus glycoprotein interactions with human and bat cells.* J Infect Dis, 2011. **204 Suppl 3**: p. S840-9.
107. Cinatl, J., et al., *Treatment of SARS with human interferons.* Lancet, 2003. **362**(9380): p. 293-4.
108. de Lang, A., et al., *Functional genomics highlights differential induction of antiviral pathways in the lungs of SARS-CoV-infected macaques.* PLoS Pathog, 2007. **3**(8): p. e112.
109. Frieman, M., M. Heise, and R. Baric, *SARS coronavirus and innate immunity.* Virus Res, 2008. **133**(1): p. 101-12.
110. Stanley Perlman, T.G., Eric J. Snijder, *Nidoviruses*2008: American Society for Microbiology.
111. Kuri, T., et al., *Species-independent bioassay for sensitive quantification of antiviral type I interferons.* Virol J, 2010. **7**: p. 50.
112. Curtis, K.M., et al., *Reverse genetic analysis of the transcription regulatory sequence of the coronavirus transmissible gastroenteritis virus.* J Virol, 2004. **78**(11): p. 6061-6.
113. Emeny, J.M. and M.J. Morgan, *Regulation of the interferon system: evidence that Vero cells have a genetic defect in interferon production.* J Gen Virol, 1979. **43**(1): p. 247-52.

114. McKimm-Breschkin, J.L. and I.H. Holmes, *Conditions required for induction of interferon by rotaviruses and for their sensitivity to its action.* Infect Immun, 1982. **36**(3): p. 857-63.
115. Mordstein, M., et al., *Lambda interferon renders epithelial cells of the respiratory and gastrointestinal tracts resistant to viral infections.* J Virol, 2010. **84**(11): p. 5670-7.
116. Prescott, J., et al., *New World hantaviruses activate IFNlambda production in type I IFN-deficient vero E6 cells.* PLoS One, 2010. **5**(6): p. e11159.
117. Lin, J.J., *Endonuclease A degrades chromosomal and plasmid DNA of Escherichia coli present in most preparations of single stranded DNA from phagemids.* Proc Natl Sci Counc Repub China B, 1992. **16**(1): p. 1-5.
118. Tischer, B.K., G.A. Smith, and N. Osterrieder, *En passant mutagenesis: a two step markerless red recombination system.* Methods Mol Biol, 2010. **634**: p. 421-30.
119. Roth, S.J., et al., *Recovery of infectious virus from full-length cowpox virus (CPXV) DNA cloned as a bacterial artificial chromosome (BAC).* Vet Res, 2011. **42**(1): p. 3.
120. Narayanan, K., C. Huang, and S. Makino, *SARS coronavirus accessory proteins.* Virus Res, 2008. **133**(1): p. 113-21.
121. Tan, Y.J., S.G. Lim, and W. Hong, *Understanding the accessory viral proteins unique to the severe acute respiratory syndrome (SARS) coronavirus.* Antiviral Res, 2006. **72**(2): p. 78-88.
122. Beard, B.C., et al., *Comparison of HIV-derived lentiviral and MLV-based gammaretroviral vector integration sites in primate repopulating cells.* Mol Ther, 2007. **15**(7): p. 1356-65.
123. Hofmann, A., et al., *Epigenetic regulation of lentiviral transgene vectors in a large animal model.* Mol Ther, 2006. **13**(1): p. 59-66.
124. Staunstrup, N.H., et al., *Hybrid lentivirus-transposon vectors with a random integration profile in human cells.* Mol Ther, 2009. **17**(7): p. 1205-14.
125. Hornung, V., et al., *5'-Triphosphate RNA is the ligand for RIG-I.* Science, 2006. **314**(5801): p. 994-7.
126. Kawai, T. and S. Akira, *Innate immune recognition of viral infection.* Nat Immunol, 2006. **7**(2): p. 131-7.
127. Thompson, M.R., et al., *Pattern recognition receptors and the innate immune response to viral infection.* Viruses, 2011. **3**(6): p. 920-40.
128. Stewart, W.E., 2nd, W.D. Scott, and S.E. Sulkin, *Relative sensitivities of viruses to different species of interferon.* J Virol, 1969. **4**(2): p. 147-53.
129. Virtue, E.R., et al., *Interferon production and signaling pathways are antagonized during henipavirus infection of fruit bat cell lines.* PLoS One, 2011. **6**(7): p. e22488.
130. Zhou, P., et al., *Type III IFNs in pteropid bats: differential expression patterns provide evidence for distinct roles in antiviral immunity.* J Immunol, 2011. **186**(5): p. 3138-47.
131. Gitlin, L., et al., *Essential role of mda-5 in type I IFN responses to polyriboinosinic:polyribocytidylic acid and encephalomyocarditis picornavirus.* Proc Natl Acad Sci U S A, 2006. **103**(22): p. 8459-64.
132. Goldsmith, C.S., et al., *Ultrastructural characterization of SARS coronavirus.* Emerg Infect Dis, 2004. **10**(2): p. 320-6.
133. Burns, J.C., et al., *Vesicular stomatitis virus G glycoprotein pseudotyped retroviral vectors: concentration to very high titer and efficient gene transfer into mammalian and nonmammalian cells.* Proc Natl Acad Sci U S A, 1993. **90**(17): p. 8033-7.
134. Tang, X.C., et al., *Prevalence and genetic diversity of coronaviruses in bats from China.* J Virol, 2006. **80**(15): p. 7481-90.
135. Dankar, S.K., et al., *Influenza A virus NS1 gene mutations F103L and M106I increase replication and virulence.* Virol J, 2011. **8**: p. 13.
136. Dediego, M.L., et al., *Pathogenicity of severe acute respiratory coronavirus deletion mutants in hACE-2 transgenic mice.* Virology, 2008. **376**(2): p. 379-89.

7 Abbreviations

BSA	Bovine Serum Albumin
CoV	Coronavirus
cDNA	Complementary DNA
DNA	Deoxyribonucleic acid
dNTPs	Deoxynucleoside triphosphate
EC_{50}	Half maximal effective concentration
EDTA	Ethylenediaminetetraacetic acid
GFP	Green Fluorescent protein
h	Hour
HA	Hemagglutinin
hACE2	Human angiotensin converting enzyme 2
IFN	Interferon
ISG	IFN-stimulated gene
kDa	Kilodalton
KPNA	Karyopherin α
min	Minutes
µL	Microliter
mL	Milliliter
mM	Millimolar
MOI	Multiplicity of infection
ng	Nanogram
nt	nucleotide
ORF	Open reading frame
PBS	Phosphate buffered saline
p.i.	Post infection
PCR	Polymerase chain reaction
PFU	Plaque forming units
Ren	*Renilla* luciferase
RhiLu	Rhinolophus lung
RNA	Ribonucleic acid

rSCV	Recombinant SARS-CoV
RT-PCR	Reverse transcription polymerase chain reaction
RVFV	Rift valley fever virus
SARS	Severe acute respiratory syndrome
sec	Second
TAE	Tris-acetate-EDTA buffer
TRS	Transcription regulatory sequence

Publications

Publication

Drexler, J. F., Gloza-Rausch, F., Glende, J., Corman, V. M., **Muth, D.**, Goettsche, M., Seebens, A., Niedrig, M., Pfefferle, S., Yordanov, S., Zhelyazkov, L., Hermanns, U., Vallo, P., Lukashev, A., Muller, M. A., Deng, H., Herrler, G., Drosten, C., *Genomic characterization of severe acute respiratory syndrome-related coronavirus in European bats and classification of coronaviruses based on partial RNA-dependent RNA polymerase gene sequences.* J Virol, 2010. **84**(21): p. 11336-49.

Oral presentations

D. Muth, J. F. Drexler, F. Gloza-Rausch, T. Binger, H. Roth, S. Pfefferle, K. Zimmermann, A. Pfeifer, C. Drosten, M. A. Müller, *The open reading frame 8 of SARS-Coronavirus displays host adaptation and has an influence on virus replication in primate and bat cell culture.* National Symposium on Zoonoses Research, 2011, Berlin.

D. Muth, M. A. Müller, J. F. Drexler, T. Binger, D. Ritz, H. Roth, S. Pfefferle, C. Drosten, *Assessment of a SARS-Coronavirus virulence factor (open reading frame 6) carried by European bat viruses.* National Symposium on Zoonoses Research, 2011, Berlin.

Erklärung zur Dissertation

Ich erkläre, dass ich

- die Dissertation persönlich, selbstständig und ohne unerlaubte fremde Hilfe angefertigt habe,
- keine anderen, als die von mir angegebenen Quellen und Hilfsmittel benutzt habe,
- diese oder eine ähnliche Arbeit an keiner anderen Universität zur Erlangung eines Titels eingereicht habe,
- noch keinen Promotionsversuch unternommen habe.

Bonn, den

_____

Doreen Muth

Danksagung

Mein besonderer Dank gilt Prof. Christian Drosten für die Bereitstellung dieses interessanten und herausfordernden Themas. Ich bedanke mich für die kompetente Betreuung und die immer wieder inspirierenden Diskussionen.

Großer Dank geht an Prof. Sahl, der sich ohne Zögern bereit erklärt hat, meine Arbeit zu begutachten.

Außerdem danke ich Prof. Misof und Prof. Müller für die Bereitschaft an der Promotionskommission teilzunehmen.

Weiterhin danke ich meinen „Ex"-Kollegen aus dem Bernhard-Nocht-Institut. Ganz besonders Petra und Susanne, die mir gezeigt haben, dass 3 Frauen auf engstem Raum nicht Krieg bedeuten. Außerdem den „Günthers" und den „Biochemikern", die unserer kleinen Enklave immer geholfen haben. Und allen danke für die unvergesslichen Stunden 100m die Straße runter außerhalb des Instituts.

Besonderer Dank gilt meinen „neuen" Kollegen in Bonn, die mich so herzlich und offen aufgenommen haben, dass der Umzug nur halb so wehgetan hat. Im Speziellen Marcel, der ein wirklich schönes Nest gebaut hat und immer für mich da ist (auch wenn er in Berlin, Dortmund, Holland,… ist). Weiterhin danke ich Tabea, Hanna und Daniel für die tatkräftige Unterstützung im Labor, am Rechner und beim Nicht-verrückt-werden. Huge thanks to Tasnim for revising my English! Danke Felix und Victor für die Bereitstellung meiner Arbeitsgrundlage in Form von Gs, As, Ts und Cs. Und danke denen, die bei der Etablierung meines Privatlebens geholfen haben…

Außerdem danke ich meinen Eltern, die immer noch nicht wissen, was ich mache, aber es trotzdem ganz toll finden, für ihre immerwährende Unterstützung. Danke Jörg, dass du schon soooo lang da bist. Danke Franzi, dass du mich einfach nicht gehen lässt.

Walk on!